Supporting Information

An Indium(I) Tetramer Bound by Anionic *N*-Heterocyclic Olefins: Ambiphilic Reactivity, Transmetallation and a Rare Indium-Imide

Samuel R. Baird,[a] Emanuel Hupf,[b] Ian C. Watson,[a] Michael J. Ferguson[a] and Eric Rivard*[a]

[a.]Department of Chemistry, University of Alberta, 11227 Saskatchewan Dr, Edmonton, Alberta, T6G 2G2, Canada

[b.]Institut für Anorganische Chemie und Kristallographie, Universität Bremen, Leobener Str. 7, 28359 Bremen, Germany

Contents:

Supporting Information

Complete Experimental Procedures

Materials and Experimentation

General: All reactions were performed using Schlenk and glovebox (Innovative Technology, Inc.) techniques under a nitrogen atmosphere. All solvents were purified using a Grubbs-type solvent purification system[S1] provided by Innovative Technology, Inc., degassed (freeze, pump, thaw method), and stored under an atmosphere of nitrogen prior to use. 2-Isopropoxy-4,4,5,5-tetramethyl-1,3,2-dioxaborolane (^{i}PrOBpin) and pinacolborane (HBpin) were purchased from Oakwood Chemical and used as received. Tris(pentafluorophenyl)borane ($B(C_6F_5)_3$) was purchased from TCI and used as received. I_2, $K[N(SiMe_3)_2]$ and ^{n}BuLi (2.5 M solution in hexanes) were purchased from Sigma-Aldrich and used as received. $SIPrCH_2$,[S2] $[(^{Me}IPrCH)Li]_2$,[S3] CpIn,[S4] $TripBH_2$,[S5] and $Ar^{Dipp}N_3$[S6] were prepared according to literature procedures [SIPr = $(H_2CNDipp)_2C$; ^{Me}IPr = $(MeCNDipp)_2C$; Ar^{Dipp} = 2,6-$Dipp_2C_6H_3$]. ^{1}H, $^{13}C\{^{1}H\}$, $^{11}B\{^{1}H\}$, $^{19}F\{^{1}H\}$, and ^{7}Li NMR spectra were recorded on 400, 500, 600 or 700 MHz Varian Inova instruments and were referenced externally to $SiMe_4$ (^{1}H, $^{13}C\{^{1}H\}$), 15% $F_3B{\bullet}Et_2O$ (^{11}B), Cl_3CF (^{19}F) and 9.7 M solution of LiCl in D_2O (^{7}Li). Elemental analyses were performed by the Analytical and Instrumentation Laboratory at the University of Alberta. Melting points were measured in sealed glass capillaries under nitrogen with a MelTemp apparatus and are uncorrected.

X-ray Crystallography

Appropriate X-ray quality crystals were coated with a small amount of hydrocarbon oil (Paratone-N) and removed from the glovebox in a vial. Crystals were mounted quickly onto a glass fiber and placed in a low temperature stream of nitrogen on the X-ray diffractometer. All data was collected using a Bruker APEX II CCD detector/D8 or PLATFORM diffractometer using Mo Kα (0.71073 Å) or Cu Kα (1.54178 Å) radiation, with the crystals cooled to -80 °C or -100 °C. The data was corrected for absorption through Gaussian integration from the indexing of crystal faces.[S7] Crystal structures were solved using intrinsic phasing (SHELXT)[S8] and refined using SHELXL-2014.[S9] The assignment of hydrogen atom positions is based on the sp^2- or sp^3-hybridization geometries of their attached carbon atoms and were given thermal parameters 20% greater than those of their parent atoms.

Synthetic Procedures

Synthesis of $[(^{Me}IPrCH)In]_4$ (1): A solution of $[(^{Me}IPrCH)Li]_2$ (0.151 g, 0.173 mmol) in 10 mL of toluene was added to a solution of CpIn (0.061 g, 0.34 mmol) in 3 mL of toluene. After one

minute the solution had turned deep red in color. After a further 40 minutes of stirring the volatiles were removed *in vacuo*, and the remaining solid residue was extracted with 18 mL of hexanes and filtered through a plug of diatomaceous earth. The resulting deep-red filtrate was concentrated to a volume of 1 mL and stored in a -35 °C freezer for 16 hours to afford deep-red microcrystals of [(^{Me}IPrCH)In]$_4$ (**1**) (0.056 g, 30%). X-ray quality crystals were obtained by dissolving **1** in 1 mL toluene and storing the solution in a –35 °C freezer for one month. ^{1}H NMR (C_6D_6, 700 MHz): δ 7.37-7.40 (overlapping multiplets, 4H, Ar*H*), 7.34-7.35 (overlapping multiplets, 8H, Ar*H*), 7.24 (t, 4H, $^3J_{HH}$ = 7.0 Hz, *p*-Ar*H*), 7.16-7.17 (overlapping multiplets, 8H, *m*-Ar*H*), 3.72 (s, 4H, C*H*In), 3.39 (sept, 8H, $^3J_{HH}$ = 7.0 Hz, C*H*(CH$_3$)$_2$), 3.29 (sept, 8H, $^3J_{HH}$ = 7.0 Hz, C*H*(CH$_3$)$_2$), 1.68 (s, 12H, CN-C*H*$_3$), 1.66 (s, 12H, CN(C*H*$_3$)), 1.64 (d, 24H, $^3J_{HH}$ = 7.0 Hz, CH(C*H*$_3$)$_2$), 1.40 (d, 24H, $^3J_{HH}$ = 7.0 Hz, CH(C*H*$_3$)$_2$), 1.30 (d, 24H, $^3J_{HH}$ = 7.0 Hz, CH(C*H*$_3$)$_2$), 1.28 (d, 24H, $^3J_{HH}$ = 7.0 Hz, CH(C*H*$_3$)$_2$). ^{13}C{^{1}H} NMR (C_6D_6, 176 MHz): δ 154.9 (N*C*N), 149.4 (Ar*C*), 147.6 (Ar*C*), 134.7 (Ar*C*), 134.5 (Ar*C*), 130.3 (Ar*C*), 128.8 (Ar*C*), 128.1 (C=*C*HIn), 126.6 (Ar*C*), 124.2 (Ar*C*), 116.6 (N*C*-CH$_3$), 115.8 (N*C*-CH$_3$), 28.8 (*C*H(CH$_3$)$_2$), 28.7 (*C*H(CH$_3$)$_2$), 26.3 (CH(*C*H$_3$)$_2$), 25.5 (CH(*C*H$_3$)$_2$), 24.2 (CH(*C*H$_3$)$_2$), 24.1 (CH(*C*H$_3$)$_2$), 10.3 (CN-*C*H$_3$), 9.9 (CN-*C*H$_3$). Anal. Calcd. for $C_{120}H_{164}In_4N_8$ (%): C 66.18, H 7.59, N 5.14; Found: C 66.11, H, 8.11, N 4.55; *Prior to collecting elemental analysis, samples were dried under prolonged vacuum.* M.p. 126 °C (decomp). *The exocyclic vinyl carbon resonance was located indirectly by HSQC and overlaps with residual benzene resonances by coincidence.* UV-vis (in hexanes): λ_{max} = 515 nm, ε = 4390 L mol^{-1} cm^{-1}; λ_{max} = 439 nm, ε = 4970 L mol^{-1} cm^{-1}.

Synthesis of (^{Me}IPrCH)In(THF)•B(C$_6$F$_5$)$_3$ (2): A solution of B(C_6F_5)$_3$ (0.052 g, 0.10 mmol) in 3 mL of benzene was added to a solution of **1** (0.055 g, 0.025 mmol) in 4 mL of benzene. After one minute of stirring the color of the reaction mixture had turned dark yellow-brown. After a further three minutes of stirring the volatiles were removed *in vacuo*, and the remaining solid was extracted in 18 mL of pentane and filtered through a plug of diatomaceous earth. The resulting orange filtrate was concentrated to volume of 1 mL and 1 mL of THF was added. Storing the solution in a -35 °C freezer for 24 hours afforded (^{Me}IPrCH)In(THF)•B(C_6F_5)$_3$ (**2**) as a bright-yellow powder (0.024 g, 21%). X-ray quality crystals of **2** were grown from a solution in pentane/THF over the course of one month. ^{1}H NMR (C_6D_6, 700 MHz) δ 7.18 (t, 1H, $^3J_{HH}$ = 7.0 Hz, *p*-Ar*H*), 7.07 (d, 2H, $^3J_{HH}$ = 7.0 Hz, *m*-Ar*H*), 7.06 (d, 2H, $^3J_{HH}$ = 7.0 Hz, *m*-Ar*H*), 6.79 (t, 1H, $^3J_{HH}$ = 7.0 Hz, *p*-Ar*H*), 3.45 (t, 4H, $^3J_{HH}$ = 7.0 Hz, OC*H*$_2$CH$_2$), 4.07 (s, 1H, C*H*In), 2.85 (sept, 4H, $^3J_{HH}$ = 7.0 Hz, C*H*(CH$_3$)$_2$), 1.42 (s, 3H, CN-C*H*$_3$), 1.36 (s, 3H, CN-C*H*$_3$), 1.31-1.32 (m, 10H, $^3J_{HH}$ = 7.0 Hz, CH(C*H*$_3$)$_2$ overlapping with OCH$_2$C*H*$_2$), 1.27 (d, 6H, $^3J_{HH}$ = 7.0 Hz, CH(C*H*$_3$)$_2$), 1.08 (d, 6H, $^3J_{HH}$ = 7.0 Hz, CH(C*H*$_3$)$_2$), 0.95 (d, 6H, $^3J_{HH}$ = 7.0 Hz, CH(C*H*$_3$)$_2$). ^{13}C{^{1}H} NMR (C_6D_6, 176 MHz): δ 159.6 (N*C*N), 148.0-148.2 (m, Ar*F*), 147.8 (Ar*C*), 147.0 (Ar*C*), 146.7-146.9 (m, Ar*F*), 144.7 (Ar*C*), 139.7-139.9 (m, Ar*F*), 138.3-138.5 (m, Ar*F*), 137.7-137.9 (m, Ar*F*), 136.3-136.5 (m, Ar*F*), 131.9 (Ar*C*), 131.0 (Ar*C*), 130.4 (Ar*C*), 129.9 (Ar*C*), 127.9 (Ar*C*), 127.8 (Ar*C*), 127.1 (Ar*C*), 124.4 (Ar*C*), 118.8 (N*C*-CH$_3$), 117.4 (N*C*-CH$_3$), 81.7 (C=*C*HIn), 67.8 (O*C*H$_2$), 28.6 (CH(*C*H$_3$)$_2$), 28.5 (CH(*C*H$_3$)$_2$), 25.2 (OCH$_2$*C*H$_2$), 24.2 (CH(*C*H$_3$)$_2$), 23.8 (CH(*C*H$_3$)$_2$), 23.4 (CH(*C*H$_3$)$_2$), 23.1 (CH(*C*H$_3$)$_2$), 8.9 (NC*C*H$_3$), 8.8 (NC*C*H$_3$). ^{11}B{^{1}H} NMR (C_6D_6, 128 MHz): δ -14.3. ^{19}F NMR (C_6D_6, 376 MHz): δ -129.8 (d, 6F, $^3J_{FF}$ = 37.6 Hz, *o*-Ar*F*), -159.0 (t, 3F, $^3J_{FF}$ = 37.6

Hz, *p*-Ar*F*), -163.7 to -163.8 (m, 6F, $^3J_{FF}$ = 37.6 Hz, *m*-Ar*F*). Anal. Calcd. for $C_{52}H_{49}BF_{15}IN_2O$ (%): C 55.34, H, 4.38, N 2.48; Found: C 55.12, H, 4.41, N, 2.50; *Prior to collecting elemental analysis, samples were dried under prolonged vacuum.* M.p. 147–149 °C.

Synthesis of (^{Me}IPrCH)In•B(C_6F_5)$_3$ (2'): A solution of B(C_6F_5)$_3$ (0.026 g, 0.051 mmol) in 1 mL of C_6D_6 was added to a solution of **1** (0.028 g, 0.013 mmol) in 1 mL of C_6D_6. After one minute of stirring the color of the reaction mixture had turned to a dark yellow-brown. After a further five minutes of stirring the reaction mixture was filtered through glass filter paper and the volatiles removed from the filtrate *in vacuo* to afford (^{Me}IPrCH)In•B(C_6F_5)$_3$ (**2'**) as an orange solid (0.040 g, 74%). ^{1}H NMR (C_6D_6, 700 MHz): δ 7.19 (t, 1H, $^3J_{HH}$ = 7.0 Hz, *p*-Ar), 7.06 (overlapping doublets, 4H, $^3J_{HH}$ = 7.0 Hz, *m*-Ar), 6.80 (t, 1, $^3J_{HH}$ = 7.0 Hz, *p*-Ar), 3.57 (s, 1H, C*H*In), 2.84 (sept, 4H, $^3J_{HH}$ = 7.0 Hz, C*H*(CH$_3$)$_2$), 1.41 (s, 3H, CN-C*H*$_3$), 1.35 (s, 3H, CN-C*H*$_3$), 1.31 (d, 6H, $^3J_{HH}$ = 7.0 Hz, CH(C*H*$_3$)$_2$), 1.28 (d, 6H, $^3J_{HH}$ = 7.0 Hz, CH(C*H*$_3$)$_2$), 1.09 (d, 6H, $^3J_{HH}$ = 7.0 Hz, CH(C*H*$_3$)$_2$), 0.94 (d, 6H, $^3J_{HH}$ = 7.0 Hz, CH(C*H*$_3$)$_2$). ^{13}C{^{1}H} NMR (C_6D_6, 176 MHz): δ 160.2 (N*C*N), 148.4-148.5 (m, Ar*F*), 148.1 (Ar*C*), 147.6 (Ar*C*), 147.1-147.2 (m, Ar*F*), 140.2-140.3 (m, Ar*F*), 138.8-138.9 (m, Ar*F*), 138.1-138.3 (m, Ar*F*), 136.7-136.9 (m, Ar*F*), 132.3 (Ar*C*), 131.2 (Ar*C*), 130.9 (Ar*C*), 130.4 (Ar*C*), 128.3 (Ar*C*), 127.7 (Ar*C*), 124.8 (Ar*C*), 119.4 (N*C*-CH$_3$), 117.8 (N*C*-CH$_3$) 83.0 (C=*C*HIn), 31.9 (*C*H(*C*H$_3$)$_2$), 28.9 (*C*H(CH$_3$)$_2$), 28.8 (*C*H(CH$_3$)$_2$), 24.6 (CH(*C*H$_3$)$_2$), 24.2 (CH(*C*H$_3$)$_2$), 23.7 (CH(*C*H$_3$)$_2$), 23.6 (CH(*C*H$_3$)$_2$), 23.0 (CH(*C*H$_3$)$_2$), 9.2 (NC*C*H$_3$), 9.1 (NC*C*H$_3$). ^{11}B{^{1}H} NMR (C_6D_6, 128 MHz): δ -14.4. ^{19}F NMR (C_6D_6, 376 MHz): δ -129.9 (d, 6F, $^3J_{FF}$ = 37.6 Hz, *o*-Ar*F*), -158.7 (t, 3F, $^3J_{FF}$ = 37.6 Hz, *p*-Ar*F*), -163.5 to -163.6 (m, $^3J_{FF}$ = 37.6 Hz, *m*-Ar*F*). Anal. Calcd. for $C_{48}H_{41}BF_{15}IN_2$ (%): C 54.57, H, 3.91, N 2.65; Found: C 56.66, H, 4.34, N, 2.76; *attempts to obtain an analytically pure sample of **2'** by recrystallization was not successful*. M.p. 92 °C (decomp).

Synthesis of (^{Me}IPrCH)B(H)Trip: To a solution of TripBH$_2$ (0.008 g, 0.04 mmol) in 2 mL of toluene was added **1** (0.020 g, 0.0092 mmol) in 2 mL of toluene. After one minute, the deep-red color of **1** had faded with bubbling being observed (H_2) and the formation of a black precipitate, presumably indium metal. After a further seven minutes of stirring, the reaction mixture was filtered through a plug of diatomaceous earth resulting in a colorless solution. The volatiles were removed *in vacuo* to afford (^{Me}IPrCH)B(H)Trip as a white solid (0.021 g, 86%). ^{1}H and ^{11}B{^{1}H} NMR spectra match previously reported literature values.[S5]

Synthesis of (^{Me}IPrCH)Bpin (3): Route A. A solution of [(^{Me}IPrCH)Li]$_2$ (0.170 g, 0.195 mmol) in 5 mL of toluene was added dropwise to a solution of ^{i}PrOBpin (79 μL, 0.39 mmol) in 3 mL of toluene. After stirring for 3 hours a pale-orange supernatant was formed along with a white precipitate. The volatiles were removed *in vacuo*, the residue was extracted with 15 mL of hexanes and filtered. The filtrate was concentrated to a volume of 1 mL and stored in a -35 °C freezer for 16 hours, leading to the formation of colorless microcrystals of (^{Me}IPrCH)Bpin (**3**) (0.044 g, 20%). X-ray quality crystals of **3** were grown from hexanes at -35 °C over the course of one month. ^{1}H NMR (C_6D_6, 700 MHz): δ 7.31 (t, 1H, $^3J_{HH}$ = 7.0 Hz, *p*-Ar*H*), 7.22 (t, 1H, $^3J_{HH}$ = 7.0 Hz, *p*-Ar*H*),

7.15 (d, 2H, $^3J_{HH}$ = 7.0 Hz, *m*-Ar*H*), 7.10 (d, 2H, $^3J_{HH}$ = 7.0 Hz, *m*-Ar*H*), 3.17 (sept, 2H, $^3J_{HH}$ = 7.0 Hz, C*H*(CH_3)$_2$), 3.07 (sept, 2H, $^3J_{HH}$ = 7.0 Hz, C*H*(CH_3)$_2$), 2.65 (s, 1H, C*H*(Bpin)), 1.54 (s, 3H, CN-C*H*$_3$), 1.51 (s, 3H, CN-C*H*$_3$), 1.50 (d, 6H, $^3J_{HH}$ = 7.0 Hz, CH(C*H*$_3$)$_2$), 1.36 (d, 6H, $^3J_{HH}$ = 7.0 Hz, CH(C*H*$_3$)$_2$), 1.24 (d, 6H, $^3J_{HH}$ = 7.0 Hz, CH(C*H*$_3$)$_2$), 1.15 (d, 6H, $^3J_{HH}$ = 7.0 Hz, CH(C*H*$_3$)$_2$), 0.89 (s, 12H, OC(C*H*$_3$)$_2$). $^{13}C\{^1H\}$ NMR (C_6D_6, 176 MHz): δ 155.9 (N*C*N), 148.6 (Ar*C*), 148.4 (Ar*C*), 134.3 (Ar*C*), 132.6 (Ar*C*), 129.6 (Ar*C*), 129.0 (Ar*C*), 124.5 (Ar*C*), 123.8 (Ar*C*), 117.7 (N*C*-CH_3), 117.0 (N*C*-CH_3), 79.9 (O*C*(CH_3)$_2$), 48.0 (=*C*HBpin), 29.1 (*C*H(CH_3)$_2$), 28.9 (*C*H(CH_3)$_2$), 24.7 (OC(*C*H_3)$_2$), 24.6 (CH(*C*H_3)$_2$), 24.0 (CH(*C*H_3)$_2$), 23.8 (CH(*C*H_3)$_2$), 9.7 (NC*C*H_3), 9.5 (NC*C*H_3). $^{11}B\{^1H\}$ NMR (C_6D_6, 128 MHz): δ 28.4. Anal. Calcd. for $C_{36}H_{53}BN_2O_2$ (%): C 77.68, H 9.60, N 5.75; Found: C 76.55, H, 9.53, N 4.98. M.p. 145–147 °C. *The exocyclic vinyl carbon resonance was not found in the $^{13}C\{^1H\}$ NMR but located indirectly by HSQC.*

Route B. To a solution of **1** (0.045 g, 0.021 mmol) in 2 mL of C_6D_6 was added HBpin (12 μL, 0.083 mmol). After one minute, the deep-red color of **1** had faded and a black precipitate had formed, presumably indium metal. After a further four minutes of stirring, the reaction mixture was filtered through a plug of diatomaceous earth resulting in a colorless solution. ^1H and $^{11}B\{^1H\}$ NMR analysis of the reaction mixture showed the formation of (^{Me}IPrCH)Bpin (**3**), which was not isolated.

Synthesis of (^{Me}IPrCH)InNAr^{Dipp} (4): A solution of [(^{Me}IPrCH)Li]$_2$ (0.029 g, 0.033 mmol) in 2 mL of toluene was added to a solution of CpIn (0.011 g, 0.061 mmol) in 2 mL of toluene. After one minute the color of the reaction mixture had turned deep red. After a further 50 minutes the reaction mixture was filtered through a plug of diatomaceous earth. To the resulting deep-red solution containing **1** was added rapidly Ar^{Dipp}N$_3$ (0.029 g, 0.066 mmol) in 2 mL of toluene. After one minute the reaction mixture became red-orange in color. After a further 40 minutes the reaction mixture was concentrated to a volume of 1 mL and placed in a -35 °C freezer for 16 hours, which afforded bright-orange microcrystals of (^{Me}IPrCH)InNAr^{Dipp} (**4**) (0.018 g, 31%). Crystals of **4** that were suitable for X-ray diffraction analysis were obtained by dissolving **4** in 1 mL of toluene and storing the solution at -35 °C for 16 hours. ^1H NMR (C_6D_6, 700 MHz): δ 7.35 (t, 1H, $^3J_{HH}$ = 7.0 Hz, *p*-Ar*H*), 7.28 (d, 2H, $^3J_{HH}$ = 7.0 Hz, *m*-Ar*H*), 7.22 (d, 2H, $^3J_{HH}$ = 7.0 Hz, *m*-Ar*H*), 7.21 (d, 2H, $^3J_{HH}$ = 7.0 Hz, *m*-Ar*H*), 7.13 (t, 1H, $^3J_{HH}$ = 7.0 Hz, *p*-Ar*H*), 7.11 (d, 2H, $^3J_{HH}$ = 7.0 Hz, *m*-Ar*H*), 7.05 (t, 1H, $^3J_{HH}$ = 7.0 Hz, *p*-Ar*H*), 7.02 (d, 2H, $^3J_{HH}$ = 7.0 Hz, *m*-Ar*H*), 6.82 (t, 1H, $^3J_{HH}$ = 7.0 Hz, *p*-Ar*H*), 6.75 (t, 1H, $^3J_{HH}$ = 7.0 Hz, *p*-Ar*H*), 3.17-3.21 (overlapping septets, 4H, $^3J_{HH}$ = 7.0 Hz, C*H*(CH_3)$_2$), 2.83 (sept, 2H, $^3J_{HH}$ = 7.0 Hz, C*H*(CH_3)$_2$), 2.73 (sept, 2H, $^3J_{HH}$ = 7.0 Hz, C*H*(CH_3)$_2$), 1.66 (s, 1H, C*H*In), 1.45 (s, 3H, CN-C*H*$_3$), 1.43 (s, 3H, CN-C*H*$_3$), 1.37 (d, 12H, $^3J_{HH}$ = 7.0 Hz, CH(C*H*$_3$)$_2$), 1.28 (d, 6H, $^3J_{HH}$ = 7.0 Hz, CH(C*H*$_3$)$_2$), 1.26 (d, 6H, $^3J_{HH}$ = 7.0 Hz, CH(C*H*$_3$)$_2$), 1.22 (d, 12H, $^3J_{HH}$ = 7.0 Hz, CH(C*H*$_3$)$_2$), 1.16 (d, 6H, $^3J_{HH}$ = 7.0 Hz, CH(C*H*$_3$)$_2$), 1.01 (d, 6H, $^3J_{HH}$ = 7.0 Hz, CH(C*H*$_3$)$_2$). $^{13}C\{^1H\}$ NMR (C_6D_6, 176 MHz): δ 162.8 (N*C*N), 158.3 (Ar*C*), 148.8 (Ar*C*), 148.7 (Ar*C*), 146.2 (Ar*C*), 143.4 (Ar*C*), 134.0 (Ar*C*), 131.9 (Ar*C*), 129.9 (Ar*C*), 129.8 (Ar*C*), 129.3 (Ar*C*), 129.2 (Ar*C*), 128.5 (Ar*C*), 128.3 (Ar*C*), 128.2 (Ar*C*), 127.7 (Ar*C*), 125.6 (Ar*C*), 124.5 (Ar*C*), 124.3 (Ar*C*), 57.6 (=*C*HIn), 30.6 (*C*H(CH_3)$_2$), 28.8 (*C*H(CH_3)$_2$), 28.6 (*C*H(CH_3)$_2$), 25.0 (CH(*C*H_3)$_2$), 24.9 (CH(*C*H_3)$_2$), 24.8 (CH(*C*H_3)$_2$), 24.7 (CH(*C*H_3)$_2$), 24.0 (CH(*C*H_3)$_2$), 23.7 (CH(*C*H_3)$_2$), 9.4 (CH(*C*H_3)$_2$), 9.2 (CH(*C*H_3)$_2$). Anal. Calcd. for $C_{80}H_{78}N_3In$ (%): C 75.37, H 8.22,

N 4.39; Found: C 68.51, H, 7.60, N 3.75; repeated attempts to obtain satisfactory elemental analysis led to low values for carbon. M.p. 203–205 °C. UV-vis (in hexanes): λ_{max} = 459 nm, ε = 3690 L mol^{-1} cm^{-1}; λ_{max} = 341 nm, ε = 8040 L mol^{-1} cm^{-1}.

Synthesis of [(SIPrCH)Li]$_2$ (5): Iodine (0.4598 g, 1.811 mmol) dissolved in 10 mL of toluene was added via cannula to a solution of SIPrCH$_2$ (0.7325 g, 1.811 mmol) in 50 mL of toluene, resulting in the immediate formation of a yellow solid. The mixture was then stirred for 1 hour. *After this point, all manipulations were performed in the absence of ambient light*. A solution of K[N(SiMe$_3$)$_2$] in 10 mL of THF (0.5060 g, 2.536 mmol) was added via cannula to the mixture, the resulting mixture was stirred for 1 hour, followed by the removal of the volatiles *in vacuo*. The residue was extracted with 100 mL of hexanes. The volatiles were removed *in vacuo* and the residue was dissolved in 15 mL of hexanes, followed by the addition of ^{n}BuLi (0.797 mL, 2.5 M solution in hexanes, 2.0 mmol). The mixture was stirred for 15 minutes, after which a white solid had formed. The supernatant was decanted away, and the volatiles were removed from the remaining white precipitate *in vacuo* to yield [(SIPrCH)Li]$_2$ (**5**) (0.379 g, 54%). X-ray quality crystals of **5** were obtained by dissolving the product in 1 mL of toluene and storing in a –35 °C freezer for 72 hours. ^{1}H NMR (C$_6$D$_6$, 700 MHz): δ 7.36 (t, 2H, $^3J_{HH}$ = 7.0 Hz, *p*-Ar*H*), 7.27 (d, 4H, $^3J_{HH}$ = 7.0 Hz, *m*-Ar*H*), 6.93 (d, 4H, $^3J_{HH}$ = 7.0 Hz, *m*-Ar*H*), 6.79 (t, 2H, $^3J_{HH}$ = 7.0 Hz, *p*-Ar*H*), 3.57 (t, 4H, $^3J_{HH}$ = 7.0 Hz, NC*H*$_2$), 3.46 (t, 4H, $^3J_{HH}$ = 7.0 Hz, NC*H*$_2$), 3.31-3.40 (overlapping multiplets, 8H, C*H*(CH$_3$)$_2$), 1.36 (d, 12H, $^3J_{HH}$ = 7.0 Hz, CH(C*H*$_3$)$_2$), 1.32 (d, 12H, $^3J_{HH}$ = 7.0 Hz, CH(C*H*$_3$)$_2$), 1.23 (d, 12H, $^3J_{HH}$ = 7.0 Hz, CH(C*H*$_3$)$_2$), 1.11 (d, 12H, $^3J_{HH}$ = 7.0 Hz, CH(C*H*$_3$)$_2$), 1.03 (s, 2H, =C*H*Li). ^{13}C{^{1}H} NMR (C$_6$D$_6$, 176 MHz): δ 161.8 (N*C*N), 150.4 (Ar*C*), 150.1 (Ar*C*), 140.6 (Ar*C*), 140.3 (Ar*C*), 128.9 (Ar*C*), 127.5 (Ar*C*), 125.8 (Ar*C*), 124.6 (Ar*C*), 123.9 (Ar*C*), 77.4 (=*C*HLi), 50.3 (N*C*H$_2$), 48.7 (N*C*H$_2$), 28.6 (*C*H(CH$_3$)$_2$), 28.5 (*C*H(CH$_3$)$_2$), 25.3 (CH(*C*H$_3$)$_2$), 24.7 (CH(*C*H$_3$)$_2$), 24.5 (CH(*C*H$_3$)$_2$), 23.9 (CH(*C*H$_3$)$_2$). ^{7}Li{^{1}H} NMR (C$_6$D$_6$, 194 MHz): δ 0.7. Anal. Calcd. for C$_{56}$H$_{78}$Li$_2$N$_4$ (%): C 81.91, H 9.57, N 6.82; Found; C 81.43, H 9.60, N 6.61; *Prior to collecting elemental analysis, samples were dried under prolonged vacuum.* M.p. 182–183 °C.

Synthesis of [(SIPrCH)In]$_4$ (6): A solution of [(SIPrCH)Li]$_2$ (**6**) (0.199 g, 0.195 mmol) in 8 mL of toluene was added to a slurry of CpIn (0.069 g, 0.38 mmol) in 8 mL of toluene. After one minute the solution had turned deep red in color. After a further 45 minutes of stirring the volatiles were removed *in vacuo*, and the remaining solid was extracted with 18 mL of hexanes and filtered through a plug of diatomaceous earth. The resulting deep-red filtrate was concentrated to a volume of 5 mL and stored in a -35 °C freezer for 16 hours, which afforded [(SIPrCH)In]$_4$ (**6**) as an analytically pure deep-orange solid (0.048 g, 24%). ^{1}H NMR (C$_6$D$_6$, 700 MHz): δ 7.38 (t, 4H, $^3J_{HH}$ = 7.0 Hz, *p*-Ar*H*), 7.30 (d, 8H, $^3J_{HH}$ = 7.0 Hz, *m*-Ar*H*), 7.16-7.18 (overlapping multiplets, 4H, $^3J_{HH}$ = 7.0 Hz, *p*-Ar*H*), 6.95 (d, 8H, $^3J_{HH}$ = 7.0 Hz, *m*-Ar*H*), 3.56 (t, 8H, $^3J_{HH}$ = 7.0 Hz, NC*H*$_2$), 3.55 (s, 4H, =C*H*In), 3.44-3.47 (overlapping multiplets, 16H, NC*H*$_2$ and C*H*(CH$_3$)$_2$), 3.30 (sept, 8H, $^3J_{HH}$ = 7.0 Hz, C*H*(CH$_3$)$_2$), 1.55 (d, 24H, $^3J_{HH}$ = 7.0 Hz, CH(C*H*$_3$)$_2$), 1.32 (d, 48H, $^3J_{HH}$ = 7.0 Hz, CH(C*H*$_3$)$_2$), 1.28 (d, 24H, $^3J_{HH}$ = 7.0 Hz, CH(C*H*$_3$)$_2$). ^{13}C{^{1}H} NMR (C$_6$D$_6$, 176 MHz): δ 157.9 (N*C*N), 149.8 (Ar*C*), 148.3 (Ar*C*), 138.5 (Ar*C*), 138.2 (Ar*C*), 130.7 (=*C*HIn), 129.9 (Ar*C*), 129.3

(Ar*C*), 126.8 (Ar*C*), 124.4 (Ar*C*), 50.7 (N*C*H_2), 50.0 (N*C*H_2), 28.9 (*C*H(CH_3)$_2$), 28.7 (*C*H(CH_3)$_2$), 25.9 (CH(*C*H_3)$_2$), 25.6 (CH(*C*H_3)$_2$), 25.2 (CH(*C*H_3)$_2$), 24.7 (CH(*C*H_3)$_2$). Anal. Calcd. for $C_{128}H_{156}N_8In_4$ (%): C 64.87, H 7.58, N 5.40; Found: C 64.56, H 7.18, N 5.01; *Prior to collecting elemental analysis, samples were dried under prolonged vacuum.* M.p. 129 °C (decomp).

Synthesis of [(^{Me}IPrCH)$_6$In$_6$P$_8$] (7): To a solution of P_4 (0.002 g, 0.02 mmol) in 4 mL of toluene was added **1** (0.032 g, 0.015 mmol) in 5 mL of toluene. After one minute of stirring the initially deep-red mixture became red-purple along with the formation of a black precipitate. After one hour the volatiles were removed *in vacuo*. 15 mL of hexanes was then added, and the mixture filtered through Celite. The filtrate was then concentrated to a volume of 1 mL and stored in a -35 °C freezer for one week affording a single X-ray quality crystal of [(^{Me}IPrCH)$_6$In$_6$P$_8$] (**7**). *Attempts to repeat the preparation of **7** on a larger scale for further characterization were unsuccessful with the major isolated product being ^{Me}IPrCH$_2$.*

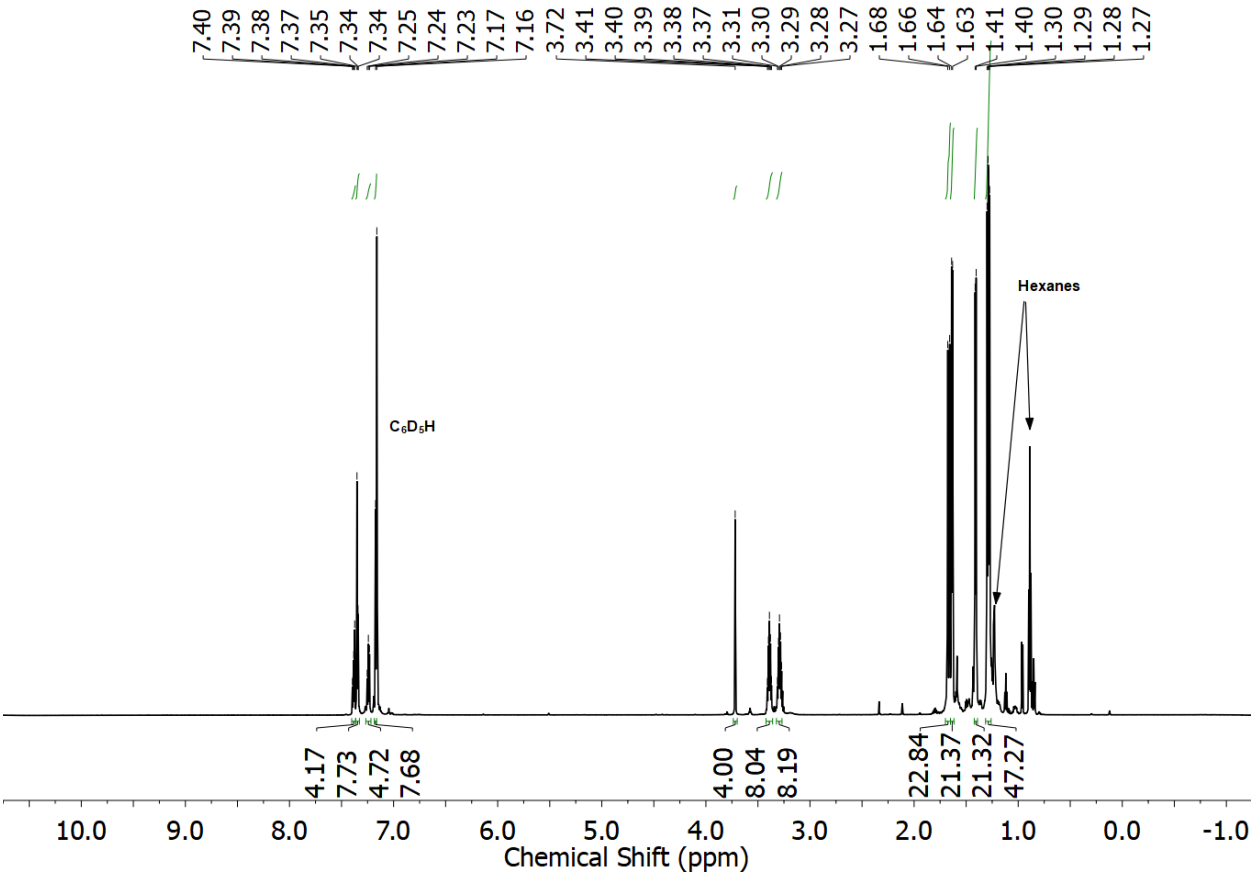

Fig. S1 ^{1}H NMR spectrum of [(^{Me}IPrCH)In]$_4$ (**1**) in C_6D_6.

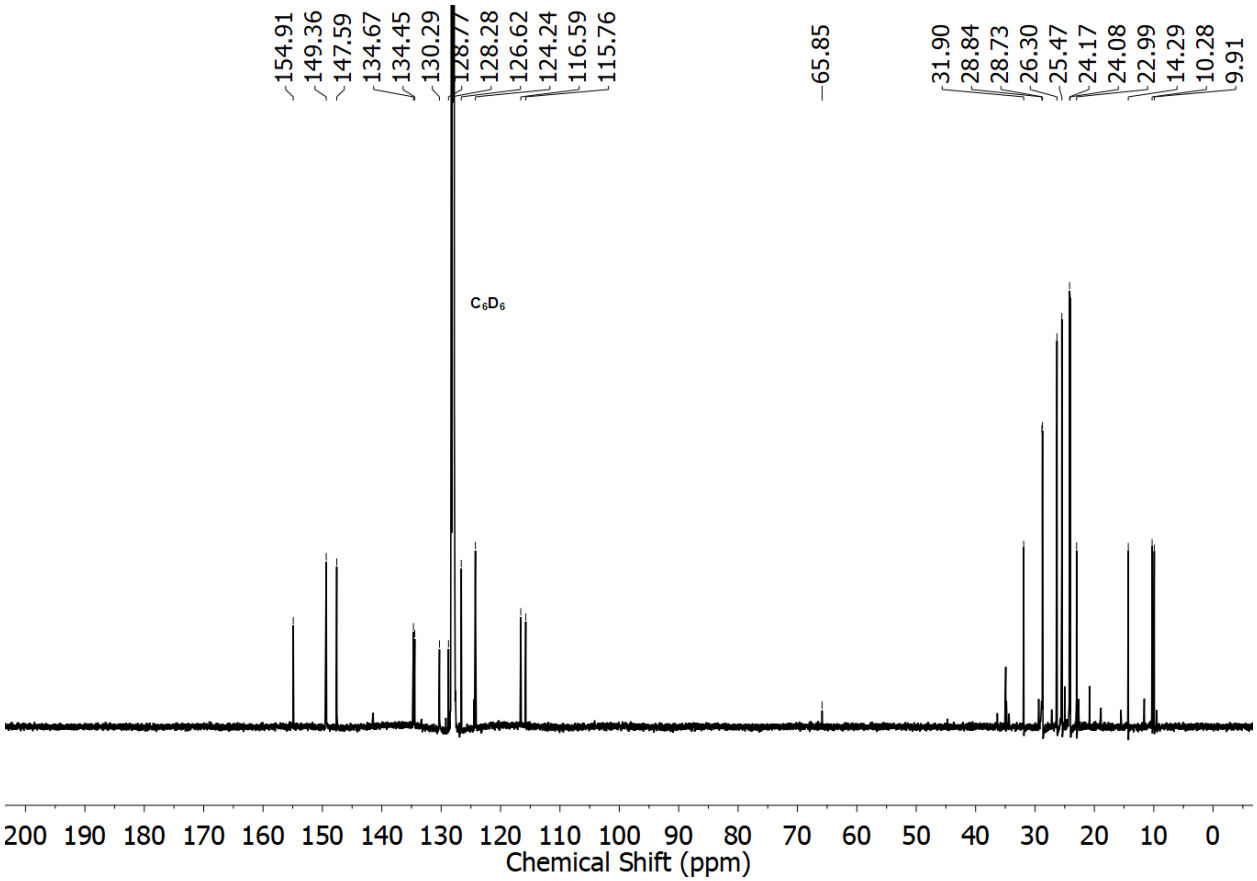

Fig. S2 $^{13}C\{^{1}H\}$ NMR spectrum of $[(^{Me}IPrCH)In]_4$ (**1**) in C_6D_6.

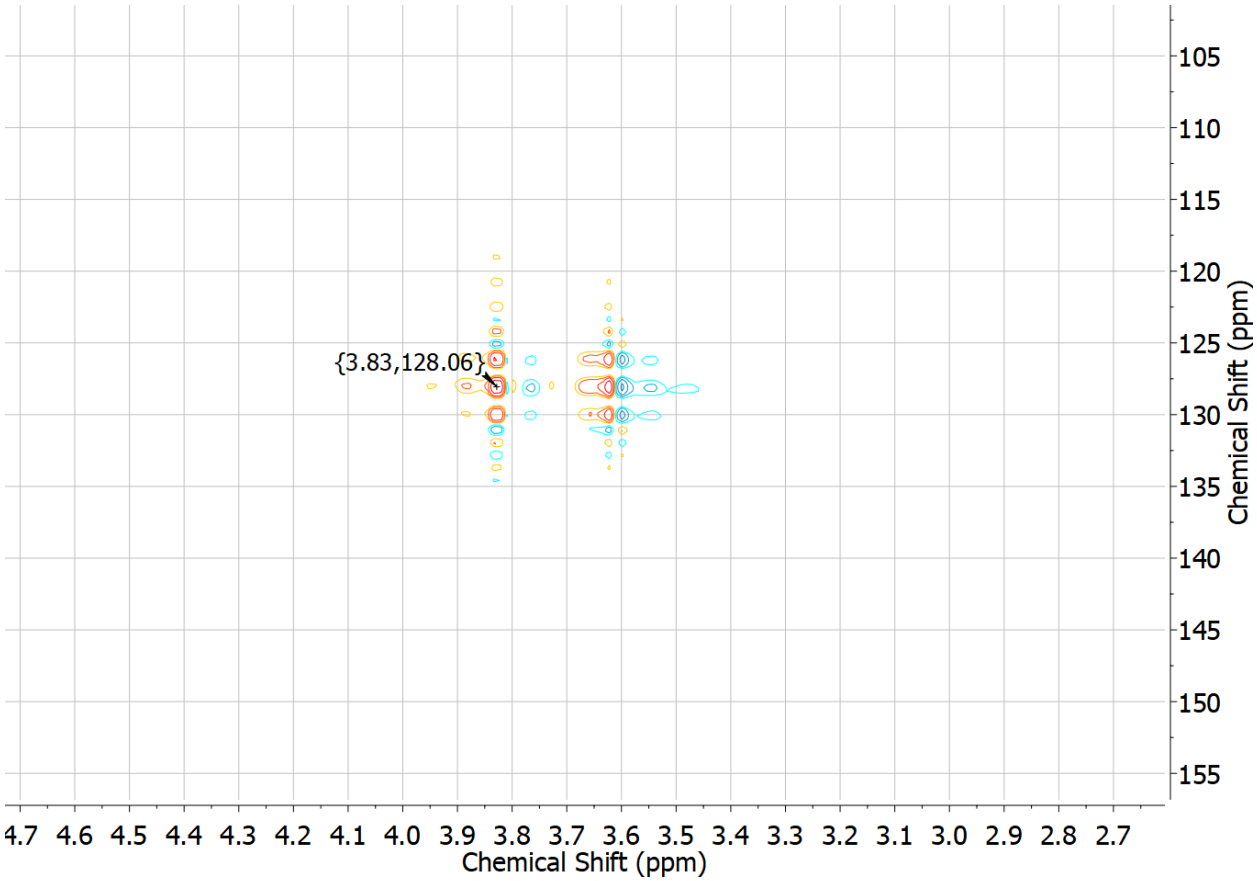

Fig. S3 ^{1}H-^{13}C HSQC NMR spectrum of [(^{Me}IPrCH)In]$_4$ (**1**) in C_6D_6.

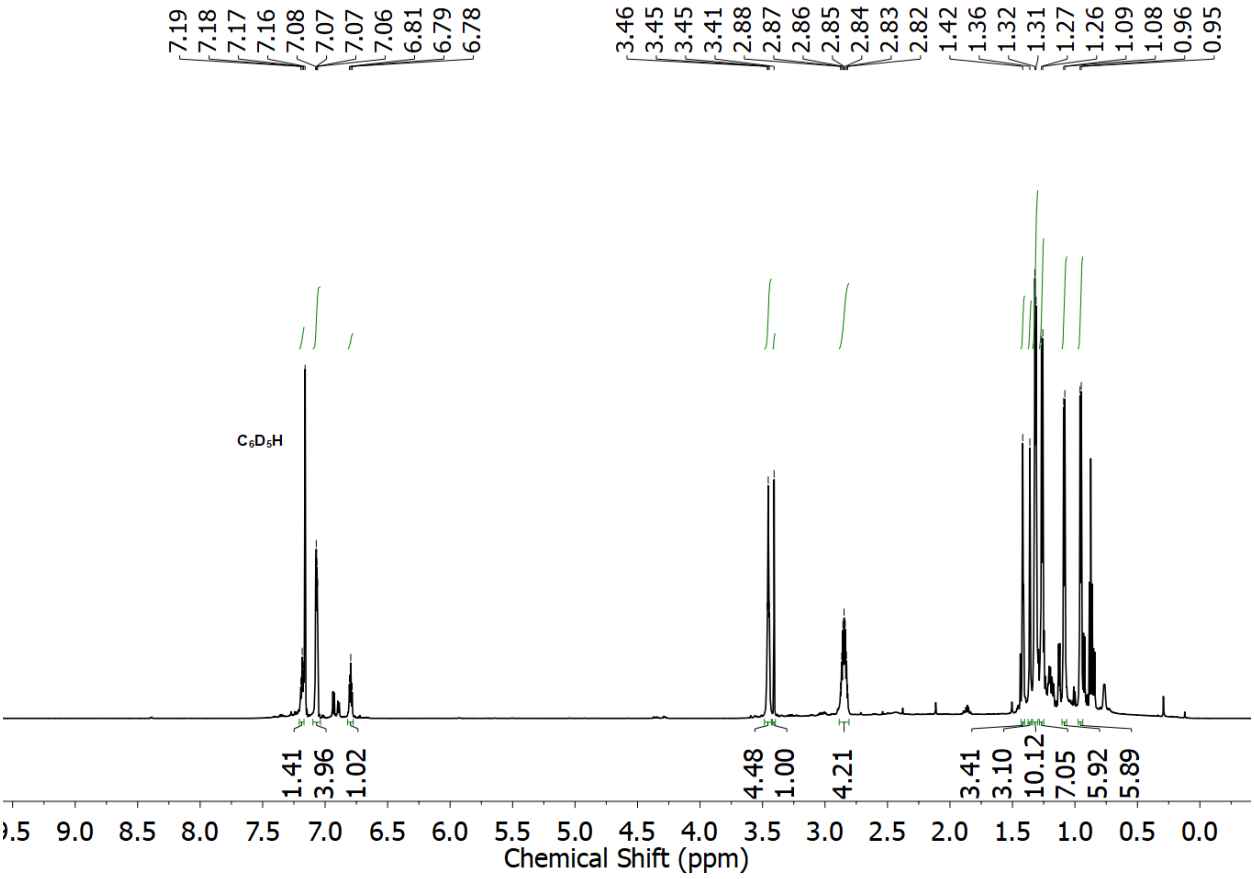

Fig. S4 ^{1}H NMR spectrum of (^{Me}IPrCH)In(THF)•B(C_6F_5)$_3$ (**2**) in C_6D_6.

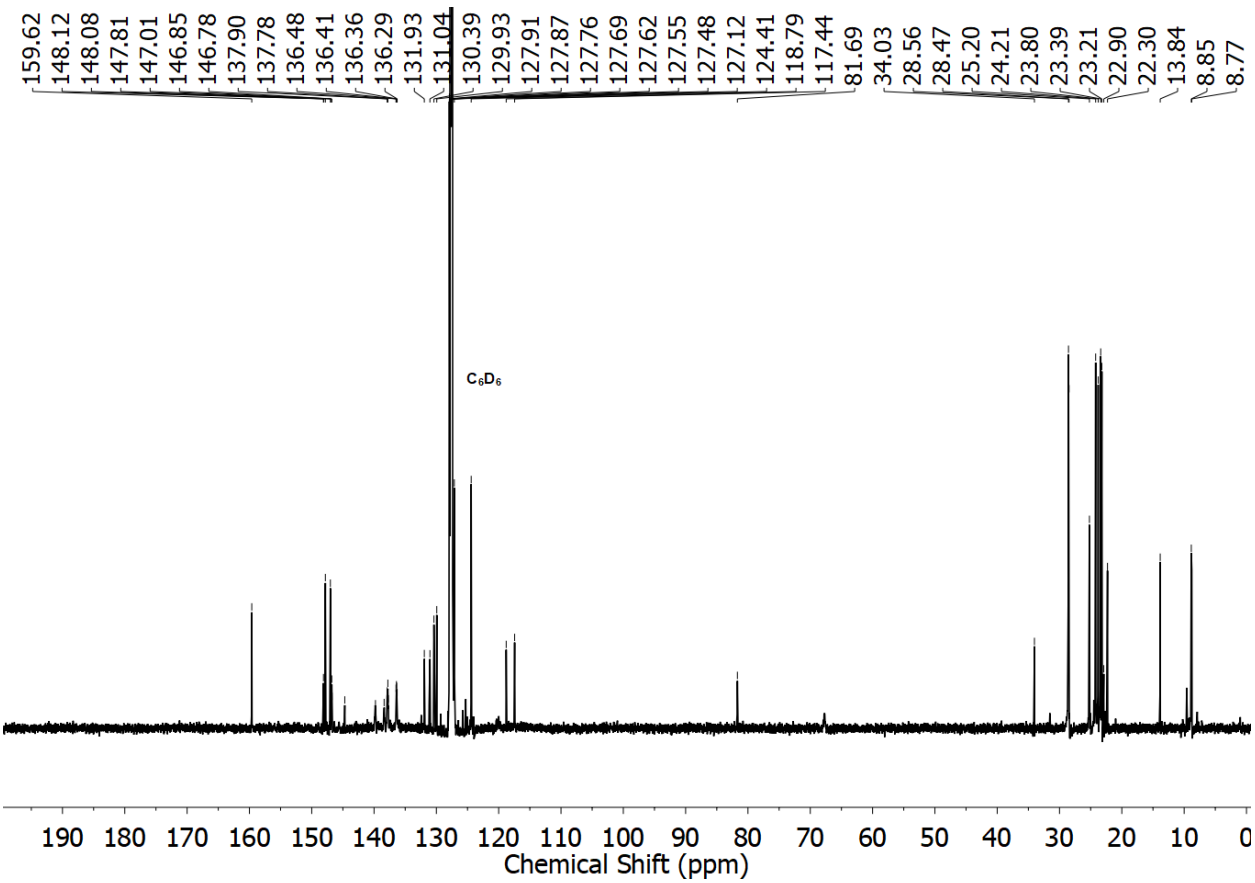

Fig. S5 $^{13}C\{^{1}H\}$ NMR spectrum of (^{Me}IPrCH)In(THF)•B(C_6F_5)$_3$ (**2**) in C_6D_6.

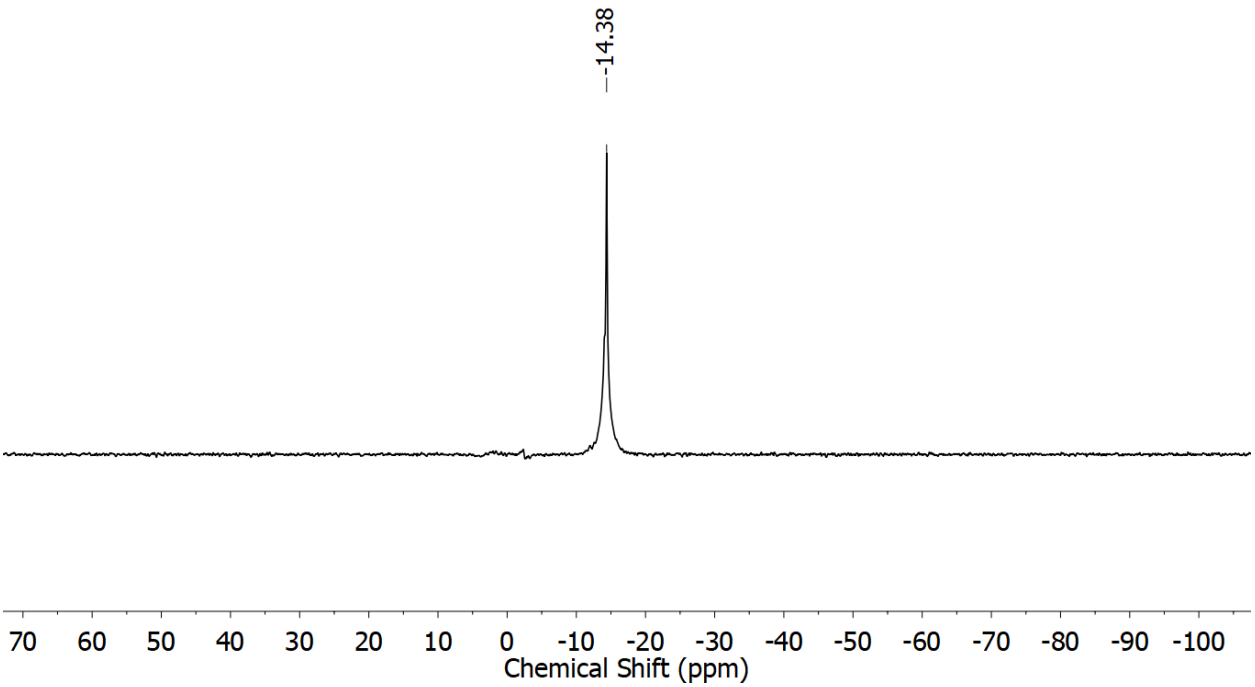

Fig. S6 $^{11}B\{^{1}H\}$ NMR spectrum of (^{Me}IPrCH)In(THF)•B(C_6F_5)$_3$ (**2**) in C_6D_6.

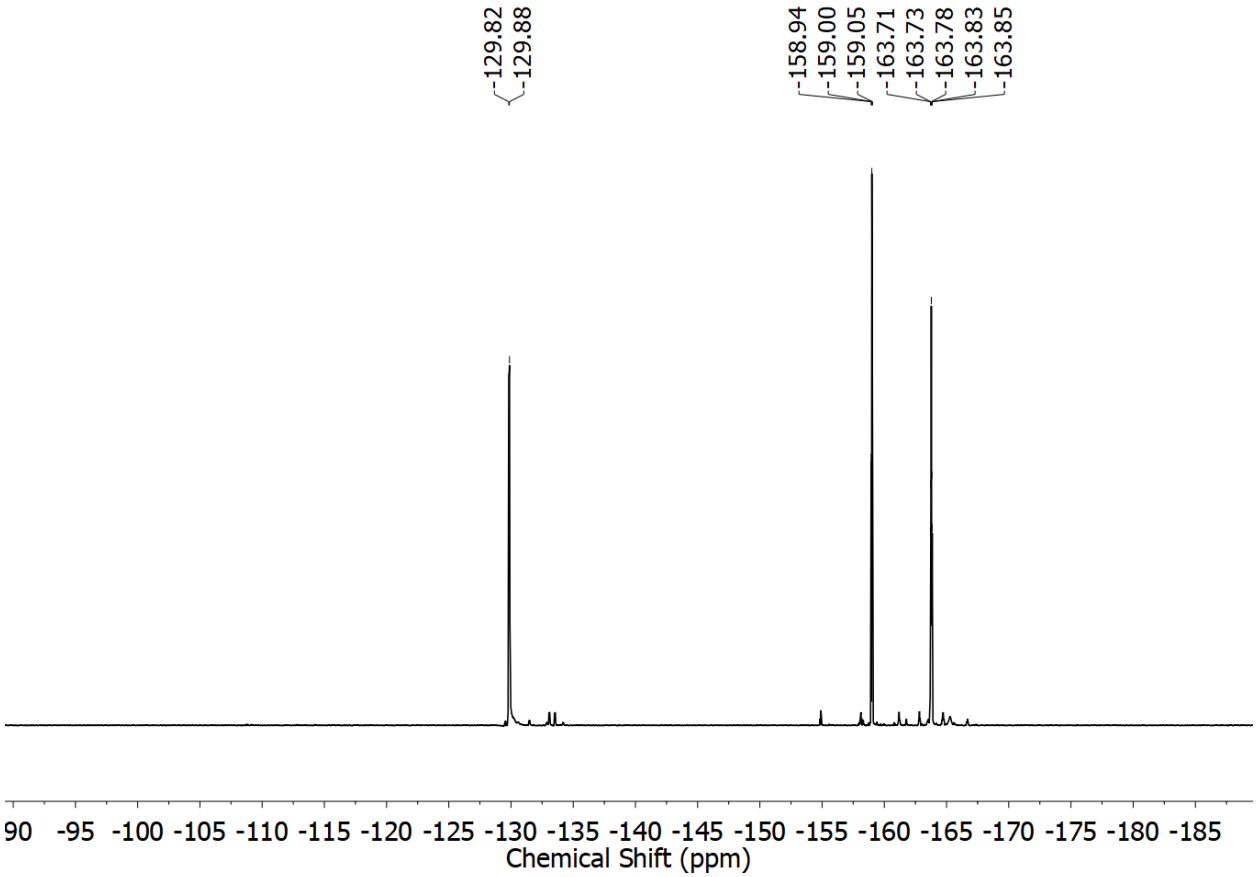

Fig. S7 ^{19}F NMR spectrum of (^{Me}IPrCH)In(THF)•B(C_6F_5)$_3$ (**2**) in C_6D_6.

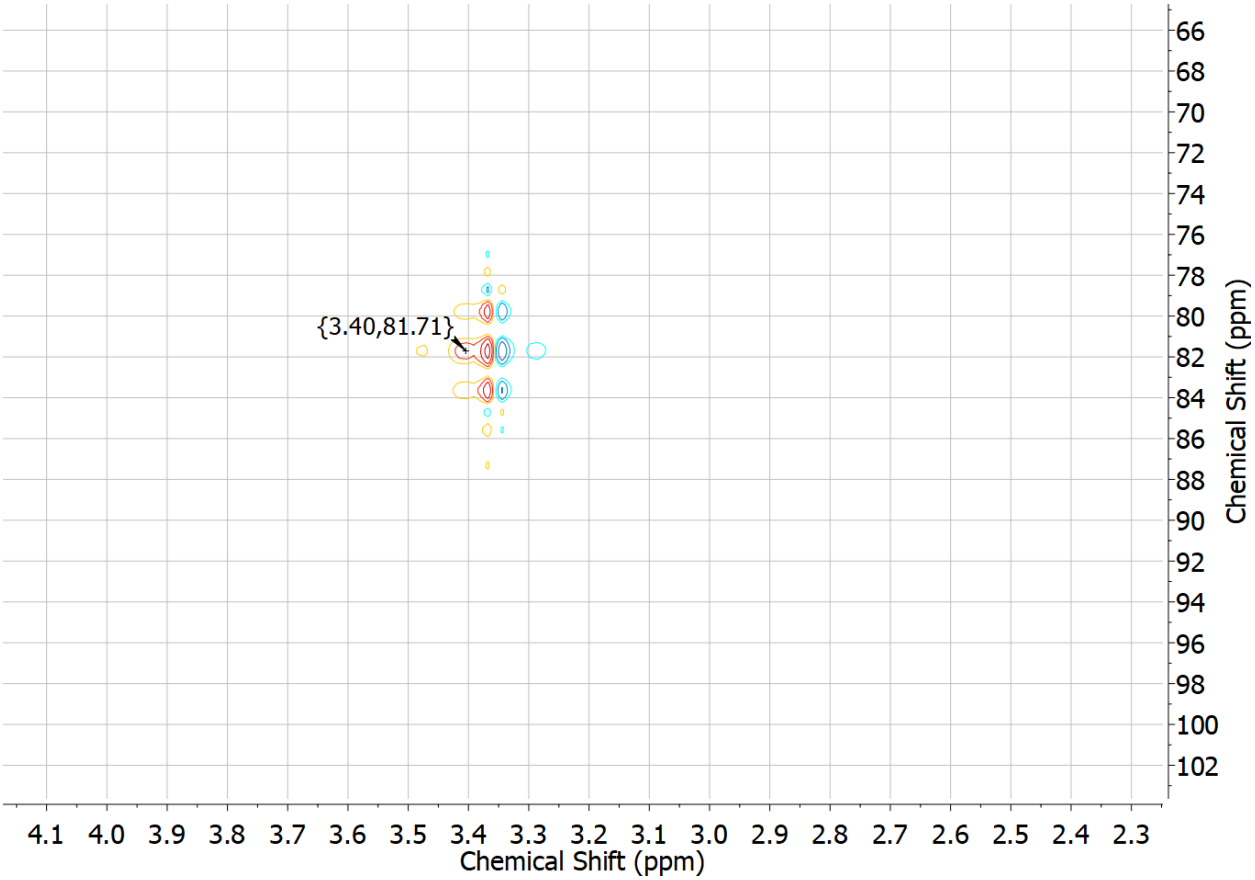

Fig. S8 ^{1}H-^{13}C HSQC spectrum of (^{Me}IPrCH)In(THF)•B(C_6F_5)$_3$ (**2**) in C_6D_6.

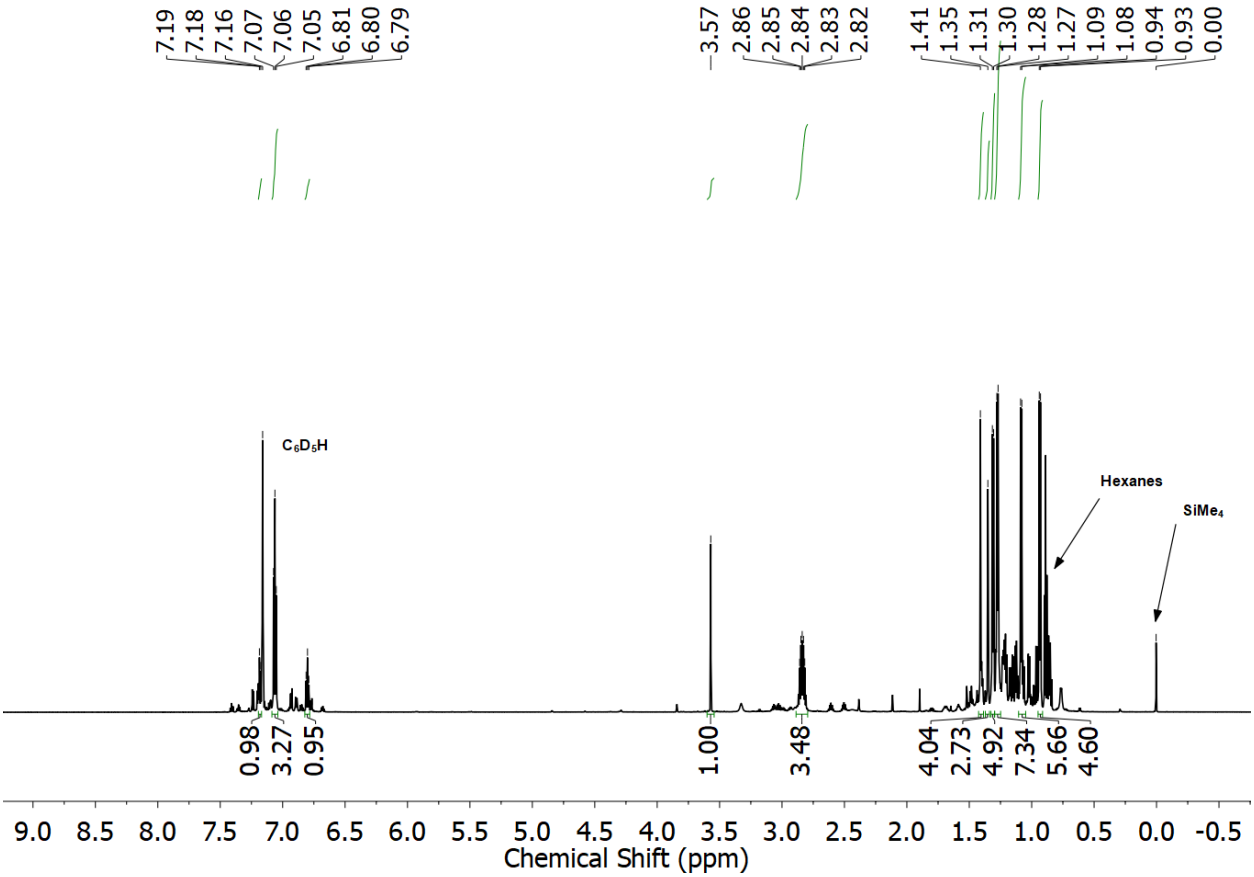

Fig. S9 ^{1}H NMR spectrum of crude (^{Me}IPrCH)In•B(C_6F_5)$_3$ (**2'**) in C_6D_6.

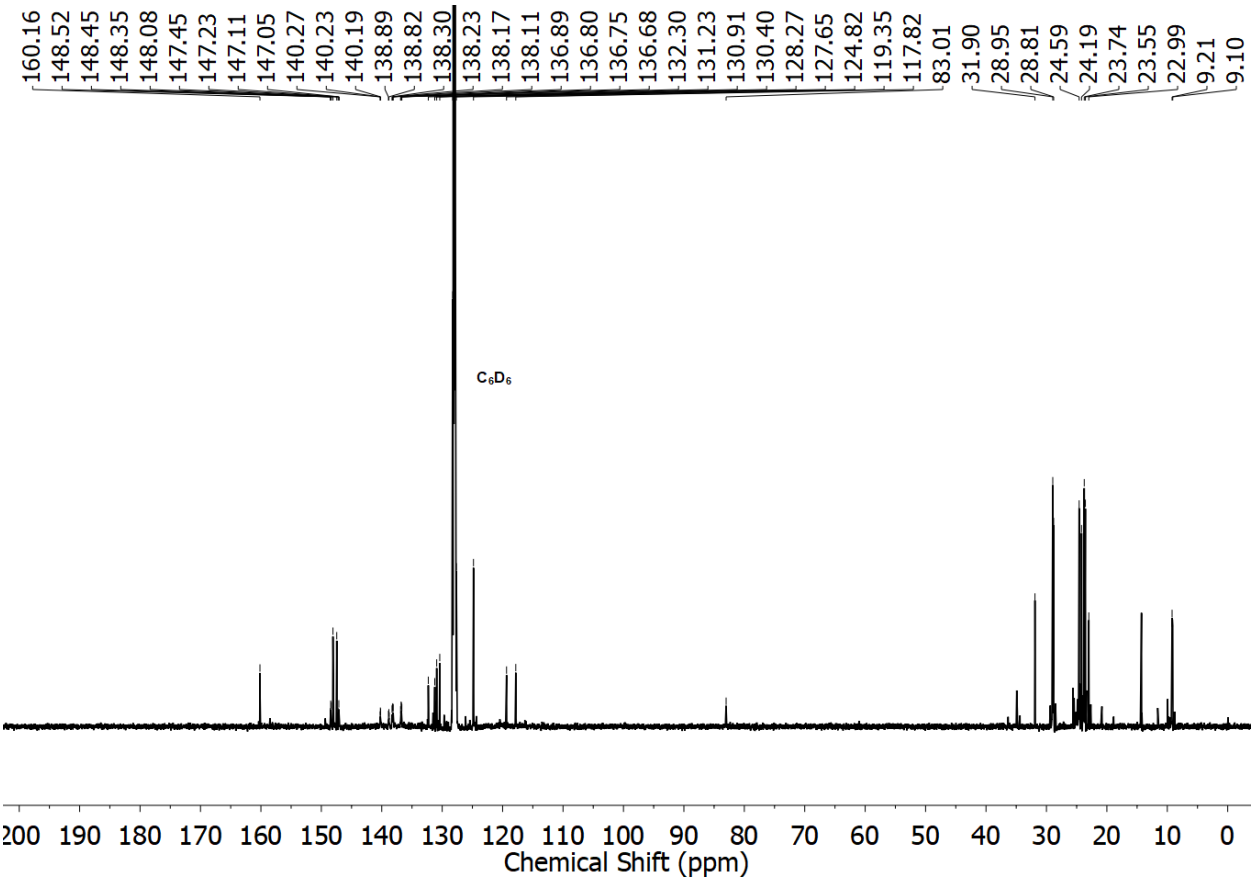

Fig. S10 $^{13}C\{^{1}H\}$ NMR spectrum of crude (^{Me}IPrCH)In•B(C_6F_5)$_3$ (**2'**) in C_6D_6.

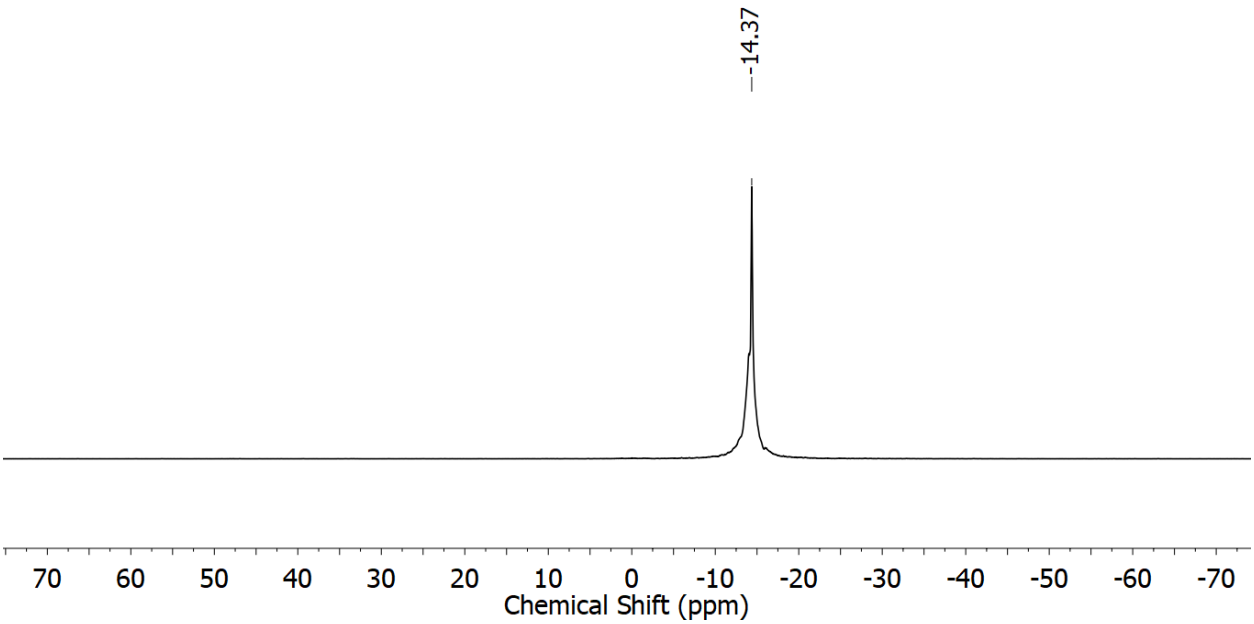

Fig. S11 $^{11}B\{^{1}H\}$ NMR spectrum of crude (^{Me}IPrCH)In•B(C_6F_5)$_3$ (**2'**) in C_6D_6.

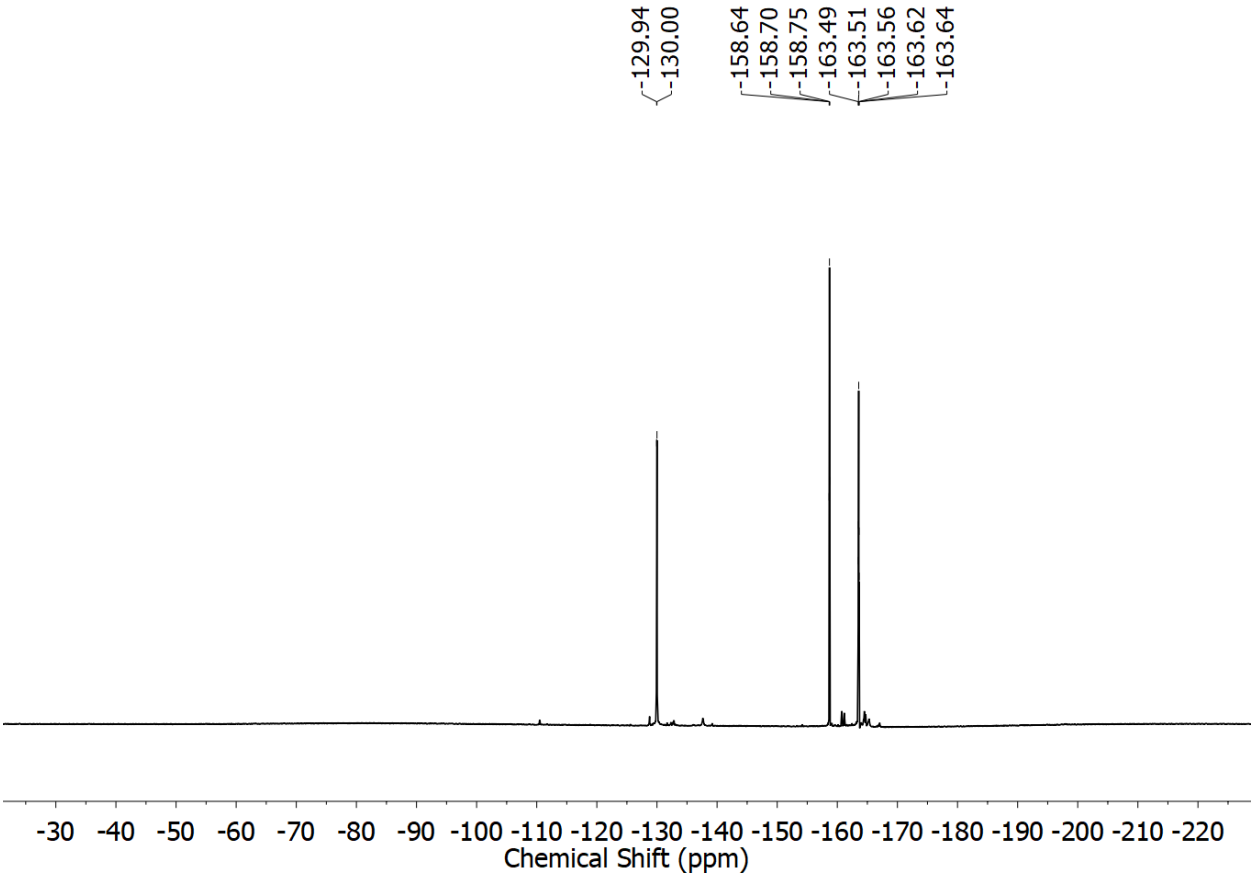

Fig. S12 ^{19}F NMR spectrum of crude (^{Me}IPrCH)In•B(C_6F_5)$_3$ (**2'**) in C_6D_6.

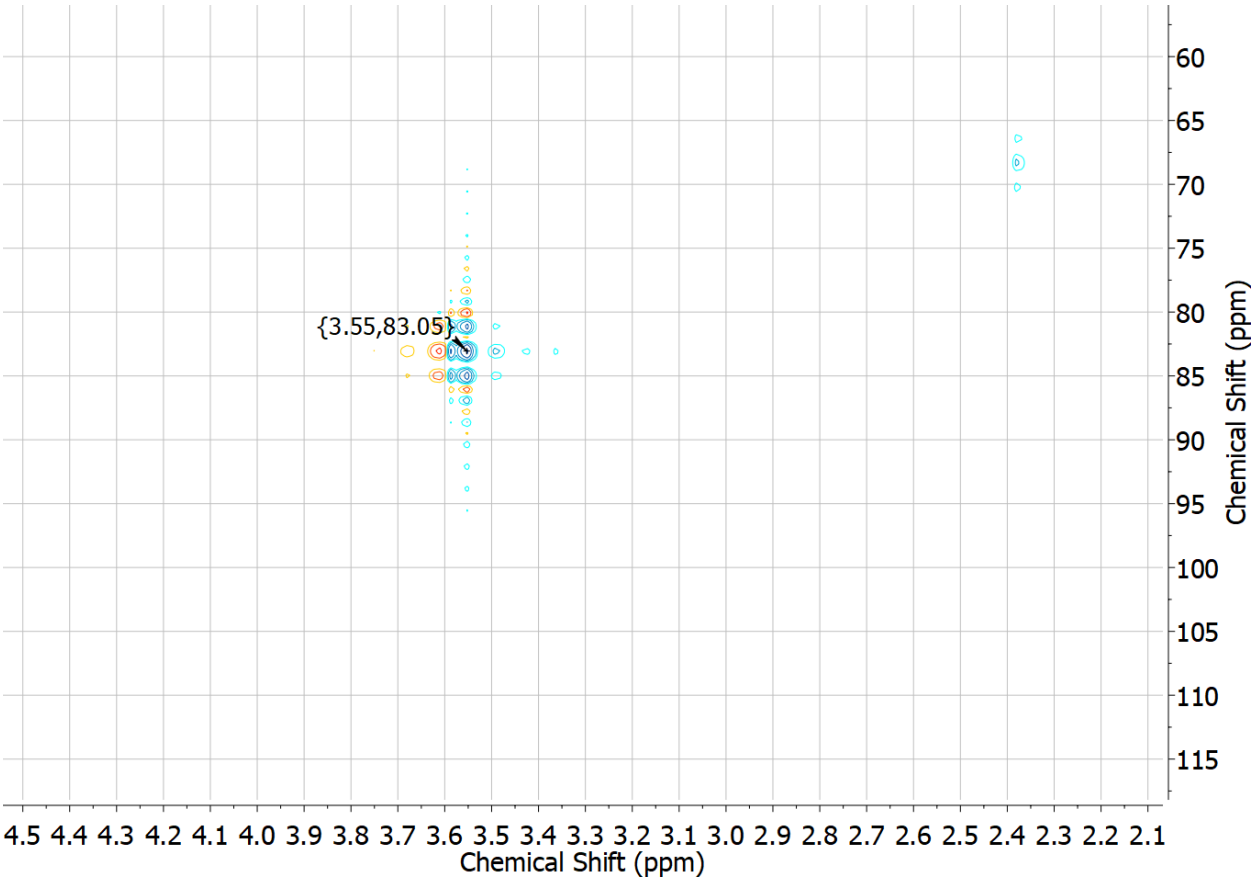

Fig. S13 ^{1}H-^{13}C HSQC spectrum of crude (^{Me}IPrCH)In•B(C_6F_5)$_3$ (**2'**) in C_6D_6.

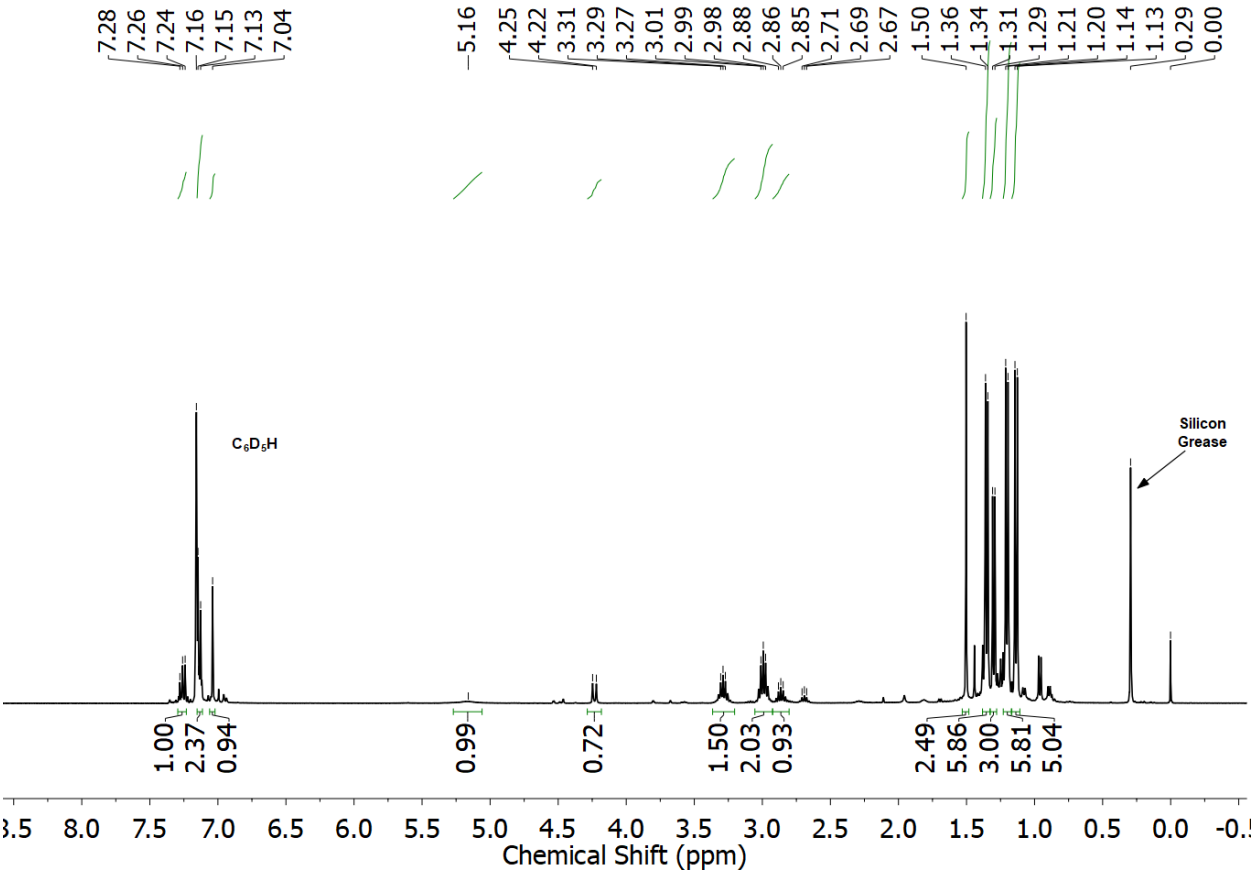

Fig. S14 ^{1}H NMR spectrum of (^{Me}IPrCH)B(H)Trip in C_6D_6 prepared by the addition of H_2BTrip to [(^{Me}IPrCH)In]$_4$ (**1**) in toluene.

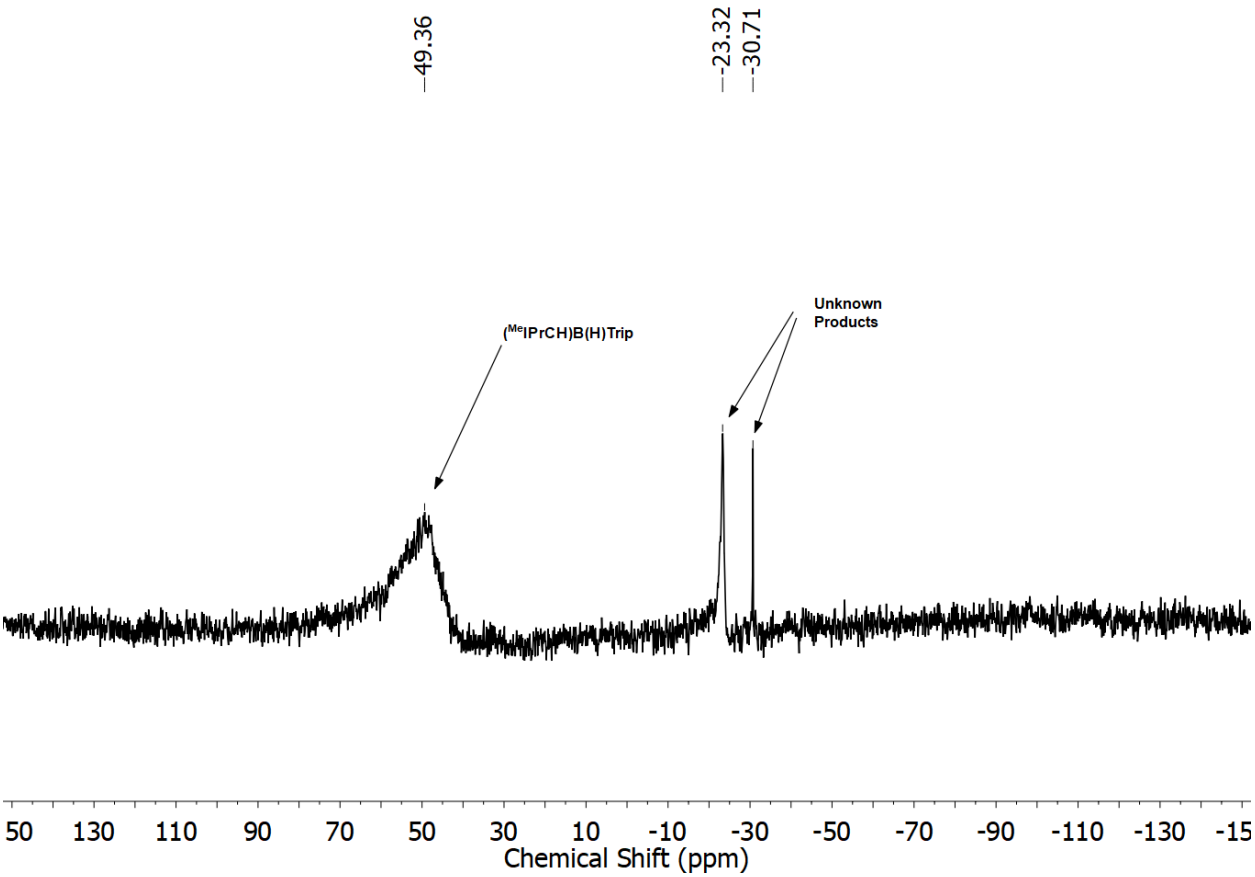

Fig. S15 $^{11}B\{^{1}H\}$ NMR spectrum of (^{Me}IPrCH)B(H)Trip in C_6D_6 prepared by the addition of H_2BTrip to [(^{Me}IPrCH)In]$_4$ (**1**) in toluene.

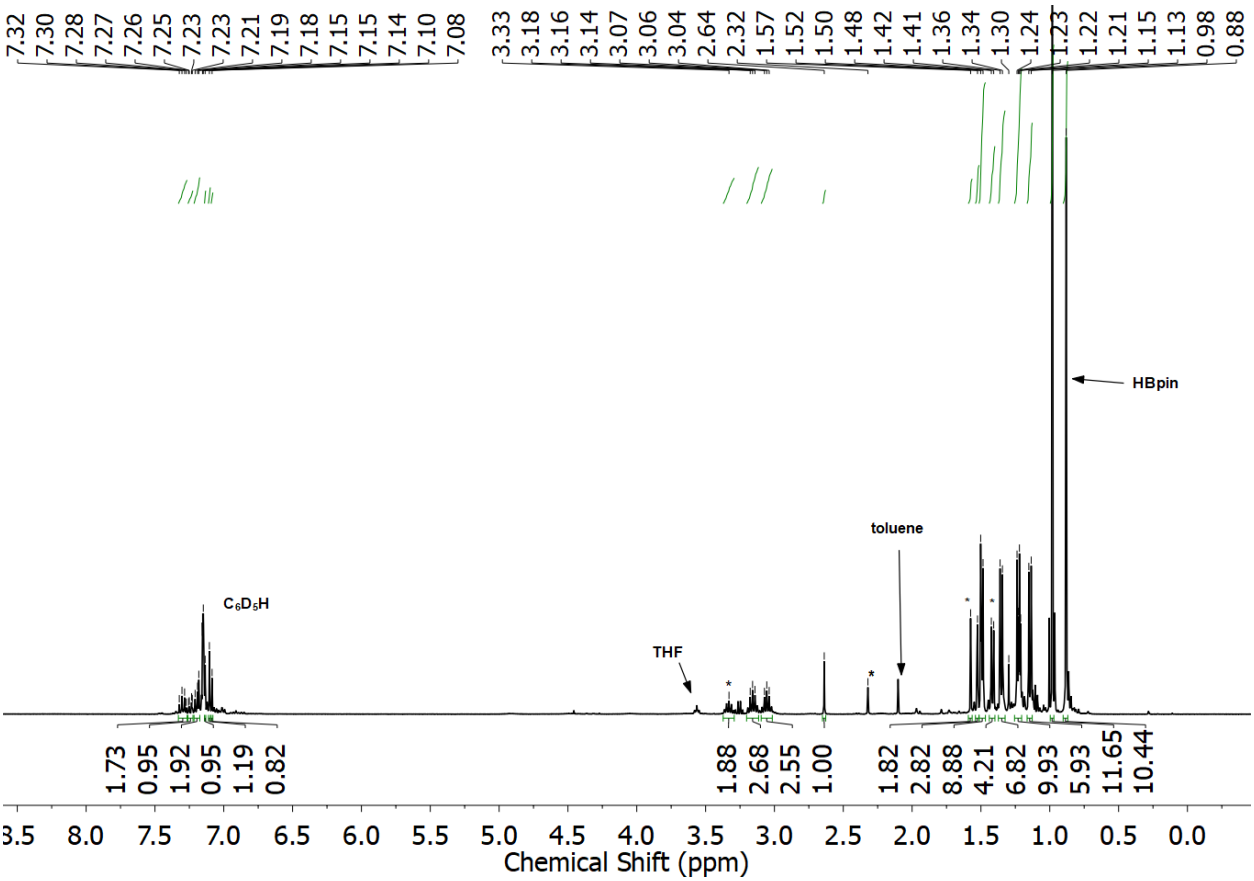

Fig. S16 ^{1}H NMR spectrum of (^{Me}IPrCH)Bpin (**3**) in C_6D_6 prepared by the addition of HBpin to [(^{Me}IPrCH)In]$_4$ (**1**) in toluene (Route B). Signals belonging to ^{Me}IPrCH$_2$ are marked by an asterisk.

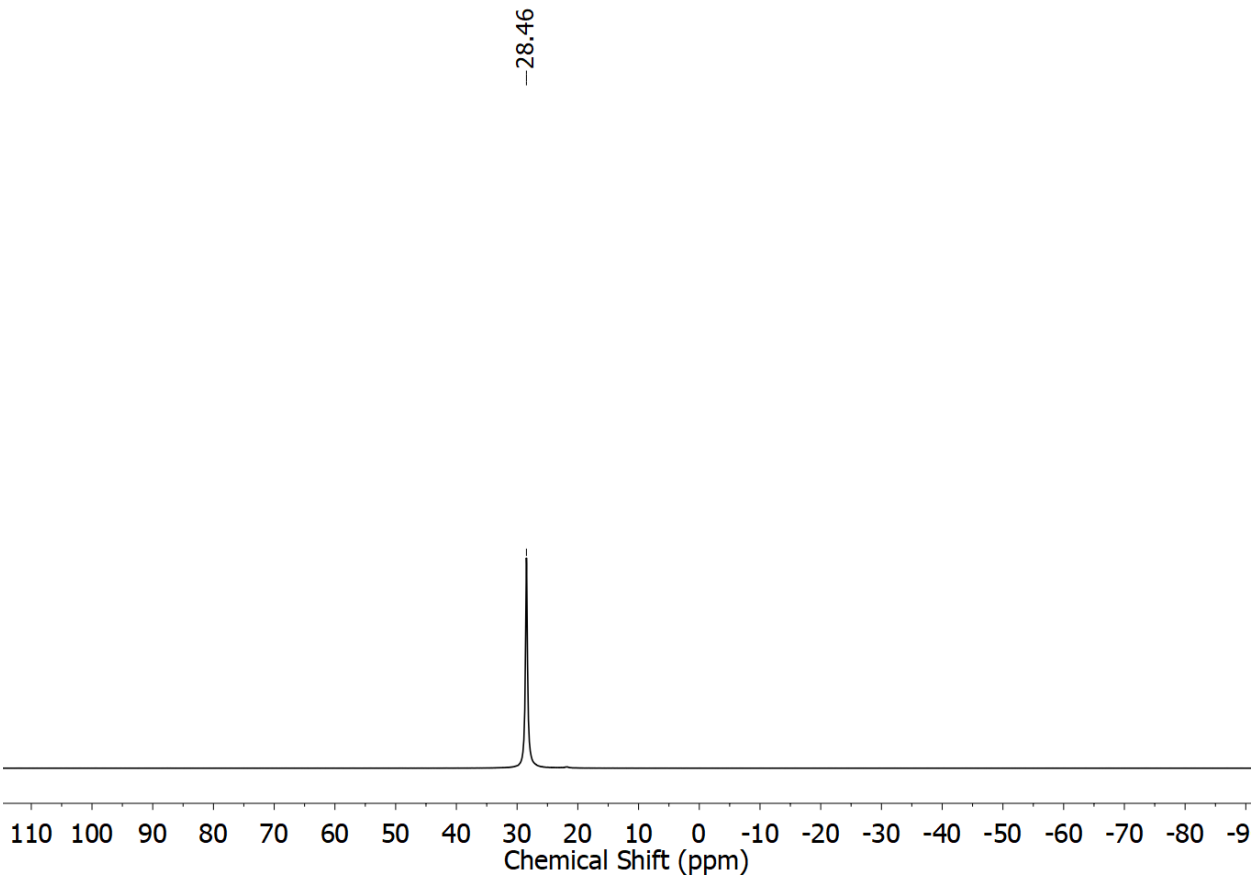

Fig. S17 $^{11}B\{^{1}H\}$ NMR spectrum of (^{Me}IPrCH)Bpin (**3**) in C_6D_6 prepared by the addition of HBpin to [(^{Me}IPrCH)In]$_4$ (**1**) in toluene (Route B).

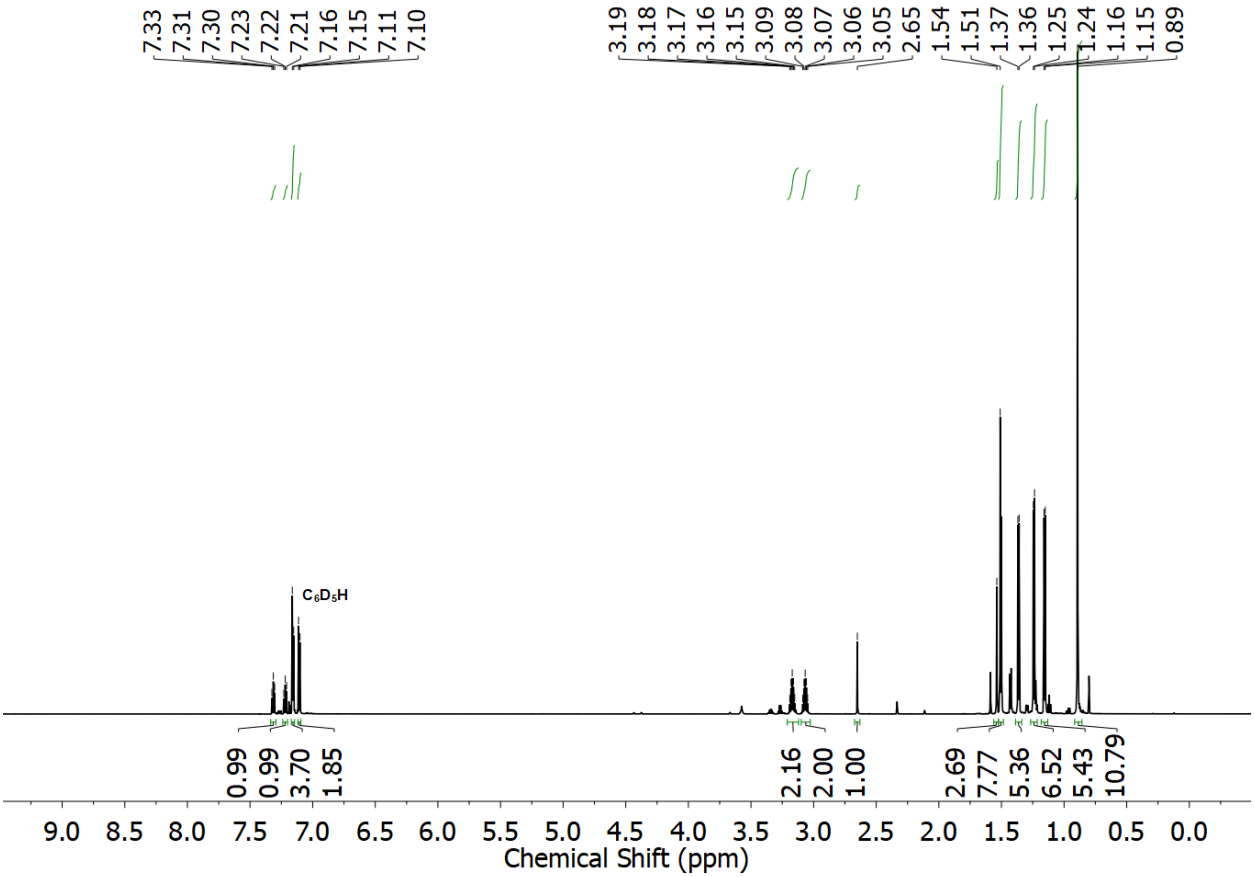

Fig. S18 ^{1}H NMR spectrum of (^{Me}IPrCH)Bpin (**3**) in C_6D_6 (prepared by Route A).

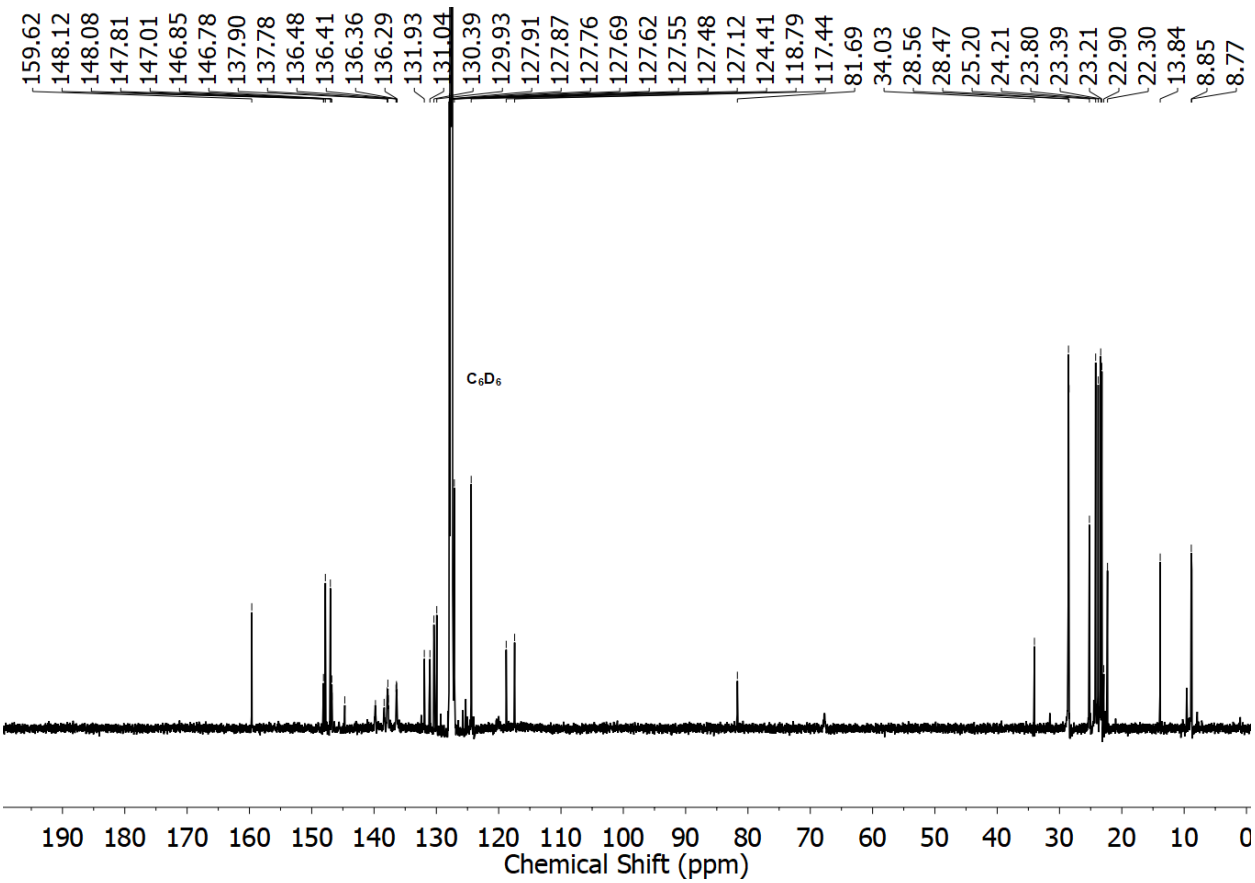

Fig. S19 $^{13}C\{^{1}H\}$ NMR spectrum of (^{Me}IPrCH)Bpin (**3**) in C_6D_6 (prepared by Route A).

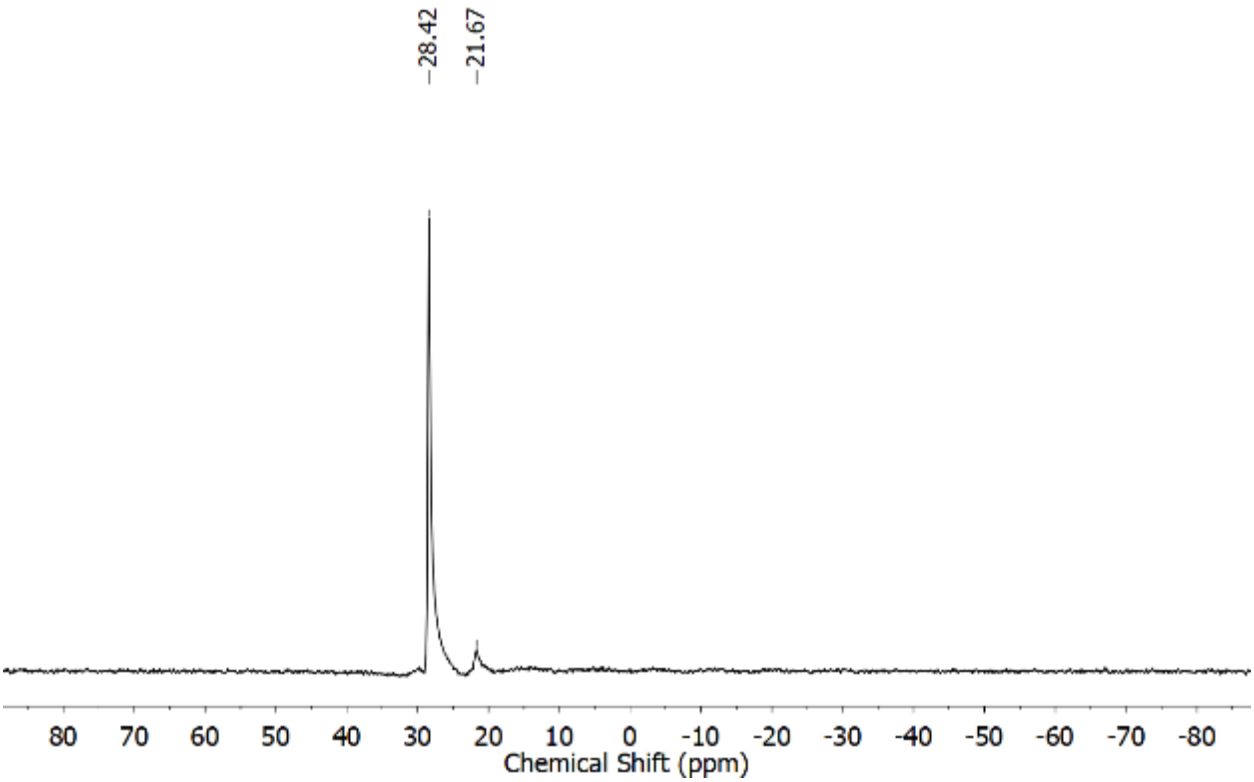

Fig. S20 $^{11}B\{^{1}H\}$ NMR spectrum of (^{Me}IPrCH)Bpin (**3**) in C_6D_6 (prepared by Route A). The peak at 21.7 is residual ^{i}PrOBpin that remains, despite recrystallization.

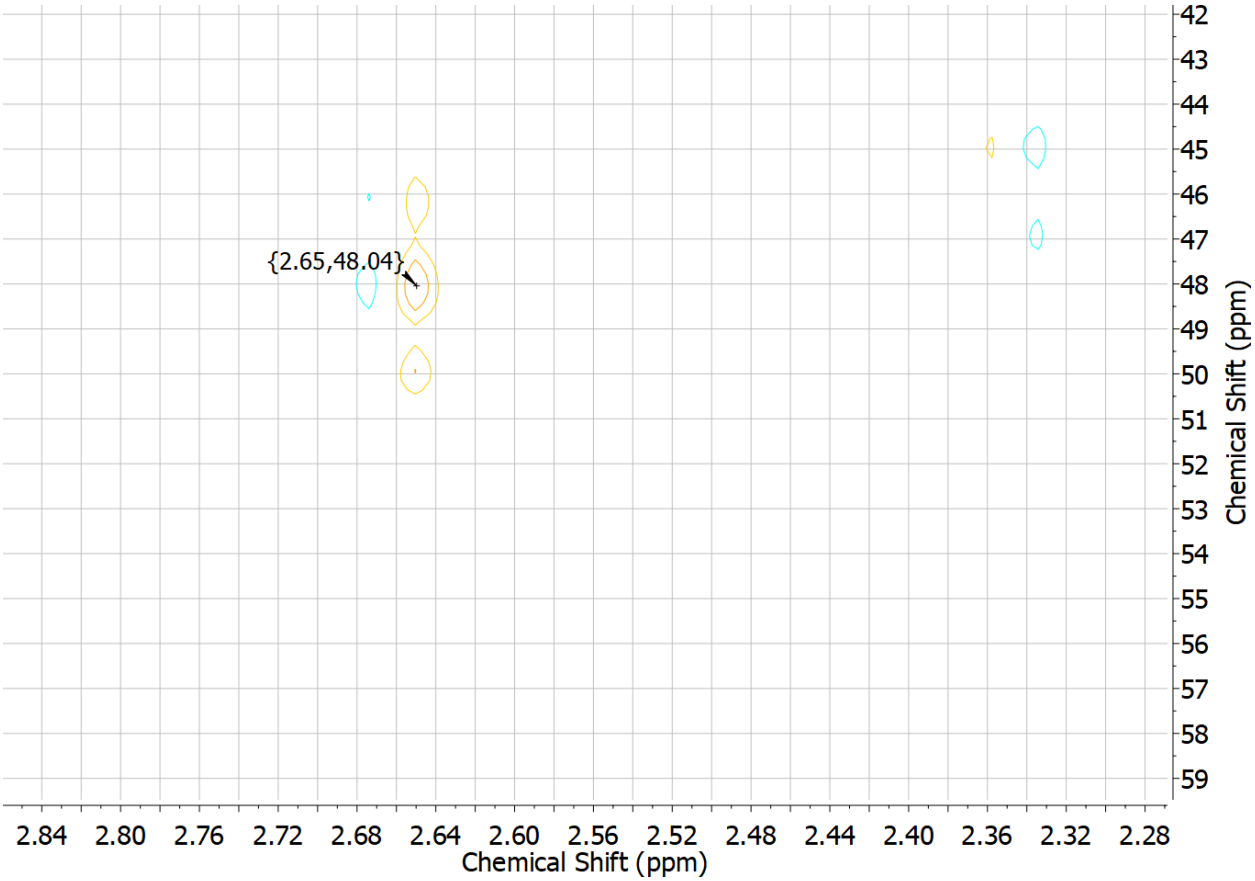

Fig. S21 ^{1}H-^{13}C HSQC spectrum of (^{Me}IPrCH)Bpin (**3**) in C_6D_6 (prepared by Route A).

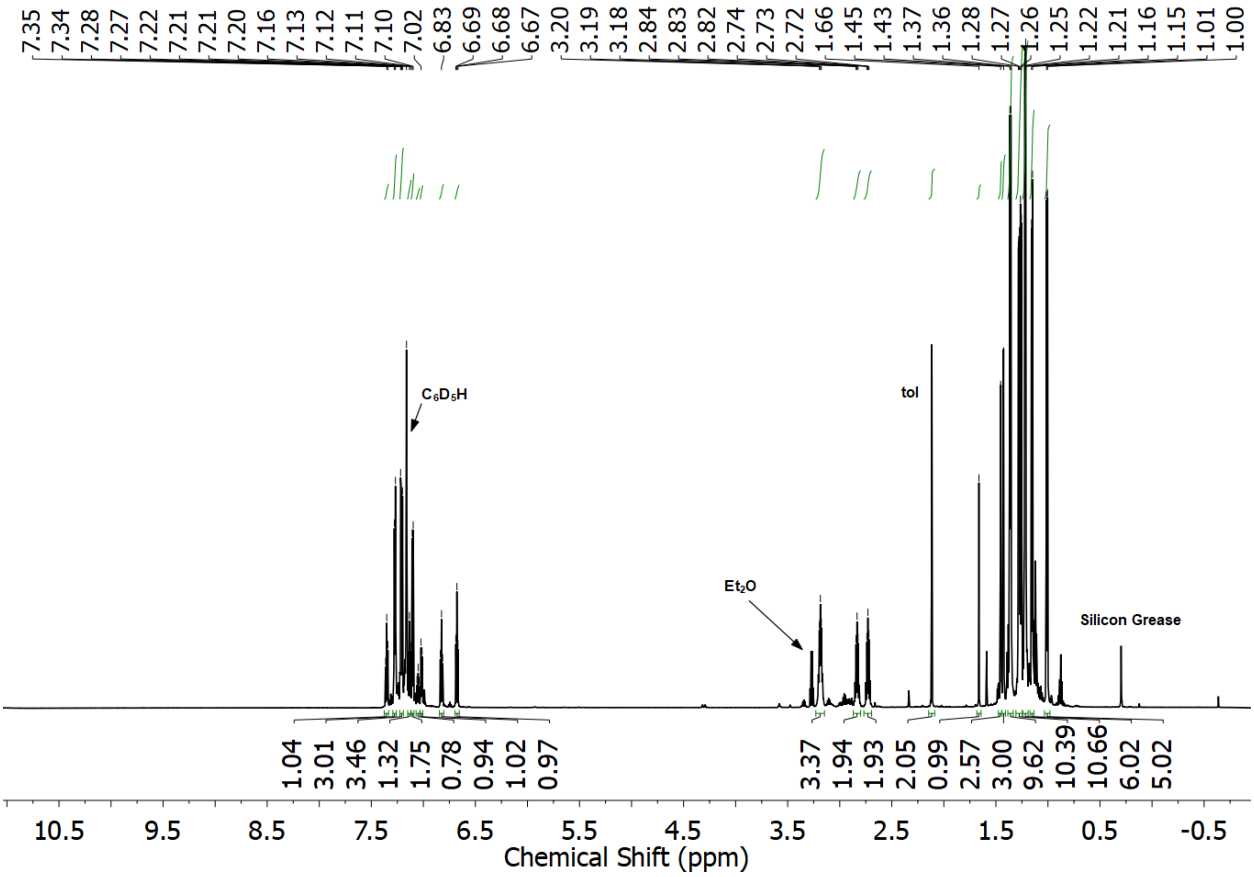

Fig. S22 ^{1}H NMR spectrum of (^{Me}IPrCH)InNAr^{Dipp} (**4**) in C_6D_6.

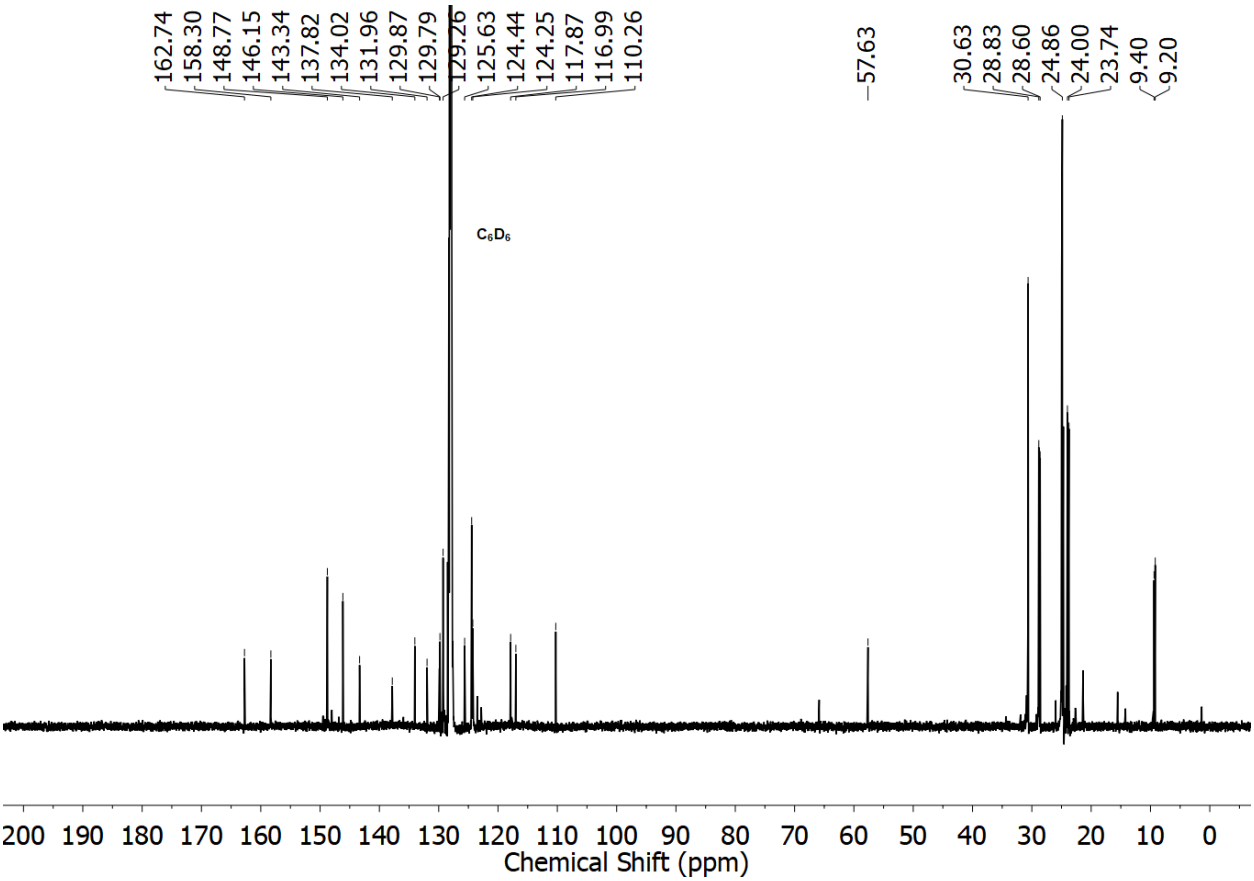

Fig. S23 $^{13}C\{^{1}H\}$ NMR spectrum of (^{Me}IPrCH)InNAr^{Dipp} (**4**) in C_6D_6.

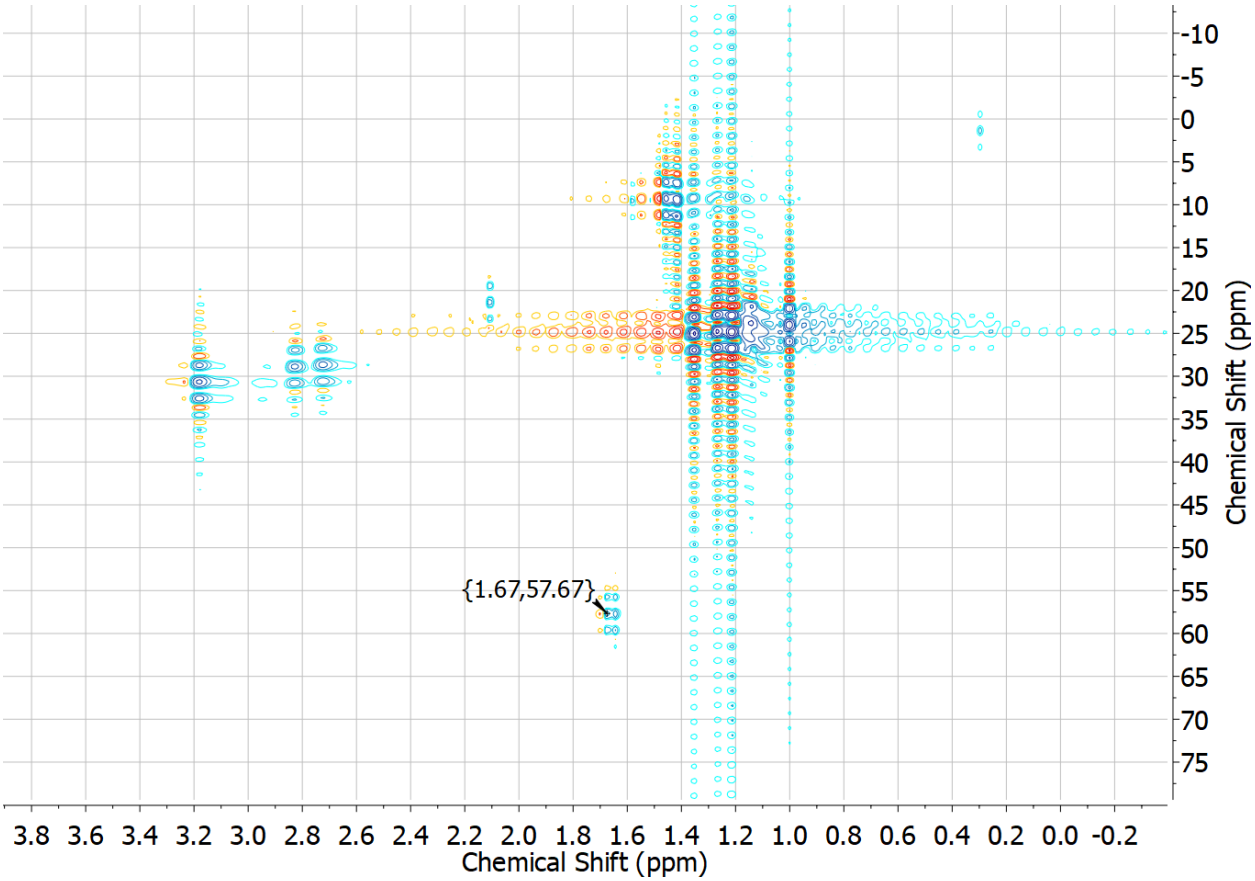

Fig. S24 ^{1}H-^{13}C HSQC spectrum of (^{Me}IPrCH)InNAr^{Dipp} (**4**) in C_6D_6.

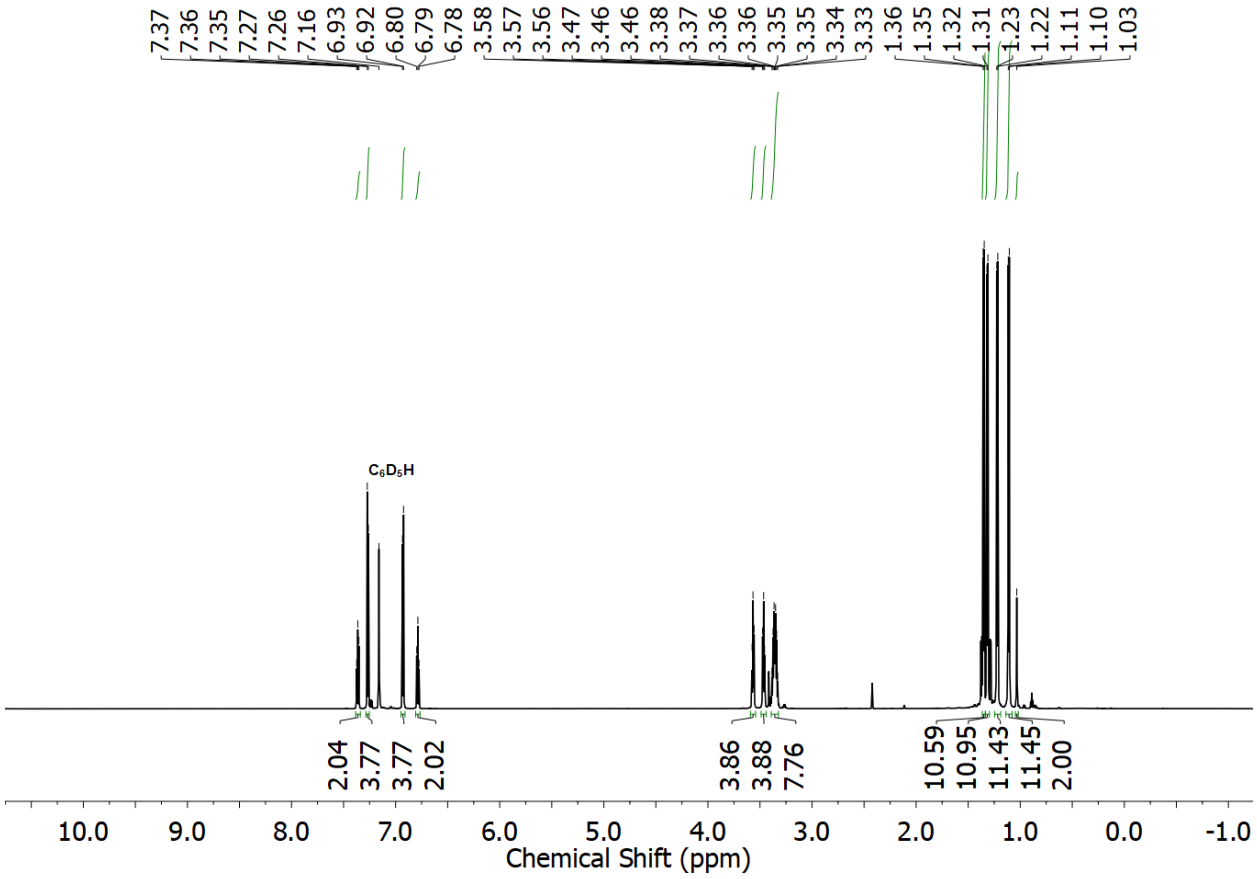

Fig. S25 ^{1}H NMR spectrum of [(SIPrCH)Li]$_2$ (**5**) in C_6D_6.

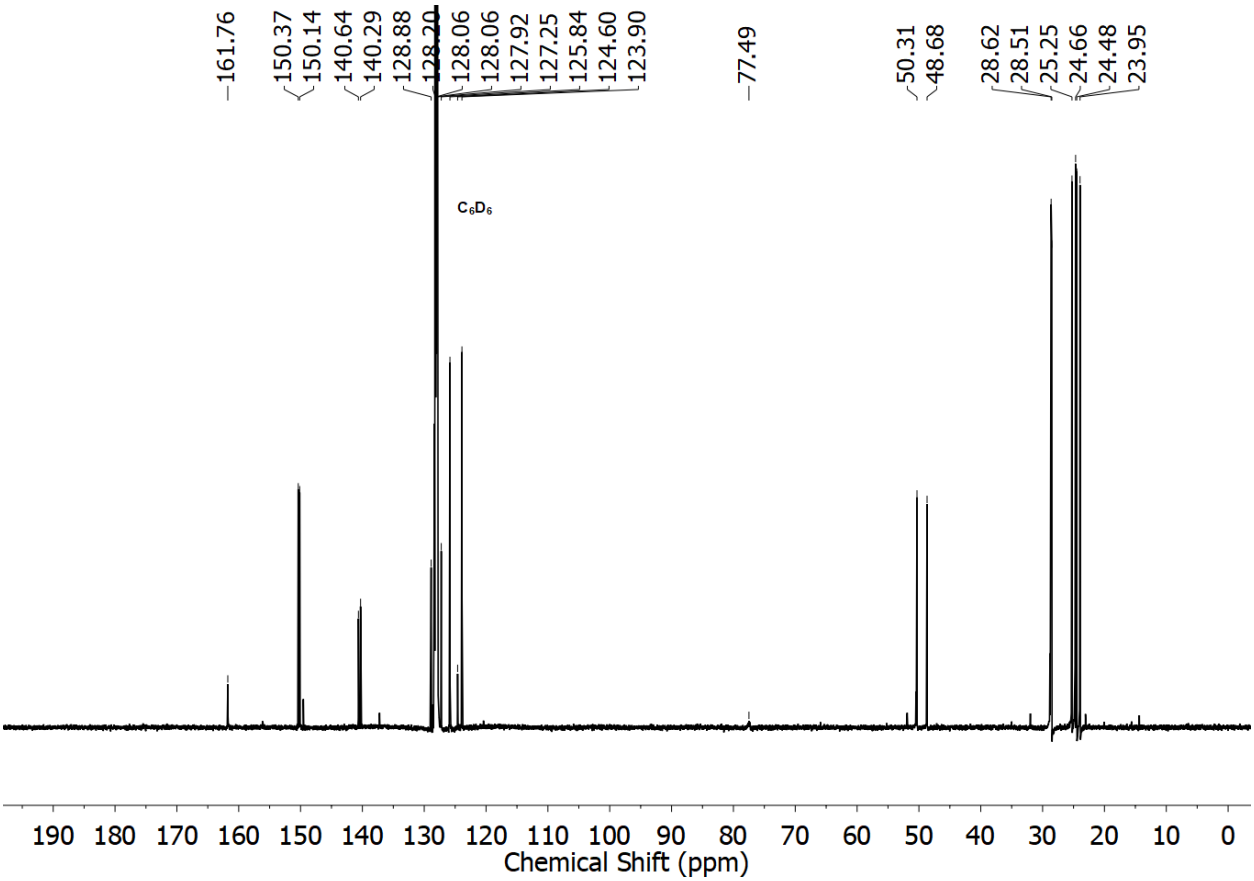

Fig. S26 $^{13}C\{^{1}H\}$ NMR spectrum of $[(SIPrCH)Li]_2$ (**5**) in C_6D_6.

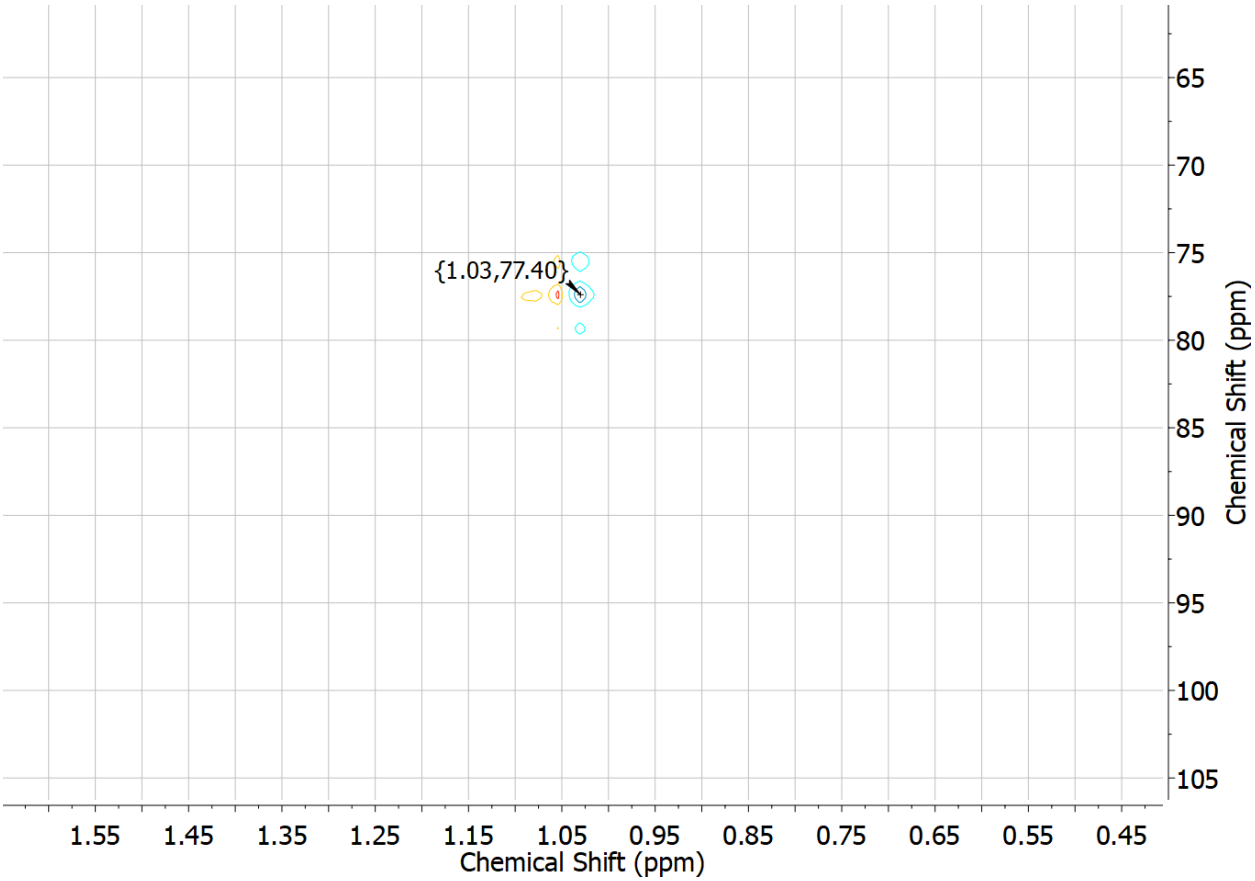

Fig. S27 ^{1}H–^{13}C HSQC NMR spectrum of $[(SIPrCH)Li]_2$ (**5**) in C_6D_6.

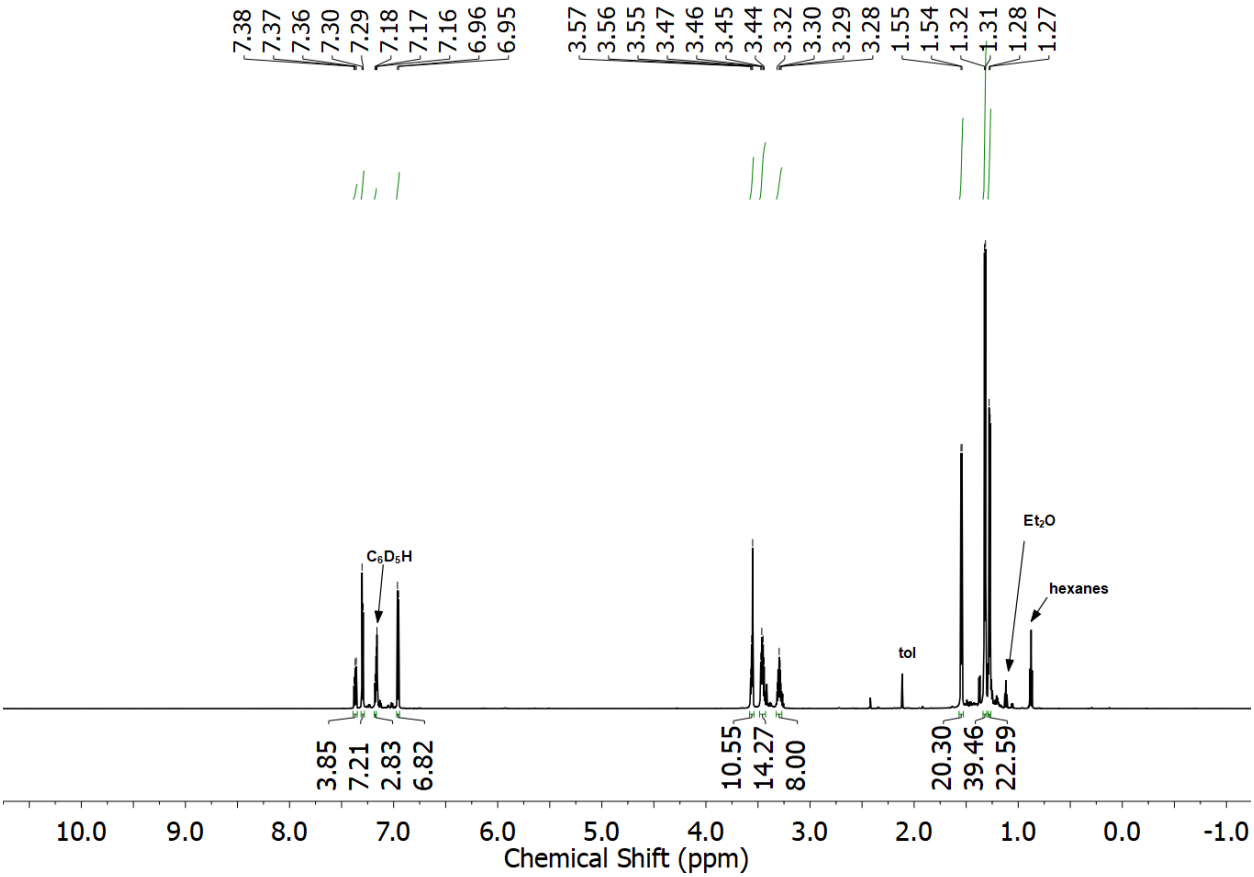

Fig. S28 ^{1}H NMR spectrum of [(SIPrCH)In]$_4$ (**6**) in C_6D_6.

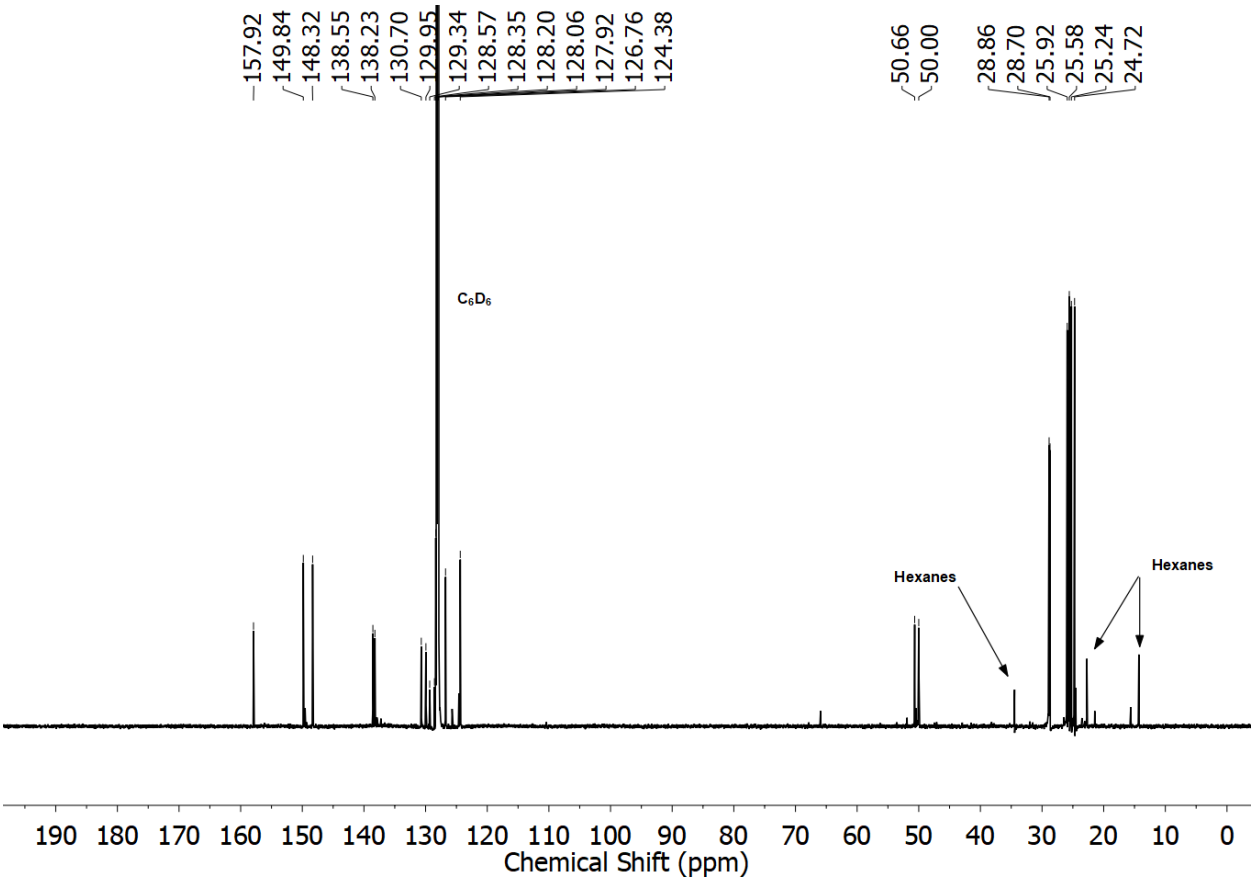

Fig. S29 $^{13}C\{^{1}H\}$ NMR spectrum of $[(SIPrCH)In]_4$ (**6**) in C_6D_6.

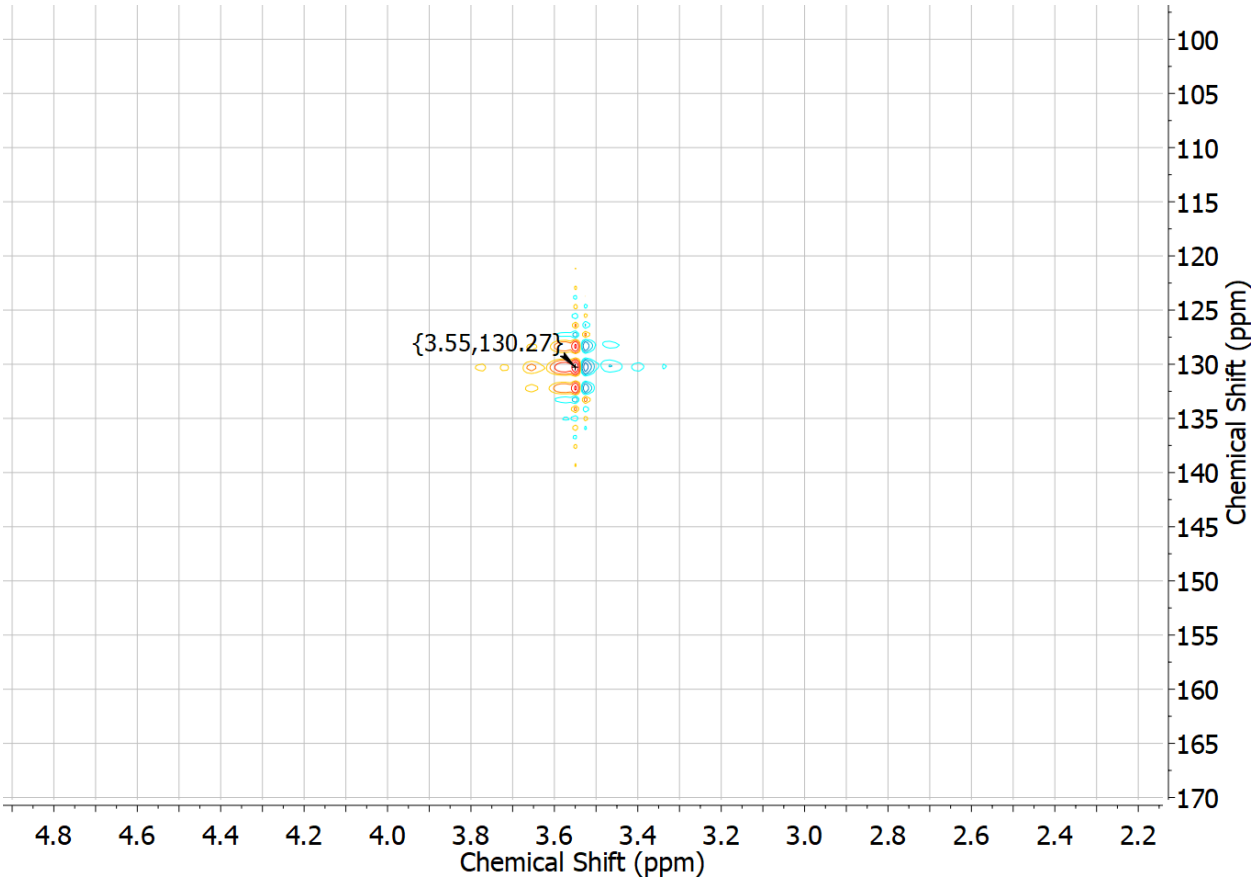

Fig. S30 $^{1}H–^{13}C$ HSQC NMR spectrum of $[(SIPrCH)In]_4$ (**6**) in C_6D_6.

Diffusion-Ordered Spectroscopy (DOSY) Experiments

Diffusion-ordered spectroscopy (DOSY) experiments were performed on a Varian 600 MHz instrument equipped with a Z-gradient HCN indirect detection probe capable of outputting 72 G/cm of gradient strength. All measurements were carried out non-spinning samples and at a calibrated temperature of 27 °C using the Oneshot45 pulse sequence.[S10,S11] For all DOSY experiments a spectral window of 7.2 kHz was used with a 3 s acquisition time and a 3 s relaxation delay with 8 scans for each gradient increment. Pulse widths and gradient strengths were optimized for each sample. A diffusion delay of 50 ms and a diffusion gradient length of 2 ms was used. Gradient strengths of 2 to 59.5 G/cm incremented in 20 steps were used. The spectra were Fourier transformed and baseline corrected prior to discrete processing, fitting the data to a double exponential fit and applying corrections for non-uniform pulse field gradients.[S12] The diffusion dimension was zero filled to 1024 data points and the directly detected dimension was zero filled to 256 K data points. DOSY experiments performed in tetrahydrofuran (THF) contained 20 % C_6D_6.

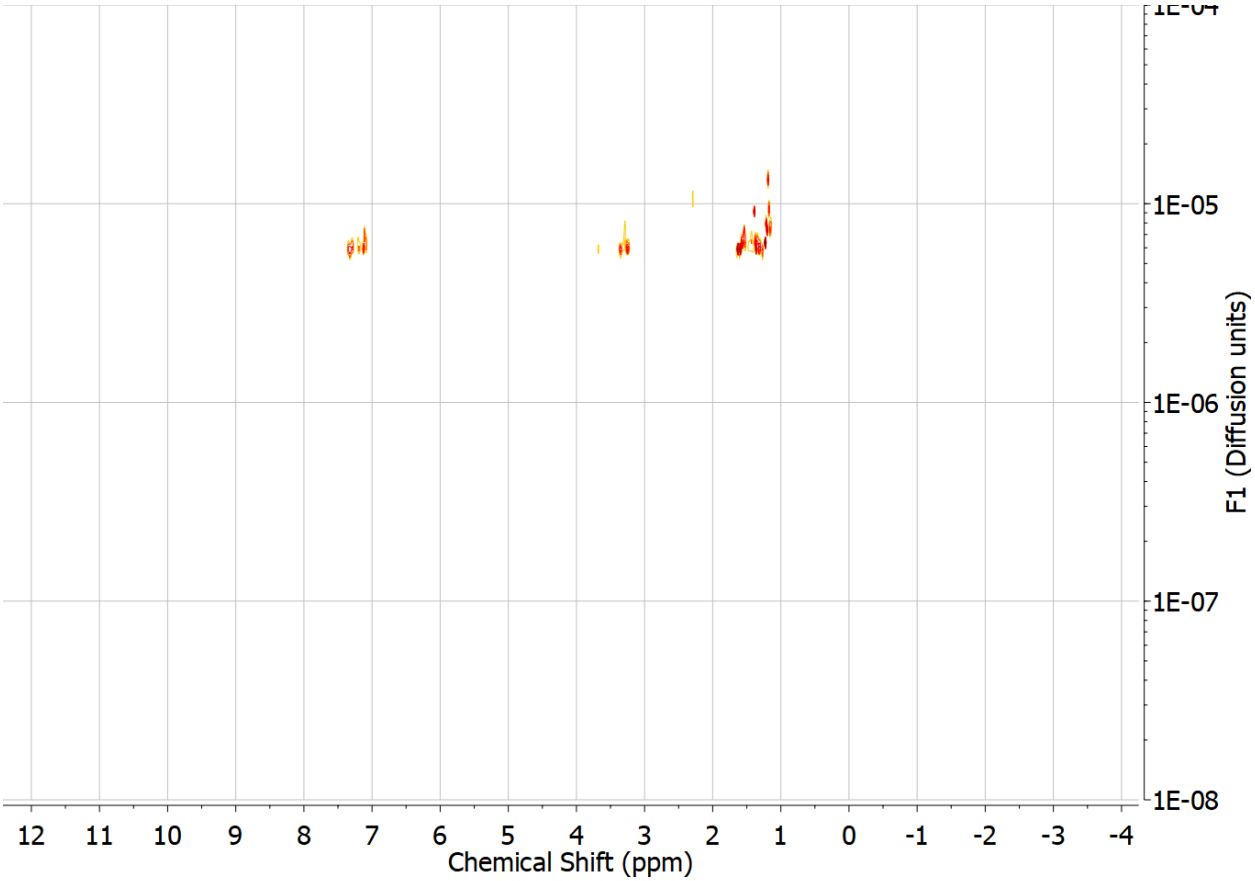

Fig. S31 DOSY NMR of [(^{Me}IPrCH)In]$_4$ (**1**) in C_6D_6.

$$H_r = \frac{k_b T}{6\pi\eta D}$$

H_r = hydrodynamic radius
k_b = Boltzmann constant
T = temperature of experiment = 300 K
η = viscosity of benzene at 300 K
D = experimentally determined diffusion coefficient

$$\frac{H_r(^{Me}IPrCH_2)}{H_r(^{Me}IPrCHIn)} = \frac{D(^{Me}IPrCHIn)}{D(^{Me}IPrCH_2)} = \frac{5 \times 10^{-10} m^2 s^{-2}}{28 \times 10^{-10} m^2 s^{-2}} = 0.18 \sim 0.20$$

The hydrodynamic radius of ^{Me}IPrCHIn is roughly 4 to 5 times that of ^{Me}IPrCH$_2$ in C_6D_6, implying that ^{Me}IPrCHIn is a tetramer in arene solutions, in line with its solid-state structure. The hydrodynamic radius of ^{Me}IPrCH$_2$ has been previously reported.[S3]

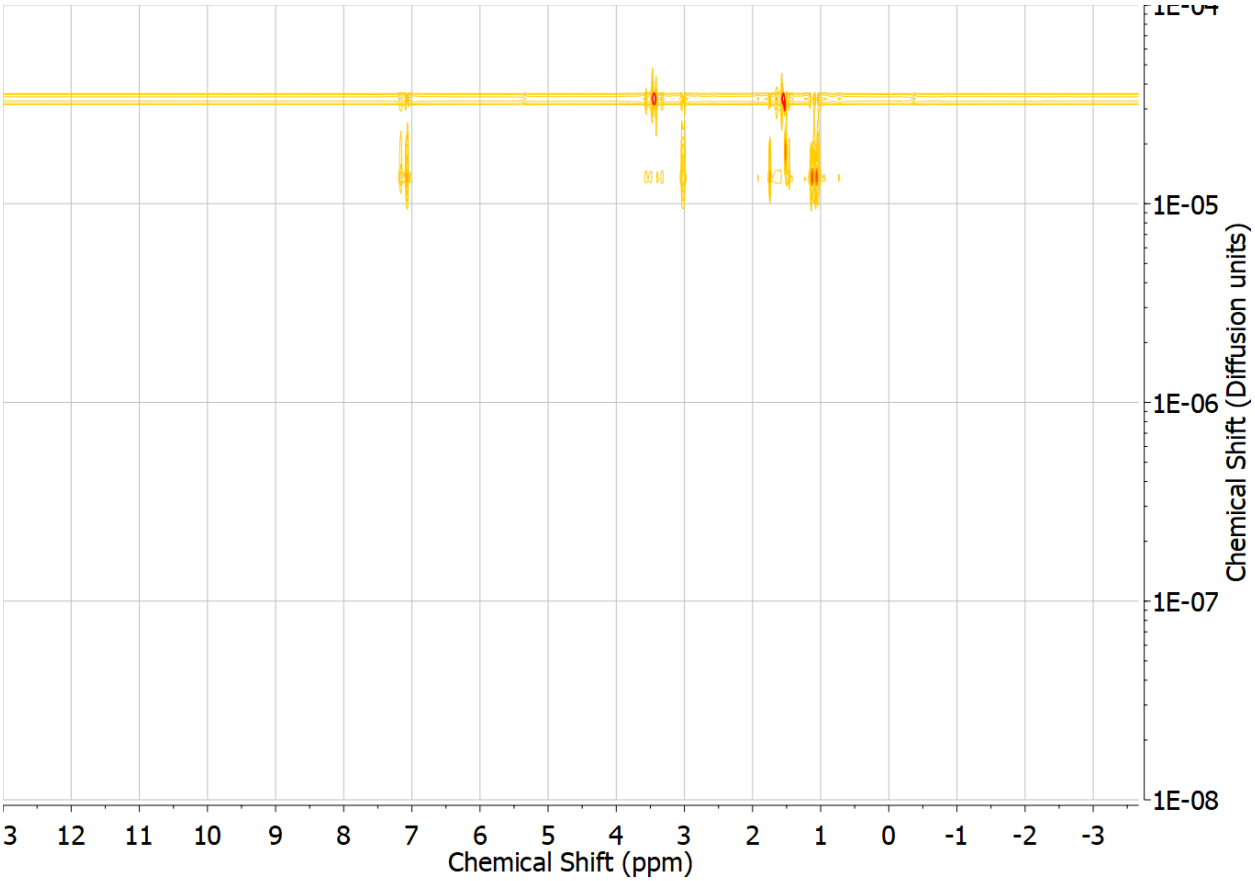

Fig. S32 DOSY NMR of ^{Me}IPrCH$_2$ in THF containing 20% C_6D_6.

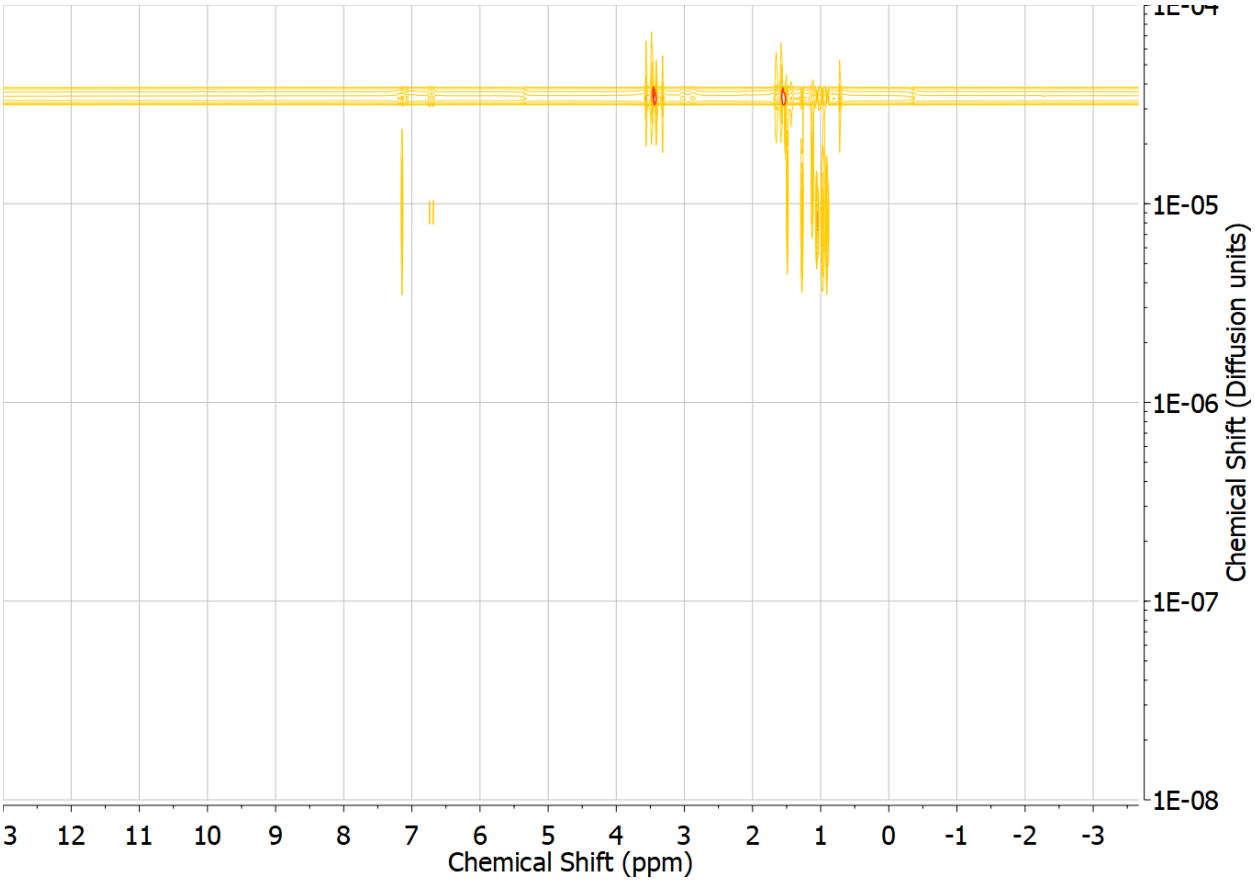

Fig. S33 DOSY NMR of [(^{Me}IPrCH)In]$_4$ (**1**) in THF containing 20% C_6D_6.

$$H_r = \frac{k_b T}{6\pi\eta D}$$

H_r = hydrodynamic radius
k_b = Boltzmann constant
T = temperature of experiment = 300 K
η = viscosity of THF at 300 K
D = experimentally determined diffusion coefficient

$$\frac{H_r(^{Me}IPrCH_2)}{H_r(^{Me}IPrCHIn)} = \frac{D(^{Me}IPrCHIn)}{D(^{Me}IPrCH_2)} = \frac{6 \times 10^{-10} m^2 s^{-2}}{11 \times 10^{-10} m^2 s^{-2}} = 0.54$$

The hydrodynamic radius of ^{Me}IPrCHIn in THF containing 20% C_6D_6 is roughly 2 times that of $^{Me}IPrCH_2$ in THF containing 20% C_6D_6, implying that ^{Me}IPrCHIn is a dimer THF.

\

Supporting Information

X-Ray Crystallographic Data

Table S1. Crystallographic details for [(^{Me}IPrCH)In]$_4$ (**1**)•2 toluene.

B. Crystal Data	
formula	$C_{134}H_{180}In_4N_8$
formula weight	2362.13
crystal color and habit[a]	blue block
crystal dimensions (mm)	0.68 × 0.20 × 0.13
crystal system	triclinic
space group	$P\bar{1}$ (No. 2)
unit cell parameters[b]	
a (Å)	16.114(3)
b (Å)	22.258(4)
c (Å)	22.529(4)
α (deg)	86.035(2)
β (deg)	78.839(2)
γ (deg)	70.732(2)
V (Å^3)	7484(2)
Z	2
ρ_{calcd} (g cm^{-3})	1.048
μ (mm^{-1})	0.650
B. Data Collection and Refinement Conditions	
diffractometer	Bruker PLATFORM/APEX II CCD[c]
radiation (λ [Å])	graphite-monochromated Mo Kα (0.71073)
temperature (°C)	–80
scan type	ω scans (0.3°) (20 s exposures)
data collection 2θ limit (deg)	52.86
total data collected	119804 (-20 ≤ h ≤ 20, -27 ≤ k ≤ 27, -28 ≤ l ≤ 28)
independent reflections	30703 (R_{int} = 0.0707)
number of observed reflections (*NO*)	20334 [$F_o^2 \geq 2\sigma(F_o^2)$]
structure solution method	intrinsic phasing (*SHELXT-2014*[d])
refinement method	full-matrix least-squares on F^2 (*SHELXL–2018*[e,f])
absorption correction method	Gaussian integration (face-indexed)
range of transmission factors	1.0000–0.6234
data/restraints/parameters	30703 / 45[g] / 1357
goodness-of-fit (*S*)[h] [all data]	1.017
final *R* indices[i]	
R_1 [$F_o^2 \geq 2\sigma(F_o^2)$]	0.0501
wR_2 [all data]	0.1484
largest difference peak and hole	1.647 and –0.726 e Å^{-3}

[a]Obtained by recrystallization from a toluene solution.

[b]Obtained from least-squares refinement of 9829 reflections with $4.58° < 2\theta < 46.06°$.

[c]Programs for diffractometer operation, data collection, data reduction and absorption correction were those supplied by Bruker.

[d]G. M. Sheldrick, *Acta Crystallogr.,* 2015, **A71**, 3–8. (*SHELXT-2014*)

[e]G. M. Sheldrick, *Acta Crystallogr.,* 2015, **C71**, 3–8. (*SHELXL-2018/3*)

[f]Attempts to refine peaks of residual electron density as disordered or partial-occupancy solvent toluene carbon atoms were unsuccessful. The data were corrected for disordered electron density through use of the SQUEEZE procedure as implemented in *PLATON* (A. L. Spek, *Acta Crystallogr.,* 2015, **C71**, 9–18. *PLATON* – a multipurpose crystallographic tool. Utrecht University, Utrecht, The Netherlands). A total solvent-accessible void volume of 1734 $Å^3$ with a total electron count of 399 (consistent with and additional 8 molecules of solvent toluene, or 4 molecules per formula unit of the indium cluster compound) was found in the unit cell.

[42he] rigid-bond restraint (**RIGU**) was applied to solvent toluene carbon atoms C11S to C17S to improve the quality of their anisotropic displacement parameters.

[h]$S = [\Sigma w(F_o^2 - F_c^2)^2/(n - p)]^{1/2}$ (n = number of data; p = number of parameters varied; $w = [\sigma^2(F_o^2) + (0.0770P)^2 + 0.8458P]^{-1}$ where $P = [\mathrm{Max}(F_o^2, 0) + 2F_c^2]/3$).

[i]$R_1 = \Sigma||F_o| - |F_c||/\Sigma|F_o|$; $wR_2 = [\Sigma w(F_o^2 - F_c^2)^2/\Sigma w(F_o^4)]^{1/2}$.

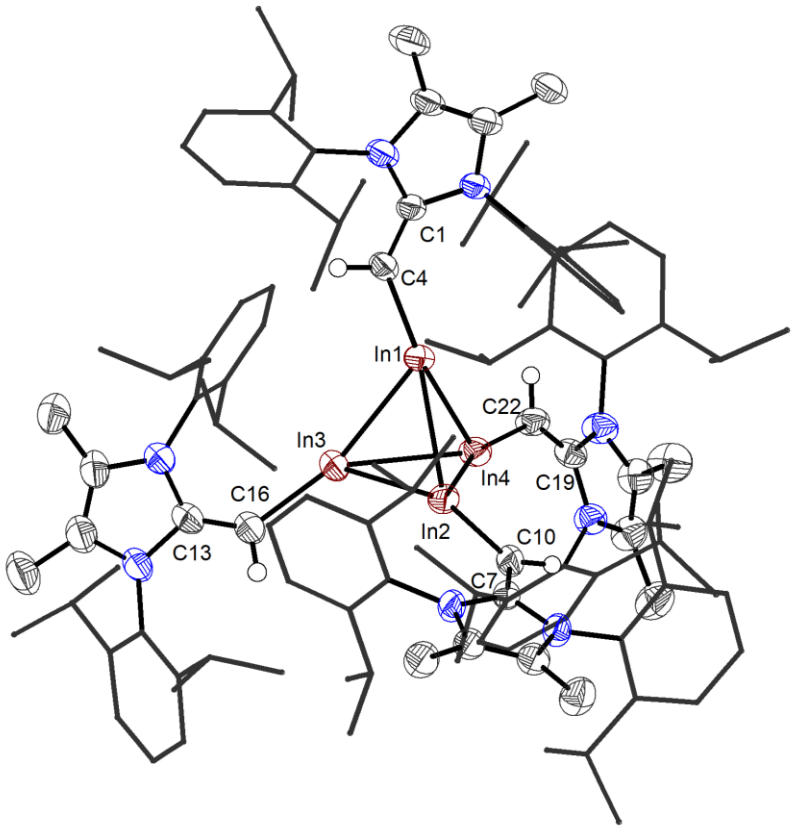

Fig. S34 Molecular structure of [(^{Me}IPrCH)In]$_4$ (**1**) with thermal ellipsoids plotted at 50% probability. All hydrogen atoms (except the vinylic hydrogen) are omitted for clarity; Dipp groups are shown as wireframes. Toluene solvate not shown for clarity. Selected bond lengths [Å] and angles [°]: In1-In2 3.0082(6), In1-In3 2.9854(5), In1-In4 2.9611(5), In1-C4 2.154(4), C1-C4 1.356(5), In2-In3 2.9565(5), In2-In4 2.9569(5), In2-C10 2.151(4), C7-C10 1.349(5), In3-In4 3.0228(6), In3-C16 2.147(4), C13-C16 1.359(6), In4-C22 2.148(4), C19-C22 1.352(5); In2-In1-In3 59.112(13), In2-In1-In4 59.380(12), In3-In1-In4 61.104(13), In1-C4-C1 134.7(3), C4-In1-In3 124.90(11).

Table S2. Crystallographic details for (^{Me}IPrCH)In(THF)•B(C_6F_5)$_3$ (**2**)•pentane.

B. Crystal Data	
formula	$C_{57}H_{61}BF_{15}InN_2O$
formula weight	1200.70
crystal color and habit[a]	yellow block
crystal dimensions (mm)	0.34 × 0.27 × 0.24
crystal system	triclinic
space group	$P\bar{1}$ (No. 2)
unit cell parameters[b]	
a (Å)	10.7833(8)
b (Å)	13.3363(10)
c (Å)	21.1279(16)
α (deg)	107.7613(11)
β (deg)	102.8104(12)
γ (deg)	91.5239(12)
V (Å^3)	2807.0(4)
Z	2
ρ_{calcd} (g cm^{-3})	1.421
μ (mm^{-1})	0.511
B. Data Collection and Refinement Conditions	
diffractometer	Bruker PLATFORM/APEX II CCD[c]
radiation (λ [Å])	graphite-monochromated Mo Kα (0.71073)
temperature (°C)	–80
scan type	ω scans (0.3°) (20 s exposures)
data collection 2θ limit (deg)	57.51
total data collected	52526 (-14 ≤ h ≤ 14, -18 ≤ k ≤ 18, -28 ≤ l ≤ 28)
independent reflections	14557 (R_{int} = 0.0283)
number of observed reflections (*NO*)	12804 [$F_o^2 \geq 2\sigma(F_o^2)$]
structure solution method	intrinsic phasing (*SHELXT-2014*[d])
refinement method	full-matrix least-squares on F^2 (*SHELXL–2018*[e])
absorption correction method	Gaussian integration (face-indexed)
range of transmission factors	0.9359–0.8825
data/restraints/parameters	14557 / 21[f] / 715
goodness-of-fit (S)[g] [all data]	1.039
final R indices[h]	
R_1 [$F_o^2 \geq 2\sigma(F_o^2)$]	0.0321
wR_2 [all data]	0.0854
largest difference peak and hole	0.584 and –0.480 e Å^{-3}

[a]Obtained by recrystallization from a pentane solution.

[b]Obtained from least-squares refinement of 9764 reflections with $4.84° < 2\theta < 56.24°$.

[c]Programs for diffractometer operation, data collection, data reduction and absorption correction were those supplied by Bruker.

[d]G. M. Sheldrick, *Acta Crystallogr.,* 2015, **A71**, 3–8. (*SHELXT-2014*)

[e]G. M. Sheldrick, *Acta Crystallogr.,* 2015, **C71**, 3–8. (*SHELXL-2018/3*)

45he C–C distances within the disordered tetrahydrofuran group were restrained to be approximately the same by use of the *SHELXL* **SAME** instruction. Likewise, the C–C distances within the solvent pentane molecule were similarly treated.

[g]$S = [\Sigma w(F_o^2 - F_c^2)^2/(n - p)]^{1/2}$ (n = number of data; p = number of parameters varied; $w = [\sigma^2(F_o^2) + (0.0411P)^2 + 1.0816P]^{-1}$ where $P = [\mathrm{Max}(F_o^2, 0) + 2F_c^2]/3$).

[h]$R_1 = \Sigma||F_o| - |F_c||/\Sigma|F_o|$; $wR_2 = [\Sigma w(F_o^2 - F_c^2)^2/\Sigma w(F_o^4)]^{1/2}$.

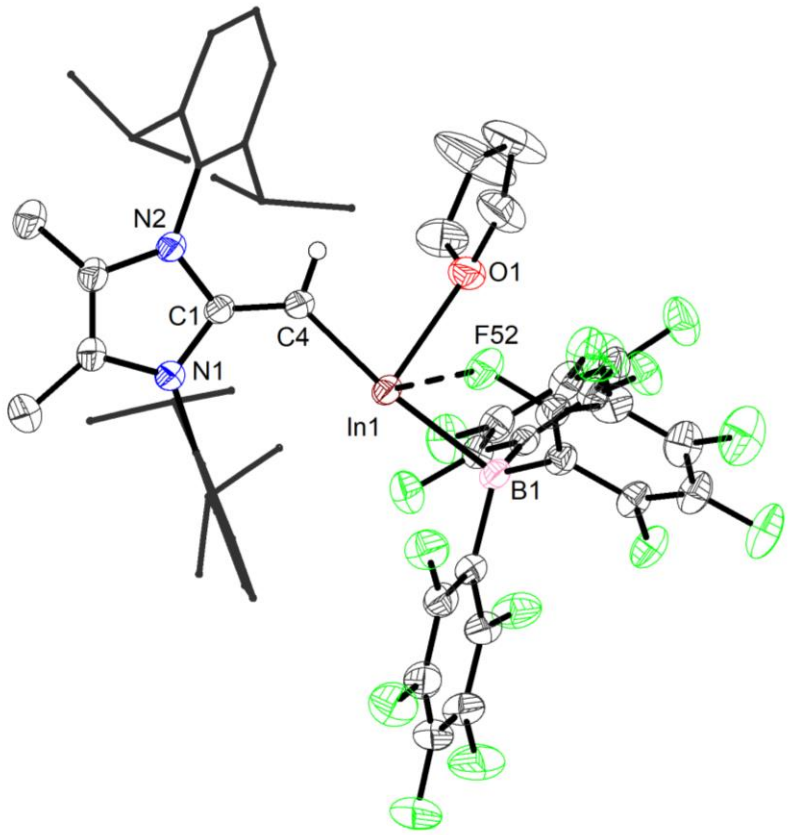

Fig. S35 Molecular structure of (^{Me}IPrCH)In(THF)•B(C_6F_5)$_3$ (**2**) with thermal ellipsoids plotted at 50% probability. All hydrogen atoms (except the vinylic hydrogen) are omitted for clarity, while all Dipp groups are shown in wireframe. Only one part of the disordered tetrahydrofuran group is shown. Pentane solvate not shown for clarity. Selected bond lengths [Å] and angles [°]: C1-C4 1.371(2), C4-In1 2.0699(16), In1-B1 2.3103(18), In1-O1 2.4734(12), In1---F52 2.7177(14); C1-C4-In1 133.12(12), C4-In1-B1 173.72(6), C4-In1-O1 83.82(6), In1-B1-C51 107.87(11), In1-B1-C61 112.84(11), In1-B1-C71 99.95(10).

Table S3. Crystallographic details for (^{Me}IPrCH)Bpin (**3**).

B. Crystal Data	
formula	$C_{36}H_{53}BN_2O_2$
formula weight	556.61
crystal colour and habit	colorless block
crystal dimensions (mm)	0.13 × 0.10 × 0.08
crystal system	monoclinic
space group	$P2_1/c$ (No. 14)
unit cell parameters[a]	
a (Å)	13.2848(3)
b (Å)	15.2957(3)
c (Å)	16.2903(4)
β (deg)	91.8769(13)
V (Å^3)	3308.42(13)
Z	4
ρ_{calcd} (g cm^{-3})	1.117
μ (mm^{-1})	0.516
B. Data Collection and Refinement Conditions	
diffractometer	Bruker D8/APEX II CCD[b]
radiation (λ [Å])	Cu Kα (1.54178) (microfocus source)
temperature (°C)	–100
scan type	ω and ϕ scans (1.0°) (5-10-15 s exposures)[c]
data collection 2θ limit (deg)	144.55
total data collected	70416 (-16 ≤ h ≤ 15, -18 ≤ k ≤ 18, -20 ≤ l ≤ 20)
independent reflections	6473 (R_{int} = 0.0622)
number of observed reflections (*NO*)	5245 [$F_o^2 \geq 2\sigma(F_o^2)$]
structure solution method	intrinsic phasing (*SHELXT-2014*[d])
refinement method	full-matrix least-squares on F^2 (*SHELXL–2018*[e])
absorption correction method	Gaussian integration (face-indexed)
range of transmission factors	0.9784–0.9161
data/restraints/parameters	6473 / 0 / 373
extinction coefficient (x)[f]	0.00105(14)
goodness-of-fit (S)[g] [all data]	1.050
final R indices[h]	
R_1 [$F_o^2 \geq 2\sigma(F_o^2)$]	0.0433
wR_2 [all data]	0.1232
largest difference peak and hole	0.329 and –0.194 e Å^{-3}

[a]Obtained from least-squares refinement of 9875 reflections with 6.66° < 2θ < 144.28°.

[b]Programs for diffractometer operation, data collection, data reduction and absorption correction were those supplied by Bruker.

[c]Data were collected with the detector set at three different positions. Low-angle (detector $2\theta = -33°$) data frames were collected using a scan time of 5 s, medium-angle (detector $2\theta = 75°$) frames using a scan time of 10 s, and high-angle (detector $2\theta = 117°$) frames using a scan time of 15 s.

[d]G. M. Sheldrick, *Acta Crystallogr.,* 2015, **A71**, 3–8. (*SHELXT-2014*)

[e]G. M. Sheldrick, *Acta Crystallogr.,* 2015, **C71**, 3–8. (*SHELXL-2018/3*)

[f]$F_c^* = kF_c[1 + x\{0.001F_c^2\lambda^3/\sin(2\theta)\}]^{-1/4}$ where k is the overall scale factor.

[g]$S = [\Sigma w(F_o^2 - F_c^2)^2/(n - p)]^{1/2}$ (n = number of data; p = number of parameters varied; $w = [\sigma^2(F_o^2) + (0.0595P)^2 + 0.8852P]^{-1}$ where $P = [\text{Max}(F_o^2, 0) + 2F_c^2]/3$).

[h]$R_1 = \Sigma||F_o| - |F_c||/\Sigma|F_o|$; $wR_2 = [\Sigma w(F_o^2 - F_c^2)^2/\Sigma w(F_o^4)]^{1/2}$.

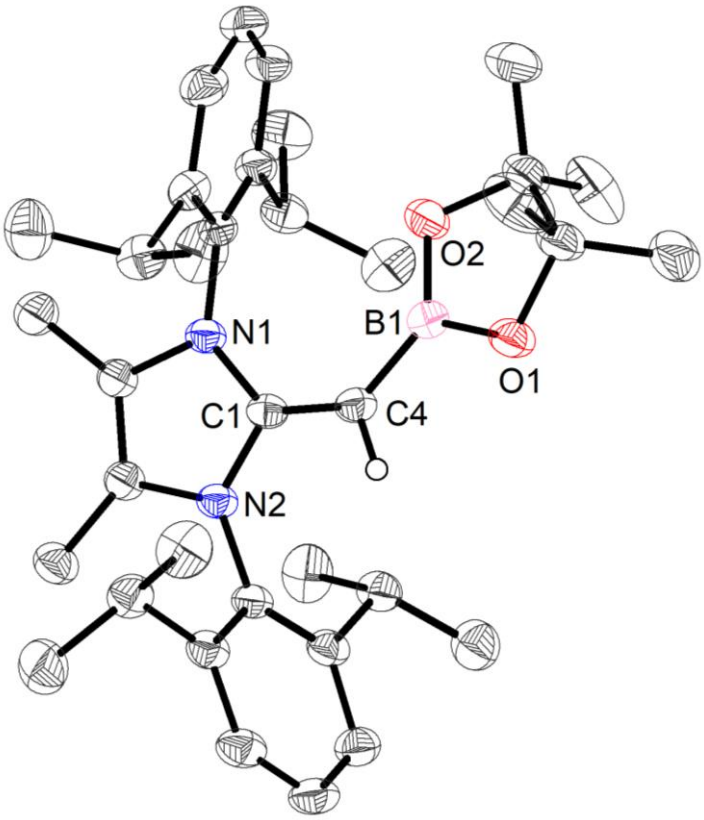

Fig. S36 Molecular structure of (^{Me}IPrCH)Bpin (**3**) with thermal ellipsoids plotted at 50% probability. All hydrogen atoms (except the vinylic hydrogen) are omitted for clarity. Selected bond lengths [Å] and angles [°]: C1-C4 1.3757(19), C4-B1 1.513(2); C1-C4-B1 134.02(12), O1-B1-O2 110.59(13).

Table S4. Crystallographic details for (^{Me}IPrCH)InNAr^{Dipp} (**4**)•toluene.

B. Crystal Data	
formula	$C_{74}H_{94}InN_3$
formula weight	1140.34
crystal colour and habit[a]	orange plate
crystal dimensions (mm)	0.37 × 0.17 × 0.05
crystal system	monoclinic
space group	$P2_1/n$ (an alternate setting of $P2_1/c$ [No. 14])
unit cell parameters[b]	
a (Å)	10.9546(16)
b (Å)	25.751(4)
c (Å)	23.267(3)
β (deg)	91.891(3)
V (Å^3)	6560.0(16)
Z	4
ρ_{calcd} (g cm^{-3})	1.155
μ (mm^{-1})	0.402
B. Data Collection and Refinement Conditions	
diffractometer	Bruker PLATFORM/APEX II CCD[c]
radiation (λ [Å])	graphite-monochromated Mo Kα (0.71073)
temperature (°C)	–80
scan type	ω scans (0.3°) (20 s exposures)
data collection 2θ limit (deg)	51.56
total data collected	80035 (-13 ≤ h ≤ 13, -31 ≤ k ≤ 31, -28 ≤ l ≤ 28)
independent reflections	12545 (R_{int} = 0.0901)
number of observed reflections (*NO*)	8925 [$F_o^2 \geq 2\sigma(F_o^2)$]
structure solution method	intrinsic phasing (*SHELXT-2014*[d])
refinement method	full-matrix least-squares on F^2 (*SHELXL–2018*[e,f])
absorption correction method	Gaussian integration (face-indexed)
range of transmission factors	1.0000–0.7633
data/restraints/parameters	12545 / 118[g] / 720
goodness-of-fit (S)[h] [all data]	1.015
final R indices[i]	
R_1 [$F_o^2 \geq 2\sigma(F_o^2)$]	0.0479
wR_2 [all data]	0.1401
largest difference peak and hole	1.006 and –0.785 e Å^{-3}

[a]Obtained by recrystallization from a toluene solution.

[b]Obtained from least-squares refinement of 9104 reflections with 4.36° < 2θ < 41.76°.

[c]Programs for diffractometer operation, data collection, data reduction and absorption correction were those supplied by Bruker.

[d]G. M. Sheldrick, *Acta Crystallogr.,* 2015, **A71**, 3–8. (*SHELXT-2014*)

[e]G. M. Sheldrick, *Acta Crystallogr.,* 2015, **C71**, 3–8. (*SHELXL-2018/3*)

[f]Attempts to refine peaks of residual electron density as disordered or partial-occupancy solvent toluene carbon atoms were unsuccessful. The data were corrected for disordered electron density through use of the SQUEEZE procedure as implemented in *PLATON* (A. L. Spek, *Acta Crystallogr.,* 2015, **C71**, 9–18. *PLATON* – a multipurpose crystallographic tool. Utrecht University, Utrecht, The Netherlands). A total solvent-accessible void volume of 872 $Å^3$ with a total electron count of 197 (consistent with 4 molecules of solvent toluene, or 1 molecule per formula unit of the indium complex) was found in the unit cell.

[51he] C–C distances within the disordered isopropyl group were restrained to be approximately the same by use of the *SHELXL* **SADI** instruction. Additionally, the C66–C70A and C66–C70B distances were similarly restrained. The rigid-bond restraint (**RIGU**) was applied to the carbon atoms of the disordered isopropyl group to improve the quality of their anisotropic displacement parameters. The phenyl ring of the disordered solvent toluene molecule was constrained to be an idealized hexagon; the C_{me}–C_{ipso} distances were restrained to be approximately the same, as were the $C_{me}\cdots C_{ortho}$ distances; the rigid-bond restraint was applied to all of the carbon atoms of the solvent toluene molecule. [total restraints: 10 **SADI**, 108 **RIGU**]

[h]$S = [\Sigma w(F_o^2 - F_c^2)^2/(n - p)]^{1/2}$ (n = number of data; p = number of parameters varied; $w = [\sigma^2(F_o^2) + (0.0770P)^2 + 0.5782P]^{-1}$ where $P = [\mathrm{Max}(F_o^2, 0) + 2F_c^2]/3$).

[i]$R_1 = \Sigma||F_o| - |F_c||/\Sigma|F_o|$; $wR_2 = [\Sigma w(F_o^2 - F_c^2)^2/\Sigma w(F_o^4)]^{1/2}$.

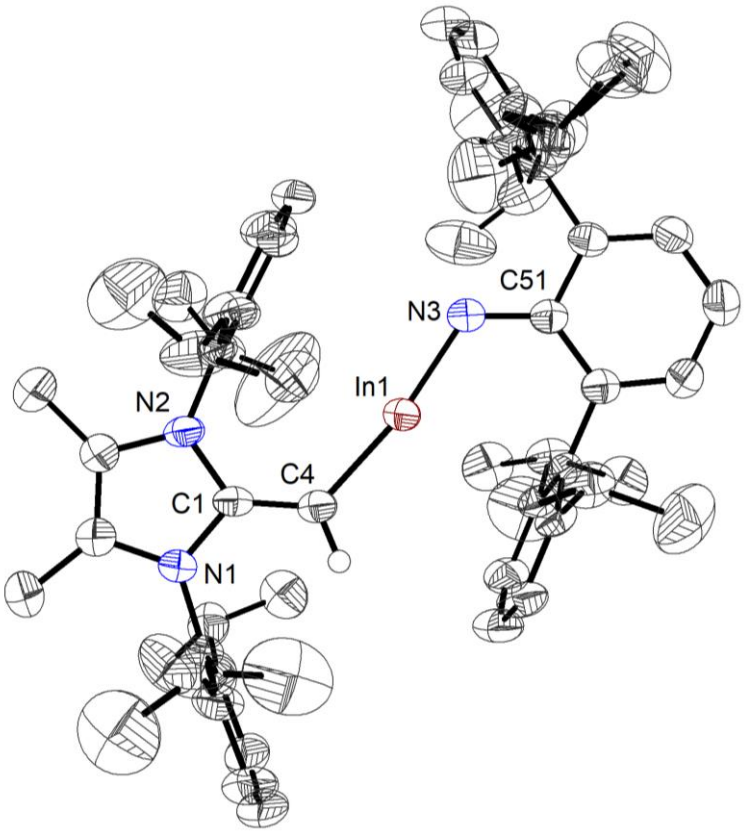

Fig. S37 Molecular structure of (^{Me}IPrCH)InNAr^{Dipp} (**4**) with thermal ellipsoids plotted at 50% probability. All hydrogen atoms (except the vinylic hydrogen) are omitted for clarity. Disordered toluene solvate not shown for clarity. Selected bond lengths [Å] and angles [°]: In1-N3 1.949(3), C4-In1 2.035(3), C1-C4 1.360(4), N3-C51 1.361(4); C1-C4-In1 128.9(2), N3-In1-C4 170.39(12), In1-N3-C51 122.5(2).

Table S5. Crystallographic details for $[(SIPrCH)Li]_2$ (**5**)•toluene.

B. Crystal Data	
formula	$C_{63}H_{86}Li_2N_4$
formula weight	913.23
crystal color and habit[a]	colorless block
crystal dimensions (mm)	0.33 × 0.30 × 0.21
crystal system	monoclinic
space group	*C*2/*c* (No. 15)
unit cell parameters[b]	
a (Å)	19.5691(4)
b (Å)	15.1755(3)
c (Å)	21.1457(4)
β (deg)	114.3497(8)
V (Å^3)	5721.1(2)
Z	4
*ρ*calcd (g cm^{-3})	1.060
μ (mm^{-1})	0.449
B. Data Collection and Refinement Conditions	
diffractometer	Bruker D8/APEX II CCD[c]
radiation (*λ* [Å])	Cu K*α* (1.54178) (microfocus source)
temperature (°C)	–100
scan type	*ω* and *ϕ* scans (1.0°) (5 s exposures)
data collection 2*θ* limit (deg)	147.73
total data collected	119852 (-24 ≤ *h* ≤ 24, -18 ≤ *k* ≤ 18, -26 ≤ *l* ≤ 26)
independent reflections	5789 (R_{int} = 0.0343)
number of observed reflections (*NO*)	5491 [$F_o^2 \geq 2\sigma(F_o^2)$]
structure solution method	intrinsic phasing (*SHELXT-2014*[d])
refinement method	full-matrix least-squares on F^2 (*SHELXL–2018*[e])
absorption correction method	Gaussian integration (face-indexed)
range of transmission factors	0.9790–0.8648
data/restraints/parameters	5789 / 0 / 349
extinction coefficient (*x*)*f*	0.00042(6)
goodness-of-fit (*S*)[g] [all data]	1.059
final *R* indices[h]	
R_1 [$F_o^2 \geq 2\sigma(F_o^2)$]	0.0388
wR_2 [all data]	0.1068
largest difference peak and hole	0.246 and –0.229 e Å^{-3}

[a]Obtained by recrystallization from a hexanes solution.
[b]Obtained from least-squares refinement of 9507 reflections with 7.66° < 2θ < 147.00°.
[c]Programs for diffractometer operation, data collection, data reduction and absorption correction were those supplied by Bruker.

[d]G. M. Sheldrick, *Acta Crystallogr.*, 2015, **A71**, 3–8. (*SHELXT-2014*)

[e]G. M. Sheldrick, *Acta Crystallogr.*, 2015, **C71**, 3–8. (*SHELXL-2018/3*)
$fF_c^* = kF_c[1 + x\{0.001F_c^2\lambda^3/\sin(2\theta)\}]^{-1/4}$ where k is the overall scale factor.
$gS = [\Sigma w(F_o^2 - F_c^2)^2/(n - p)]^{1/2}$ (n = number of data; p = number of parameters varied; $w = [\sigma^2(F_o^2) + (0.0520P)^2 + 2.8094P]^{-1}$ where $P = [\mathrm{Max}(F_o^2, 0) + 2F_c^2]/3$).
[h]$R1 = \Sigma||F_o| - |F_c||/\Sigma|F_o|$; $wR2 = [\Sigma w(F_o^2 - F_c^2)^2/\Sigma w(F_o^4)]^{1/2}$.

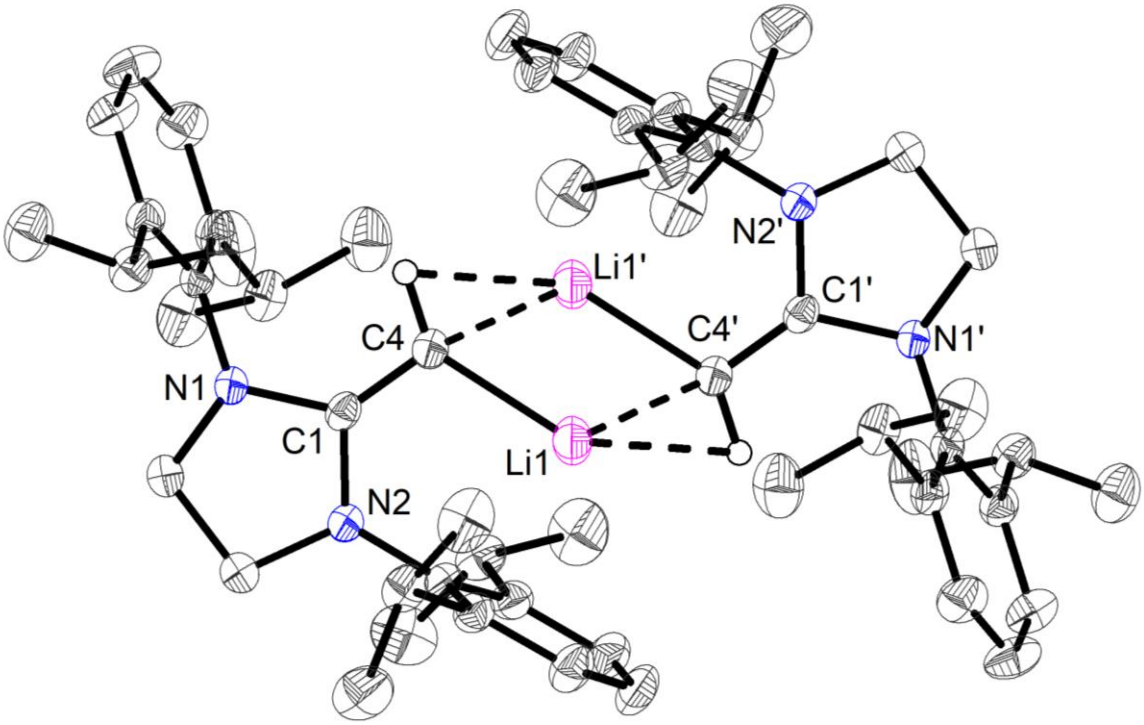

Fig. S38 Molecular structure of $[(SIPrCH)Li]_2$ (**5**) with thermal ellipsoids plotted at 50% probability. All hydrogen atoms (except the vinylic hydrogen) are omitted for clarity. Toluene solvate not shown for clarity. Selected bond lengths [Å] and angles [°]: C4-Li1 2.072(2), C1-C4 1.3440(13), C4-Li1′ 2.122(2); C1-C4-Li1 147.92(10), C1-C4-Li1′ 112.37(9).

Table S6. Crystallographic details for [(^{Me}IPrCH)$_6$In$_6$P$_8$] (**7**).

B. Crystal Data	
formula	$C_{204}H_{302}In_6N_{12}P_8$
formula weight	3859.24
crystal color and habit[a]	purple block
crystal dimensions (mm)	0.35 × 0.09 × 0.05
crystal system	triclinic
space group	$P\bar{1}$ (No. 2)
unit cell parameters[b]	
a (Å)	17.9240(3)
b (Å)	18.1563(3)
c (Å)	19.0661(3)
α (deg)	66.0552(7)
β (deg)	69.6779(7)
γ (deg)	71.9143(8)
V (Å^3)	5212.76(15)
Z	1
ρ_{calcd} (g cm^{-3})	1.229
μ (mm^{-1})	6.171
B. Data Collection and Refinement Conditions	
diffractometer	Bruker D8/APEX II CCD[c]
radiation (λ [Å])	Cu Kα (1.54178) (microfocus source)
temperature (°C)	–100
scan type	ω and ϕ scans (1.0°) (5 s exposures)
data collection 2θ limit (deg)	145.17
total data collected	237205 (-22 ≤ h ≤ 22, -21 ≤ k ≤ 19, -23 ≤ l ≤ 23)
independent reflections	19848 (R_{int} = 0.0447)
number of observed reflections (*NO*)	18289 [$F_o^2 \geq 2\sigma(F_o^2)$]
structure solution method	intrinsic phasing (*SHELXT-2014*[d])
refinement method	full-matrix least-squares on F^2 (*SHELXL–2018*[e,f])
absorption correction method	Gaussian integration (face-indexed)
range of transmission factors	0.8060–0.3321
data/restraints/parameters	19848 / 0 / 934
goodness-of-fit (S)[g] [all data]	1.038
final R indices[h]	
R_1 [$F_o^2 \geq 2\sigma(F_o^2)$]	0.0237
wR_2 [all data]	0.0645
largest difference peak and hole	0.834 and –0.554 e Å^{-3}

[a]Obtained by recrystallization from a hexanes solution.

[b]Obtained from least-squares refinement of 9206 reflections with $5.44° < 2\theta < 144.70°$.

[c]Programs for diffractometer operation, data collection, data reduction and absorption correction were those supplied by Bruker.

[d]G. M. Sheldrick, *Acta Crystallogr.,* 2015, **A71**, 3–8. (*SHELXT-2014*)

[e]G. M. Sheldrick, *Acta Crystallogr.,* 2015, **C71**, 3–8. (*SHELXL-2018/3*)

[f]Attempts to refine peaks of residual electron density as disordered or partial-occupancy solvent hexane carbon atoms were unsuccessful. The data were corrected for disordered electron density through use of the SQUEEZE procedure as implemented in *PLATON* (A. L. Spek, *Acta Crystallogr.,* 2015, **C71**, 9–18. *PLATON* – a multipurpose crystallographic tool. Utrecht University, Utrecht, The Netherlands). A total solvent-accessible void volume of 1177 $Å^3$ with a total electron count of 195 (consistent with 4 molecules of solvent hexane) was found in the unit cell.

[g]$S = [\Sigma w(F_o^2 - F_c^2)^2/(n - p)]^{1/2}$ (n = number of data; p = number of parameters varied; $w = [\sigma^2(F_o^2) + (0.0337P)^2 + 2.7250P]^{-1}$ where $P = [\text{Max}(F_o^2, 0) + 2F_c^2]/3$).

[h]$R_1 = \Sigma||F_o| - |F_c||/\Sigma|F_o|$; $wR_2 = [\Sigma w(F_o^2 - F_c^2)^2/\Sigma w(F_o^4)]^{1/2}$.

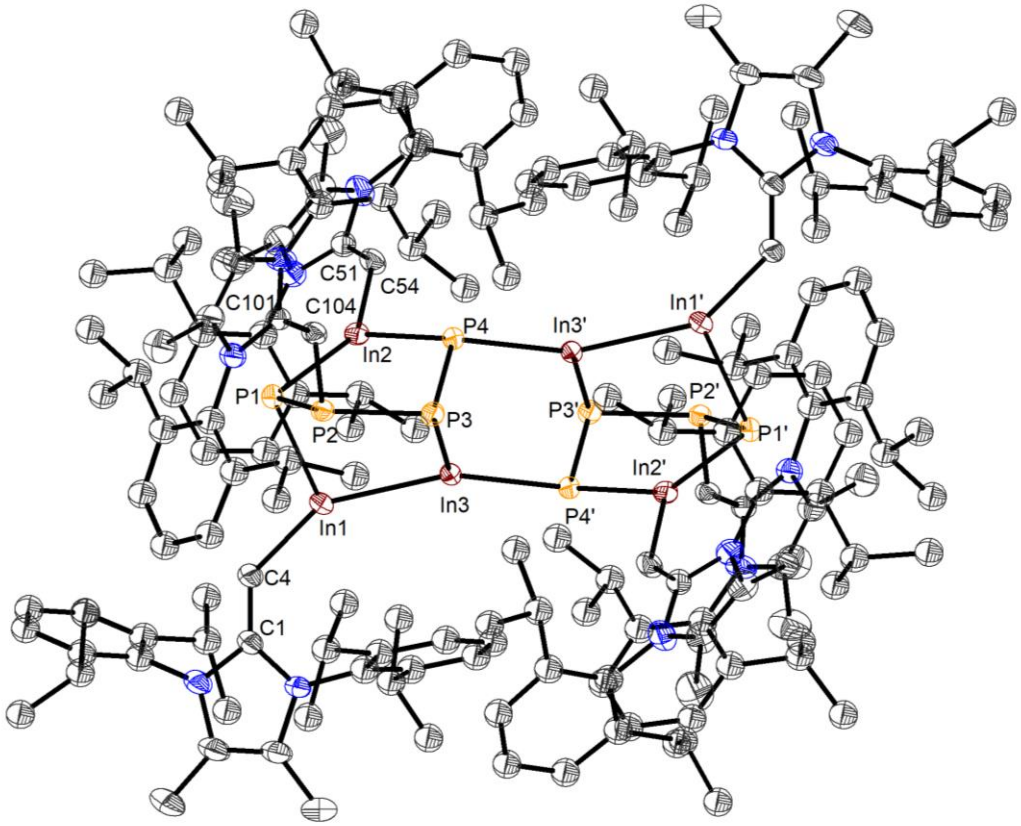

Fig. S39 Molecular structure of [(^{Me}IPrCH)$_6$In$_6$P$_8$] (**7**) with thermal ellipsoids plotted at 50% probability. All hydrogen atoms are omitted for clarity. Selected bond lengths [Å] and angles [°]: C4-In1 2.1065(19), In1-P1 2.5623(5), In1-In3 2.73726(16), C54-In2 2.1008(18), In2-P1 2.4936(4), In2-P4 2.5274(5), C104-P2 1.7863(18), P1-P2 2.2346(6), P2-P3 2.2374(6), P3-P4 2.2045(6), P4-In3′ 2.5702(2); C1-C4-In1 135.06(15), C4-In1-In3 147.91(5), In1-In3-P4′ 80.913(13), In3-P3-P4 73.145(18), In3-P4′-P3′ 107.68(2), P4-P3-P2 102.21(2), P3-P2-P1 113.87(2), P1-P2-C104 104.23(7), P3-P2-C104 98.69(6), P2-P1-In2 101.88(2), In1-P2-In2 89.2719(14), P1-In2-C54 145.42(5), P4-In2-C54 110.21(5).

Density Functional Theory (DFT) Computations and UV-Vis Data

All computations were performed with Gaussian16.[S13] Gas-phase geometries were optimized using density functional theory (DFT) with the B3LYP functional[S14] and the cc-pVDZ basis set.[S15] For indium, the cc-pVDZ-PP basis set[S16] was used in conjunction with effective core potentials, as obtained from the Basis Set Exchange Library.[S17] Frequency analyses confirmed all obtained structures to be local minima on the potential energy surfaces. Optimized geometries, orbitals and Atoms-in-Molecules (AIM) molecular graphs were visualized with Visual Molecular Dynamics (VMD).[S18] NBO analyses were performed with NBO 6.0[S19] and the wavefunction files were used for a topological analysis of the electron density according to the Atoms-In-Molecules partitioning scheme[S20] using AIMAll.[S21] The NCI grids were computed with NCIplot[S22] The vertical excitation energies of the first fifty singlet states have been predicted by TD-DFT computations using the same level of theory as stated above using the respective optimized gas-phase S_0 geometries of **1** and **4**. Computations regarding $[(^{Me}IPrCH)In]_4$ (**1**), were conducted on the truncated model $[(^{Me}IPhCH)In]_4$ (**1^{M}**) ($^{Me}IPhCH$ = $[(MeCNPh)_2C=CH]^-$) wherein the isopropyl groups were removed from the aryl rings. For comparison the first ten singlet states have been computed for $[InC(SiMe_3)_3]_4$, notably, for $[InC(SiMe_3)_3]_4$ two geometries have been obtained, which both represent minima on the potential energy surface by a subsequent frequency analysis.

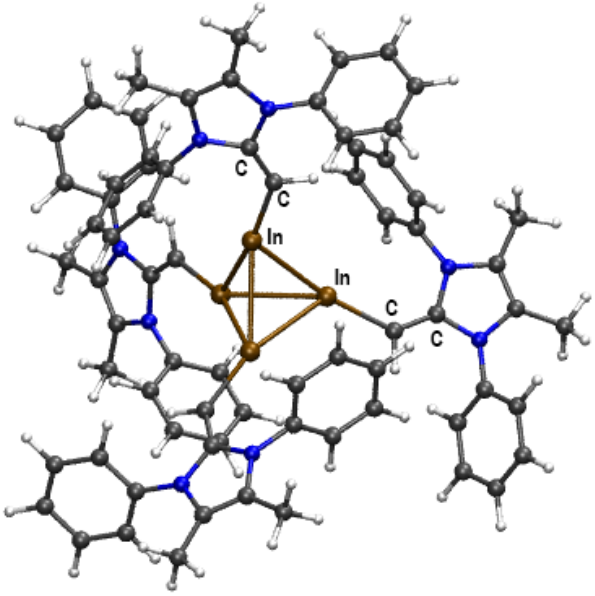

(a)

Bond	Calculated	Experimental
C–C (avg)	1.367	1.345(5)
C–In (avg)	2.190	2.150(4)
In–In (avg)	3.088	2.9818(5)

(b)

Bond	WBI	Atom	Q_{NPA}
C–C	1.650	In	0.498
C–In	0.574	C	-0.971
In–In	0.578	-	-

Table S7. Optimized gas-phase geometry of $[(^{Me}IPhCH)In]_4$ (**1^{M}**) (B3LYP/cc-pVDZ(-PP)) with (*a*) calculated bond lengths of $[(^{Me}IPhCH)In]_4$ (**1^{M}**) and experimental bond lengths of $[(^{Me}IPrCH)In]_4$ (**1**) [Å], and (*b*) Wiberg bond indices (WBI) and natural charges (Q_{NPA}).

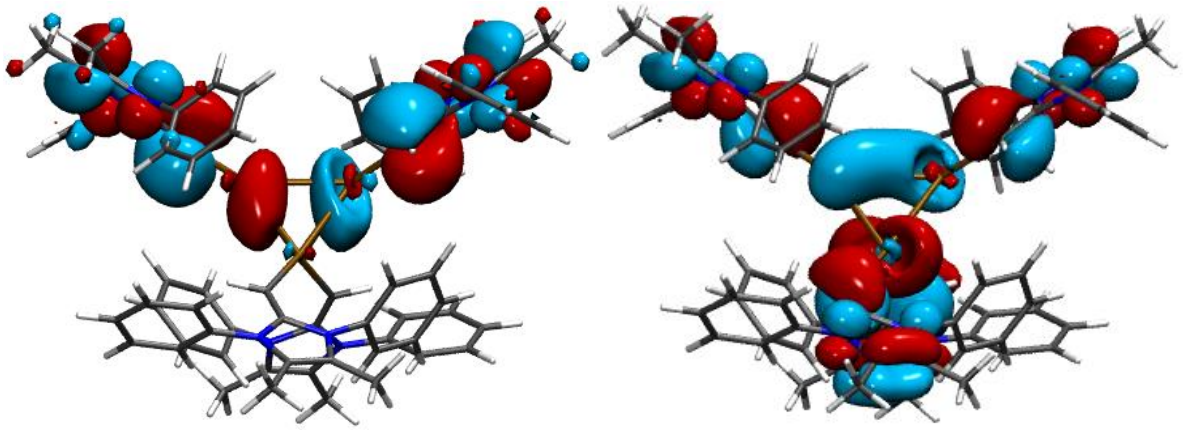

Fig. S40 HOMO-1 (left) and HOMO (right) of [(^{Me}IPhCH)In]$_4$ (**1^{M}**). Computed at the B3LYP/cc-pVDZ(-PP) level of theory.

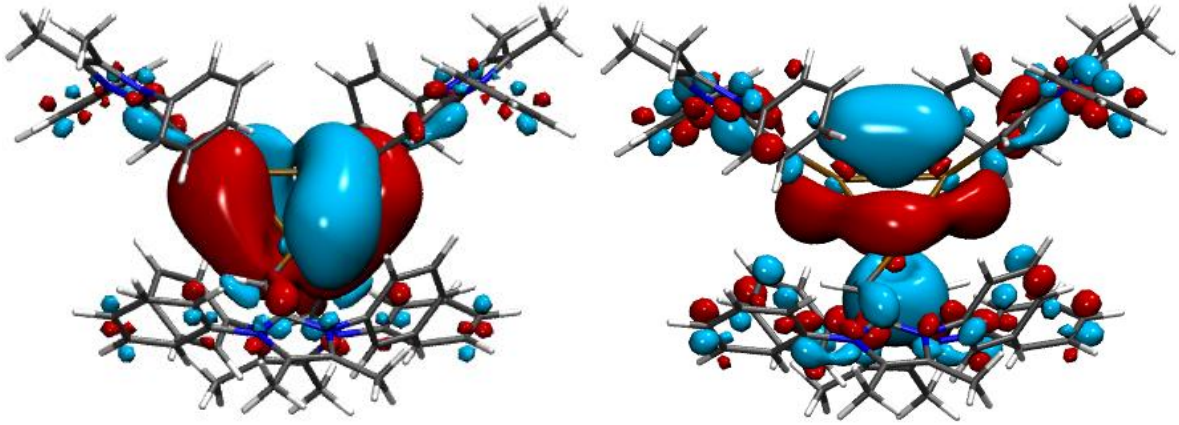

Fig. S41 LUMO (left) and LUMO+1 (right) of [(^{Me}IPhCH)In]$_4$ (**1^{M}**). Computed at the B3LYP/cc-pVDZ(-PP) level of theory.

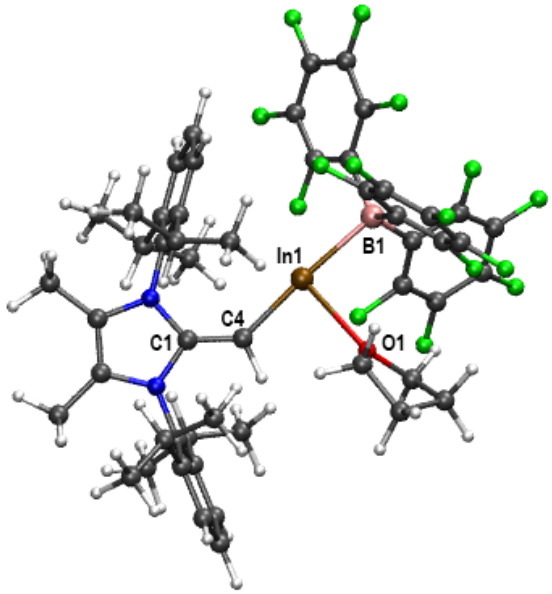

(a)

Bond	Calculated	Experimental
C1–C4	1.383	1.371(2)
C4–In1	2.107	2.0699(16)
In1–B1	2.359	2.3103(18)
In1–O1	2.610	2.4734(12)

(b)

Bond	WBI	Atom	Q_{NPA}
C1–C4	1.538	In1	1.465
C4–In1	0.552	B1	-0.019
In1–B1	0.660	C1	0.461
-	-	C4	-1.092
-	-	O1	-0.648

Table S8. Optimized gas-phase geometry of (^{Me}IPrCH)In(THF)•B(C_6F_5)$_3$ (**2**) (B3LYP/cc-pVDZ(-PP)) with (*a*) calculated and experimental bond lengths [Å], and (*b*) Wiberg bond indices (WBI) and natural charges (Q_{NPA}).

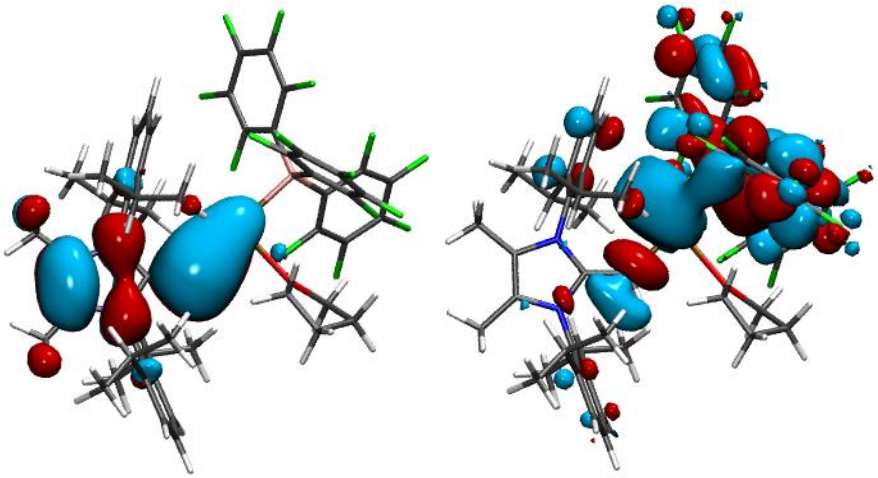

Fig. S42 HOMO (left) and LUMO (right) of (^{Me}IPrCH)In(THF)•B(C_6F_5)$_3$ (**2**). Computed at the B3LYP/cc-pVDZ(-PP) level of theory.

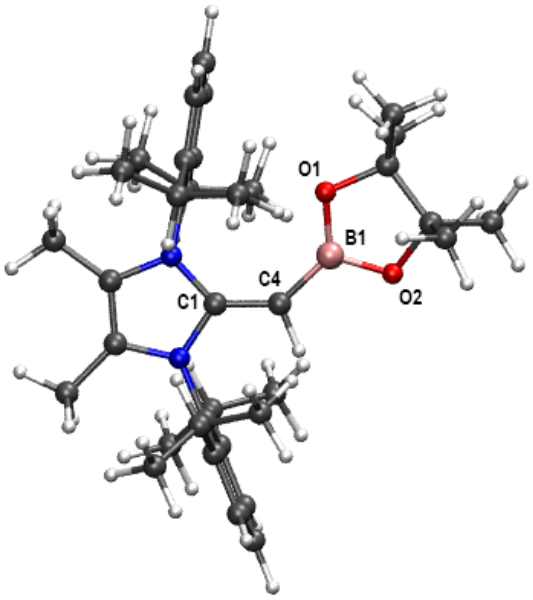

(a)

Bond	Calculated	Experimental
C1–C4	1.385	1.3757(19)
C4–B1	1.513	1.513(2)
B1–O1	1.394	1.3948(19)
B1–O2	1.400	1.3770(19)

(b)

Bond	WBI	Atom	Q_{NPA}
C1–C4	1.489	B1	1.132
C4–B1	1.038	C4	-0.874
B1–O1	0.823	C1	0.502
B1–O2	0.821	O1	-0788
-	-	O2	-0.782

Table S9. Optimized gas-phase geometry of (^{Me}IPrCH)Bpin (**3**) (B3LYP/cc-pVDZ) with (*a*) calculated and experimental bond lengths [Å], and (*b*) Wiberg bond indices (WBI) and natural charges (Q_{NPA}).

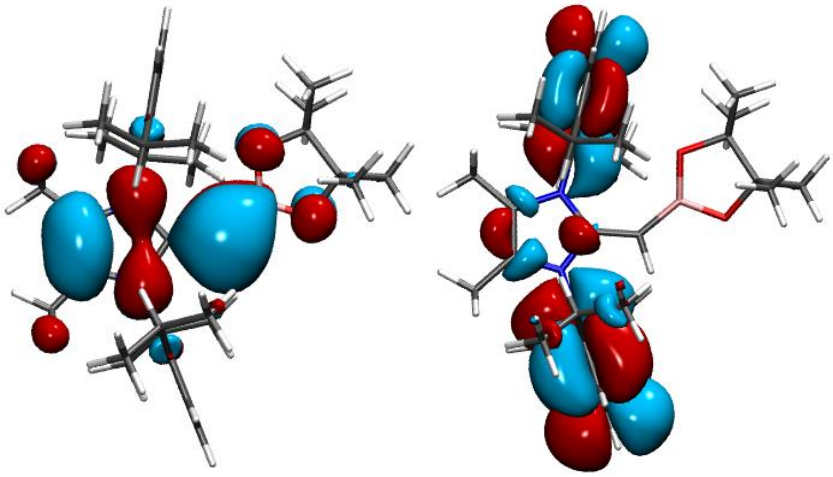

Fig. S43 HOMO (left) and LUMO (right) of (^{Me}IPrCH)Bpin (**3**). Computed at the B3LYP/cc-pVDZ level of theory.

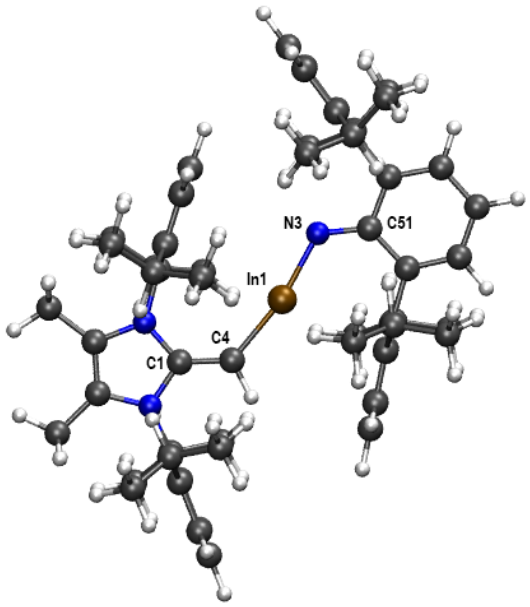

(a)

Bond	Calculated	Experimental
In1–C4	2.071	2.035(3)
In1–N3	1.974	1.949(3)
C1–C4	1.381	1.360(4)
N3–C51	1.366	1.361(4)

(b)

Bond	WBI	Atom	Q_{NPA}
In1–C4	0.683	In1	1.463
In1–N3	0.963	N3	-0.997
C1–C4	1.529	C4	-1.045
N3–C51	1.323	C1	0.461
-	-	C51	0.216

Table S10. Optimized gas-phase geometry of (^{Me}IPrCH)InNAr^{Dipp} (**4**) (B3LYP/cc-pVDZ(-PP)) with (*a*) calculated and experimental bond lengths [Å], and (*b*) Wiberg bond indices (WBI) and natural charges (Q_{NPA}).

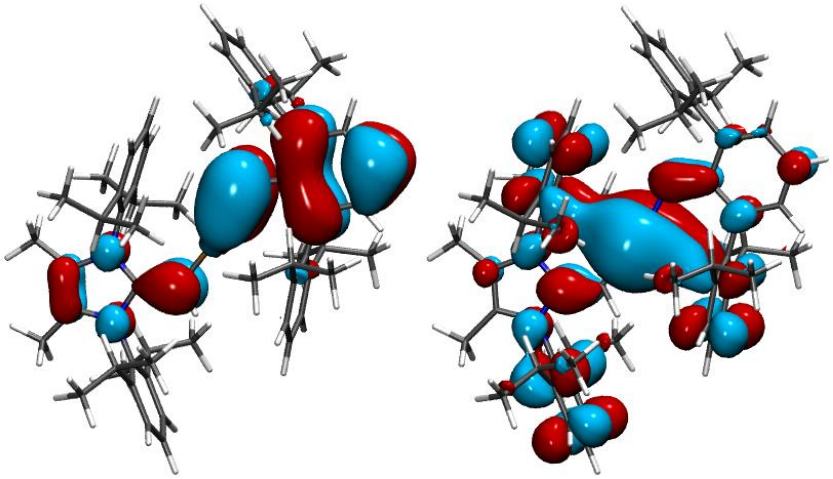

Fig. S44 HOMO (left) and LUMO (right) of (^{Me}IPrCH)InNAr^{Dipp} (**4**). Computed at the B3LYP/cc-pVDZ(-PP) level of theory.

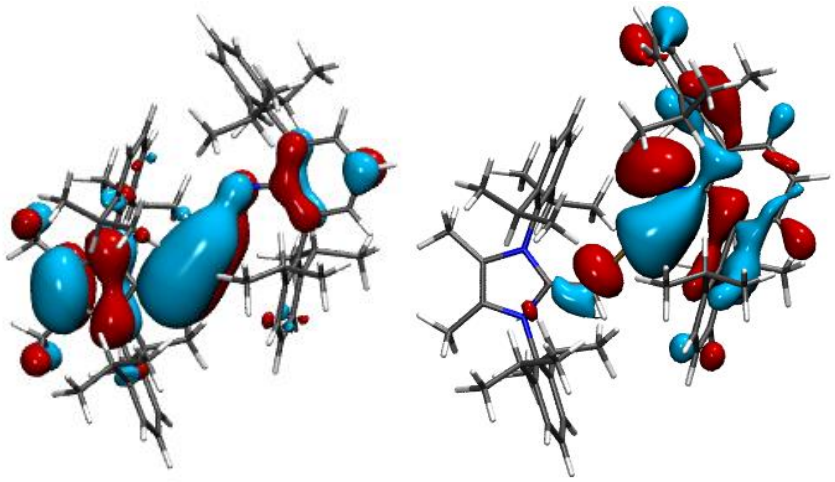

Fig. S45 HOMO-1 (left) and HOMO-2 (right) of (^{Me}IPrCH)InNAr^{Dipp} (**4**). Computed at the B3LYP/cc-pVDZ(-PP) level of theory.

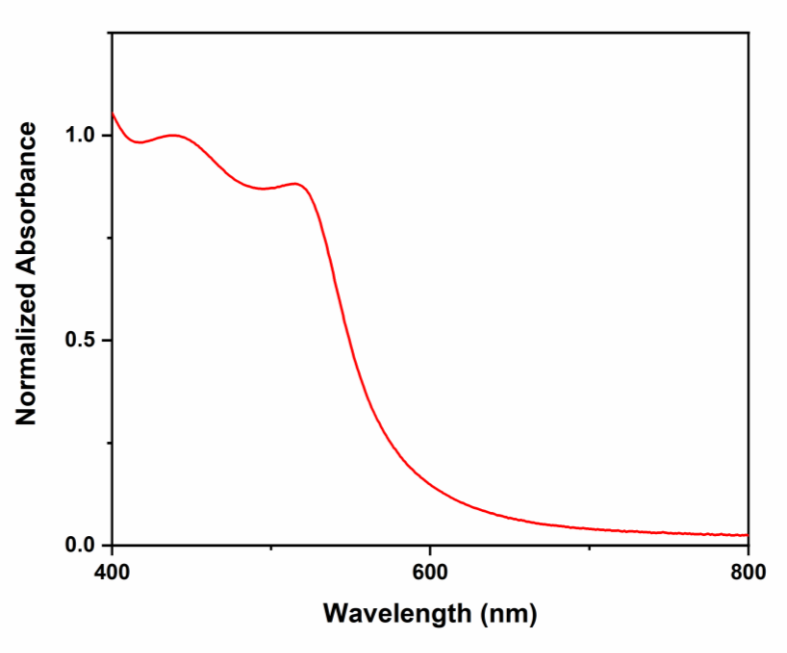

Fig. S46 Experimentally determined UV-vis spectrum of [(^{Me}IPrCH)In]$_4$ (**1**) in hexanes.

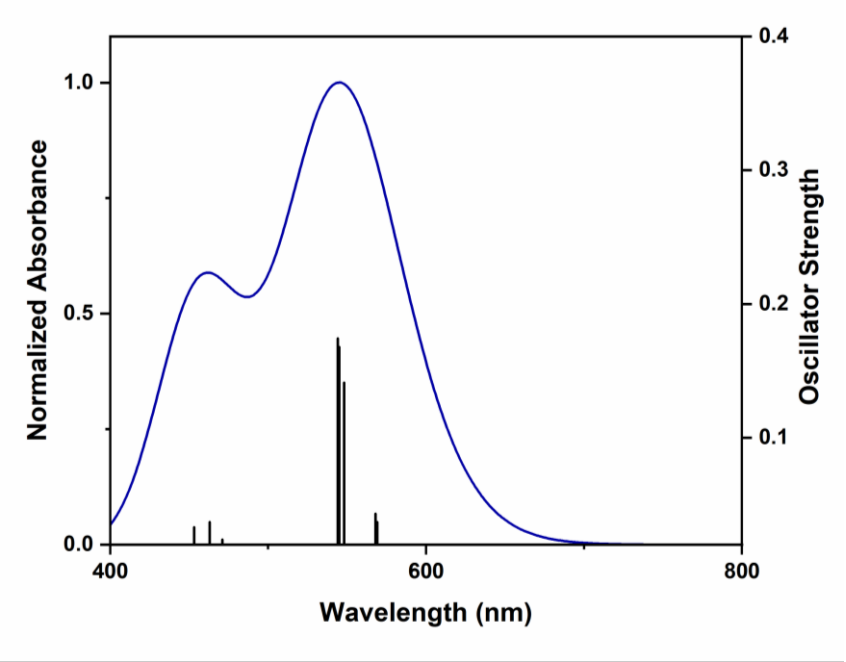

Fig. S47 Computed UV-vis spectrum and corresponding oscillator strengths for [(^{Me}IPhCH)In]$_4$ (**1^{M}**). Computed at the B3LYP/cc-pVDZ(-PP) level of theory.

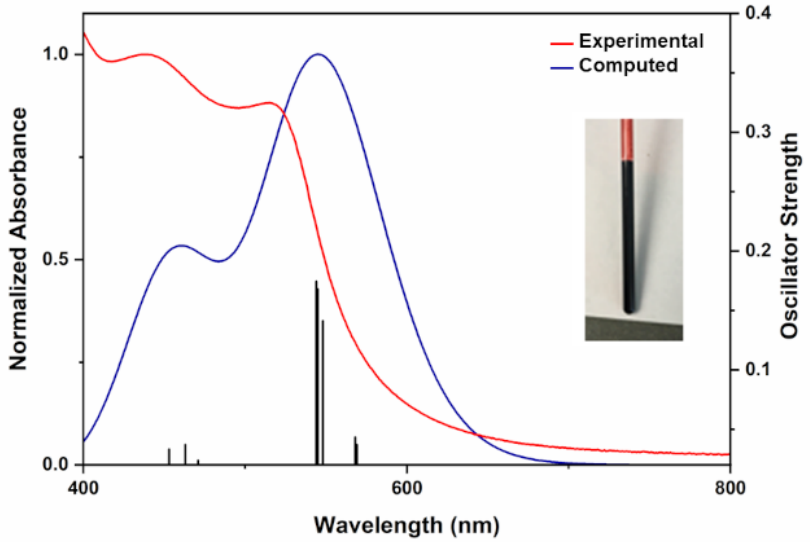

Fig. S48 Experimentally determined UV-vis spectrum of [(^{Me}IPrCH)In]$_4$ (**1**) in hexanes with computed UV-vis spectra overlay with corresponding oscillator strengths for [(^{Me}IPhCH)In]$_4$ (**1^{M}**). Computed at B3LYP/cc-pVDZ(-PP) level of theory with inlay of **1** in a benzene solution in an NMR tube.

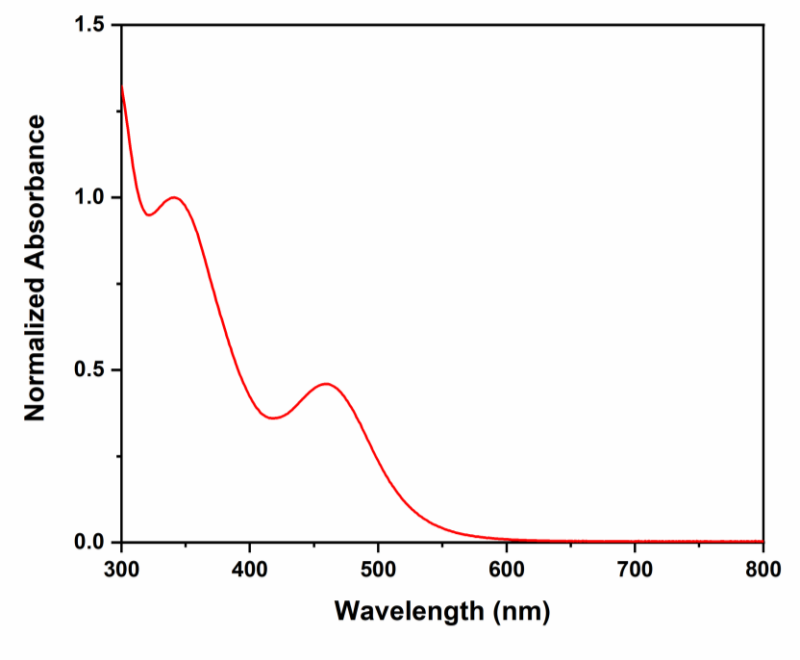

Fig. S49 Experimentally determined UV-vis spectrum of (^{Me}IPrCH)InNAr^{Dipp} (**4**) in hexanes.

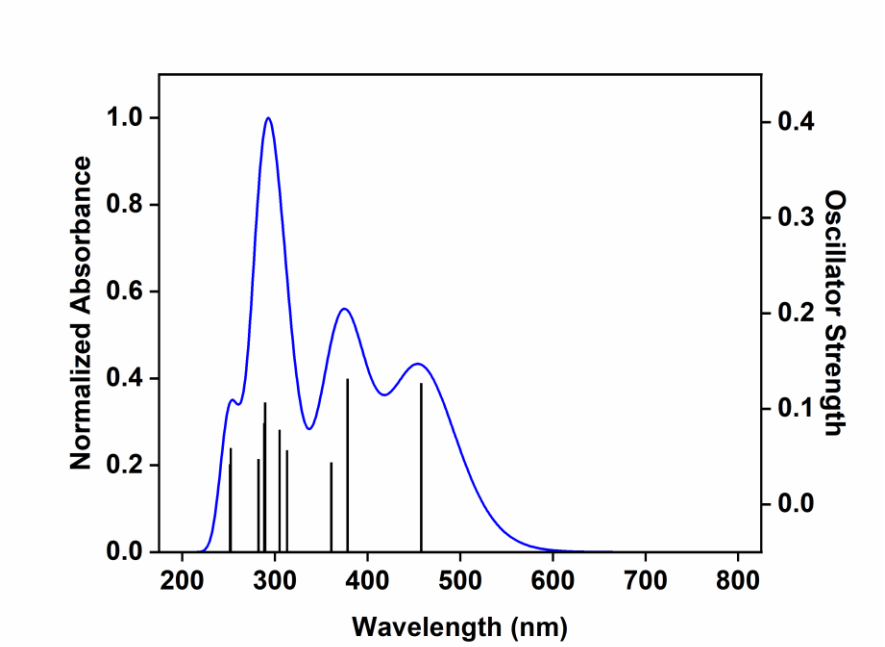

Fig. S50 Computed UV-vis spectrum and corresponding oscillator strengths for (^{Me}IPrCH)InNAr^{Dipp} (**4**). Computed at B3LYP/cc-pVDZ(-PP) level of theory.

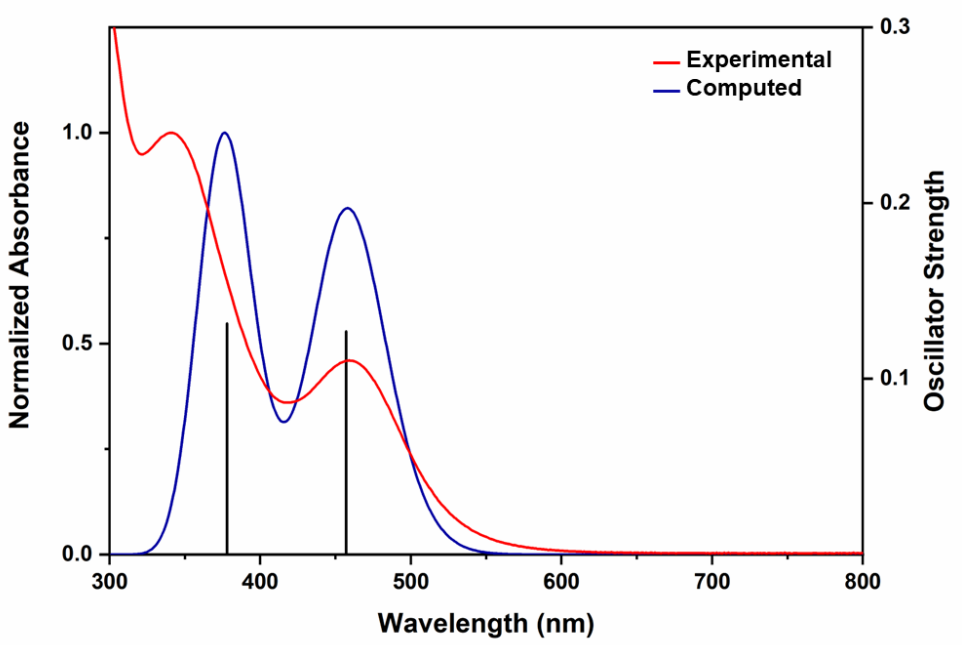

Fig. S51 Experimentally determined UV-vis spectrum of (^{Me}IPrCH)InNAr^{Dipp} (**4**) in hexanes with computed UV-vis spectra overlay with corresponding oscillator strengths for the two most bathochromic shifted absorption maxima. Computed at the B3LYP/cc-pVDZ(-PP) level of theory.

Table S11. S_0-S_n Transitions of [(^{Me}IPhCH)In]$_4$ (**1^{M}**) with oscillator strengths of f ≥ 0.0200 and contributing MOs with CI > |0.25| at the B3LYP/cc-pVDZ(PP) level of theory.

Transition	
$S_0 \rightarrow S_2$ (569.3 nm, f = 0.0371)	HOMO – 1 → LUMO (CI = 0.65)
$S_0 \rightarrow S_3$ (568.2 nm, f = 0.0433)	HOMO – 2 → LUMO (CI = 0.65)
$S_0 \rightarrow S_4$ (549.0 nm, f = 0.1412)	HOMO → LUMO + 1 (CI = 0.68)
$S_0 \rightarrow S_5$ (545.2 nm, f = 0.1678)	HOMO – 2 → LUMO + 1 (CI = 0.61)
$S_0 \rightarrow S_6$ (544.5 nm, f = 0.1744)	HOMO – 1 → LUMO + 1 (CI = 0.62)
$S_0 \rightarrow S_7$ (517.9 nm, f = 0.0436)	HOMO – 3 → LUMO (CI = 0.69)
$S_0 \rightarrow S_{13}$ (472.0 nm, f = 0.0239)	HOMO – 2 → LUMO + 10 (CI = 0.35)
$S_0 \rightarrow S_{14}$ (471.9 nm, f = 0.0220)	HOMO – 1 → LUMO + 11 (CI = 0.33)
$S_0 \rightarrow S_{18}$ (463.2 nm, f = 0.0358)	HOMO → LUMO + 2 (CI = 0.27) HOMO → LUMO + 9 (CI = 0.27)
$S_0 \rightarrow S_{19}$ (463.0 nm, f = 0.0371)	HOMO → LUMO + 3 (CI = 0.27) HOMO → LUMO + 8 (CI = 0.29)
$S_0 \rightarrow S_{27}$ (454.5 nm, f = 0.0234)	HOMO – 1 → LUMO + 4 (CI = 0.27)
$S_0 \rightarrow S_{29}$ (453.9 nm, f = 0.0331)	HOMO – 5 → LUMO (CI = 0.25) HOMO – 5 → LUMO + 1 (CI = 0.27) HOMO – 2 → LUMO + 4 (CI = 0.32)
$S_0 \rightarrow S_{39}$ (436.2 nm, f = 0.0208)	HOMO → LUMO + 17 (CI = 0.45)

Table S12. S_0-S_n Transitions of (^{Me}IPrCH)InNAr^{Dipp} (**4**) with oscillator strengths of f ≥ 0.0200 and contributing MOs with CI > |0.25| at the B3LYP/cc-pVDZ(PP) level of theory.

Transition	
$S_0 \rightarrow S_2$ (457.7 nm, f = 0.1270)	HOMO → LUMO (CI = 0.67)
$S_0 \rightarrow S_8$ (378.3 nm, f = 0.1316)	HOMO → LUMO + 7 (CI = 0.69)
$S_0 \rightarrow S_{10}$ (360.8 nm, f = 0.0438)	HOMO – 1→ LUMO (CI = 0.68)
$S_0 \rightarrow S_{15}$ (336.0 nm, f = 0.0388)	HOMO – 1 → LUMO + 4 (CI = 0.67)
$S_0 \rightarrow S_{20}$ (313.0 nm, f = 0.0565)	HOMO → LUMO +11 (CI = 0.68)
$S_0 \rightarrow S_{21}$ (304.9 nm, f = 0.0781)	HOMO – 1 → LUMO + 7 (CI = 0.69)
$S_0 \rightarrow S_{25}$ (289.35 nm, f = 0.1066)	HOMO – 2 → LUMO + 3 (CI = 0.26) HOMO – 2 → LUMO + 5 (CI = 0.50) HOMO → LUMO + 12 (CI = 0.29)
$S_0 \rightarrow S_{27}$ (288.4 nm, f = 0.0849)	HOMO → LUMO + 12 (CI = 0.64)
$S_0 \rightarrow S_{30}$ (282.2 nm, f = 0.0474)	HOMO – 2 → LUMO + 6 (CI = 0.63)
$S_0 \rightarrow S_{41}$ (259.3 nm, f = 0.0355)	HOMO – 2 → LUMO + 8 (CI = 0.35) HOMO → LUMO + 16 (CI = 0.53)
$S_0 \rightarrow S_{48}$ (252.3 nm, f = 0.0588)	HOMO – 1 → LUMO +12 (CI = 0.64)
$S_0 \rightarrow S_{49}$ (251.4 nm, f = 0.0419)	HOMO – 2 → LUMO + 8 (CI = 0.40) HOMO → LUMO + 16 (CI = 0.31)

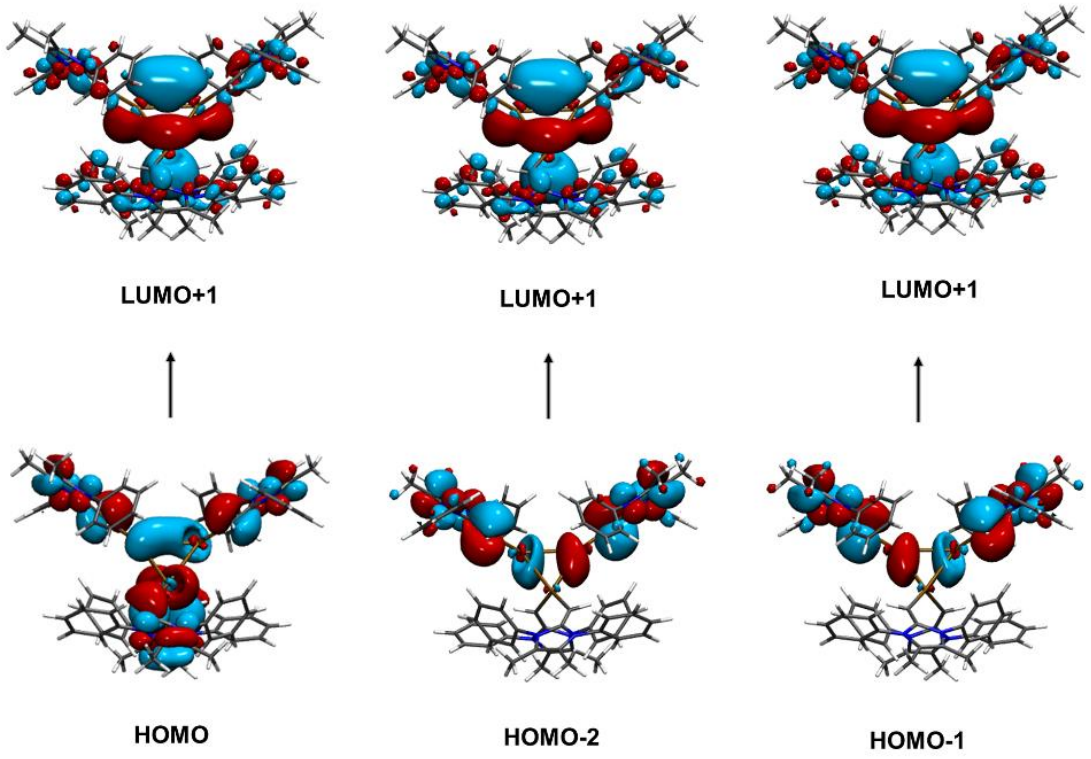

Fig. S52 Contributing MOs of the three dominant transitions at 549.0 nm (left), 545.2 nm (middle) and 544.5 nm (right) of [(^{Me}IPhCH)In]$_4$ (**1^{M}**).

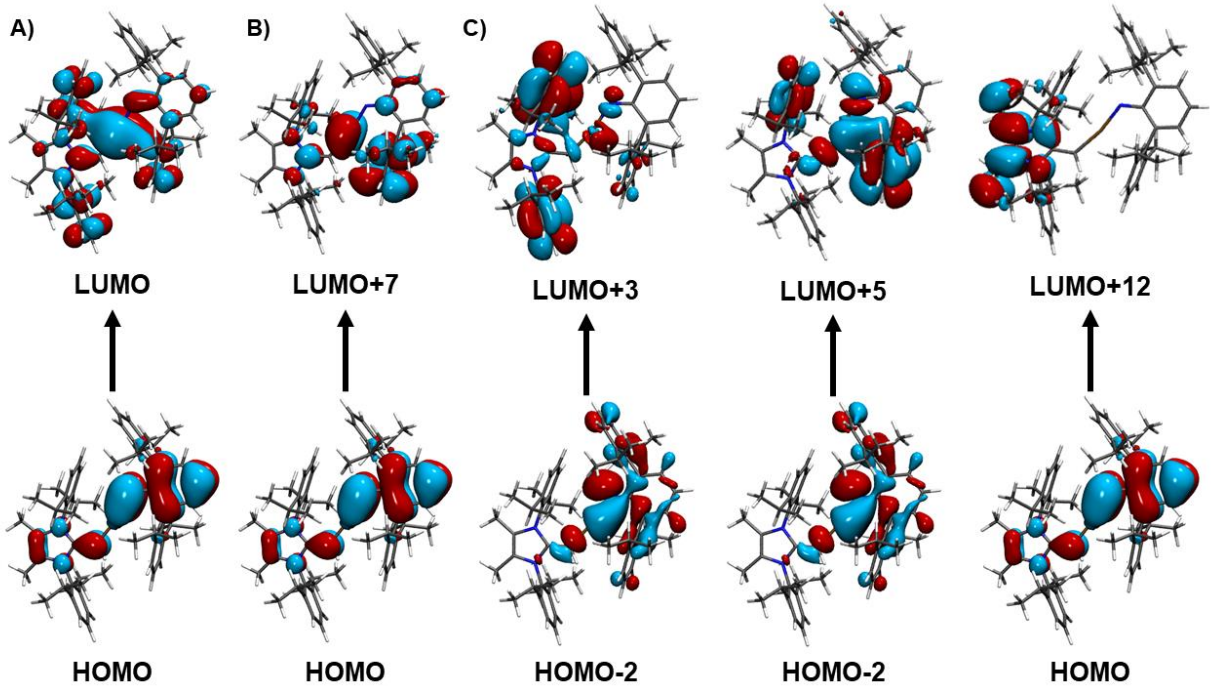

Fig. S53 Contributing MOs of the three dominant transitions at 457.7 nm (*a*), 378.3 nm (*b*) and 289.4 nm (*c*) of (^{Me}IPrCH)InNAr^{Dipp} (**4**).

Table S13. Nature of transitions of $[InC(SiMe_3)_3]_4$ with oscillator strengths of f > 0.0000 at the B3LYP/cc-pVDZ(PP) level of theory for two different geometries, both representing minima on the potential energy surface. The energetically order of the MOs are different in both geometries (Fig. S54)

Transition	
Geometry A	
$S_0 \rightarrow S_4$ (512.12 nm, f = 0.0071)	HOMO – 2 → LUMO (CI = 0.63)
$S_0 \rightarrow S_5$ (511.69 nm, f = 0.0071)	HOMO → LUMO + 1 (CI = 0.56)
$S_0 \rightarrow S_6$ (511.48 nm, f = 0.0070)	HOMO – 1 → LUMO + 1 (CI = 0.55)
Geometry B	
$S_0 \rightarrow S_4$ (511. 80 nm, f = 0.0072)	HOMO – 2 → LUMO (CI = –0.17) HOMO – 2 → LUMO + 1 (CI = 0.17) HOMO – 1 → LUMO (CI = 0.14) HOMO – 1 → LUMO + 1 (CI = 0.27) HOMO → LUMO (CI = 0.54) HOMO → LUMO + 1 (CI = –0.17)
$S_0 \rightarrow S_5$ (511.67 nm, f = 0.0072)	HOMO – 2 → LUMO (CI = 0.26) HOMO – 2 → LUMO + 1 (CI = 0.23) HOMO – 1 → LUMO (CI = 0.45) HOMO → LUMO + 1 (CI = 0.38)
$S_0 \rightarrow S_6$ (511. 38 nm, f = 0.0072)	HOMO – 2 → LUMO (CI = –0.12) HOMO – 2 → LUMO + 1 (CI = 0.53) HOMO – 1 → LUMO (CI = –0.28) HOMO – 1 → LUMO + 1(CI = –0.31) HOMO → LUMO + 4 (CI = –0.12)

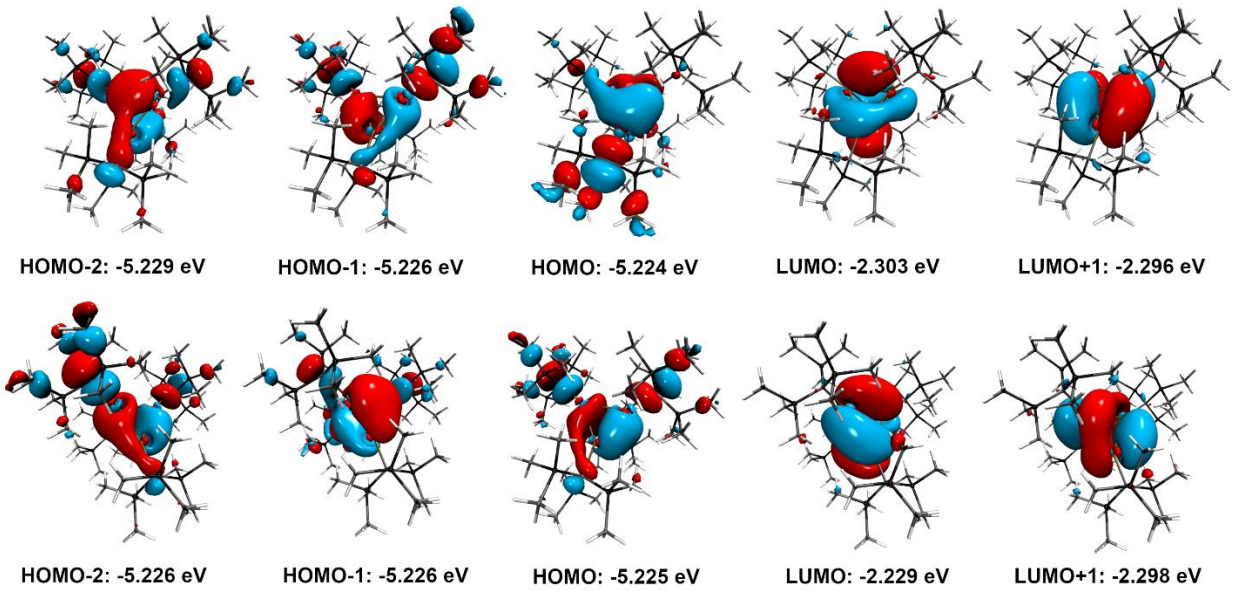

Fig. S54 MOs with respective energies for geometry A (top) and geometry B (bottom) for $[InC(SiMe_3)_3]_4$. Due to very similar energies of the MOs, the HOMO-1/HOMO as well as LUMO/LUMO+1 are swapped in both geometries.

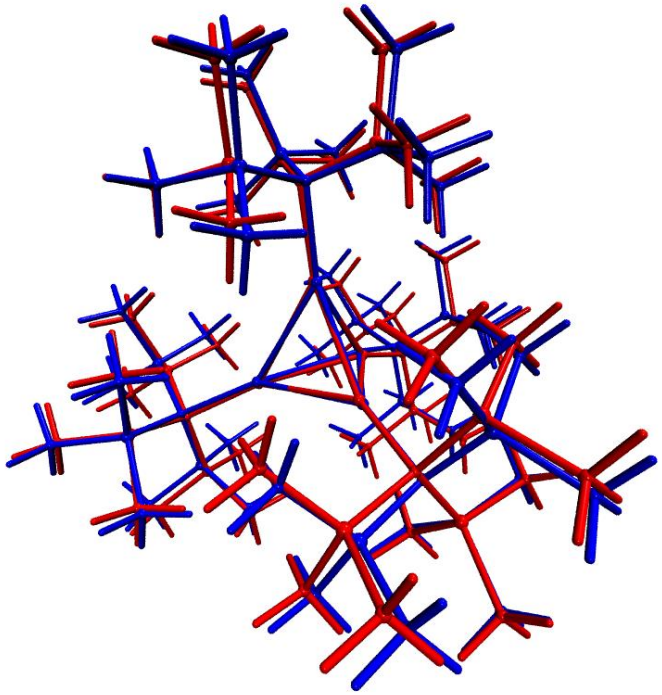

Fig. S55 Superposition of Geometries A (red) and B (blue). Total energy difference is 0.0000888 hartree (= 0.23 kJ/mol)

Table S14. Thermochemistry data for [(^{Me}IPhCH)In]$_4$ (**1^{M}**), monomeric (^{Me}IPhCH)In, HBpin, (^{Me}IPhCH)Bpin, InH, (^{Me}IPhCH)In^{III}(H)Bpin and a potential transition state (^{Me}IPhCH)-BH(In)pin (Fig. S56).

Energy	**[(^{Me}IPhCH)In]$_4$**	**(^{Me}IPhCH)In**	**HBpin**	**(^{Me}IPhCH)-In(H)Bpin**
ε_0	–3983.539892	–995.8765545	–411.8830582	–1407.7326499
ZPE	1.210447	0.302203	0.188693	0.488587
E_{tot}	1.296793	0.322051	0.198323	0.519959
H_{corr}	1.297737	0.322995	0.199267	0.520903
G_{corr}	1.055592	0.250076	0.156093	0.421952
ε_0 + ZPE	–3982.329445	–995.574352	–411.694366	–1407.244063
$\varepsilon_0 + E_{tot}$	–3982.243099	–995.554504	–411.684735	–1407.212691
$\varepsilon_0 + H_{corr}$	–3982.242155	–995.553560	–411.683791	–1407.211747
$\varepsilon_0 + G_{corr}$	–3982.484300	–995.626479	–411.726965	–1407.310698

Energy	**(^{Me}IPhCH)Bpin**	**InH**	**TS_(^{Me}IPhCH)-BH(In)pin**
ε_0	–1216.9861534	–190.7808603	–1407.775358
ZPE	0.484309	0.003227	0.492833
E_{tot}	0.512261	0.005594	0.522280
H_{corr}	0.513205	0.006539	0.523224
G_{corr}	0.424870	–0.017046	0.430647
ε_0 + ZPE	–1216.501844	–190.777633	–1407.282525
$\varepsilon_0 + E_{tot}$	–1216.473892	–190.775266	–1407.253078
$\varepsilon_0 + H_{corr}$	–1216.472948	–190.774322	–1407.252134
$\varepsilon_0 + G_{corr}$	–1216.561283	–190.797906	–1407.344711

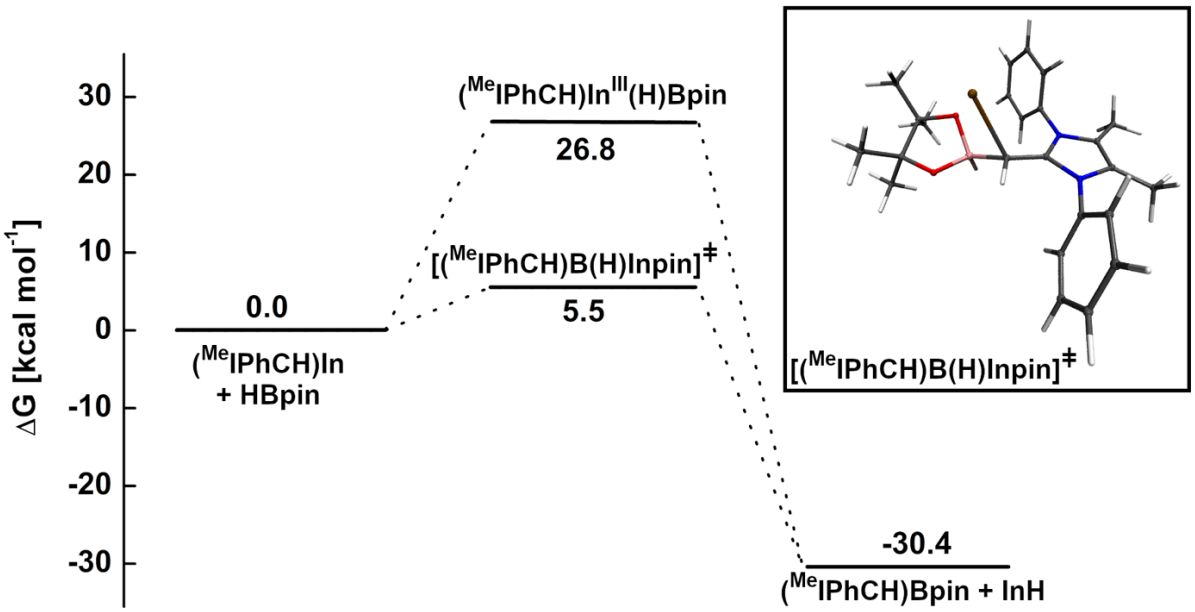

Fig. S56 Possible reaction mechanism of the reaction of tetramer $\mathbf{1^M}$ with HBpin. The (^{Me}IPhCH)BH(In)pin represents a transition state, all other geometries are minima on the potential energy surface.

Table S15. Topological and integrated bond properties from the AIM analysis of compound **4** and the model compounds RNInR′ (R = H, Ph; R′ = H, Ph, HC=CH_2, HC=C(NHCH)$_2$).

Species	Contact or basin	d [Å]	ρ(r) [eÅ^{-3}]	$\nabla^2\rho(r)$ [eÅ^{-5}]	ε	G/ρ(r) [a.u.]	H/ρ(r) [a.u.]	δ(A|B)
4	In1-N4	1.975	0.81	10.8	0.06	1.21	–0.28	1.13
	In1-C8	2.072	0.73	4.9	0.13	0.85	–0.37	0.92
	N4-C76	1.366	2.16	–23.8	0.08	0.56	–1.33	1.23
	C8-C5	1.381	2.04	–17.1	0.33	0.41	–1.00	1.44
	In1⋯C47	3.406	0.07	0.6	5.59	0.57	0.09	0.04
	In1⋯H64	3.259	0.03	0.3	0.70	0.52	0.14	0.02
	In1⋯H73	3.259	0.03	0.3	0.70	0.52	0.14	0.02
	In1⋯C114	2.951	0.13	1.0	0.07	0.54	–0.01	0.10
HNInH	In–N	1.918	0.90	12.2	0.11	1.29	–0.34	1.73
PhNInH	In–N	1.923	0.87	13.0	0.04	1.36	–0.31	1.51
	N–C	1.376	2.07	–22.8	0.04	0.64	–1.41	1.13
PhNInPh	In–N	1.936	0.85	12.3	0.05	1.31	–0.30	1.44
	N–C	1.378	2.08	–22.9	0.05	0.61	–1.38	1.14
	In–C	2.139	0.67	4.1	0.05	0.78	–0.35	0.83
PhNInCHCH$_2$	In–N	1.933	0.85	12.5	0.05	1.33	–0.30	1.45
	N–C	1.375	2.09	–23.1	0.05	0.63	–1.40	1.14
	In–C	2.129	0.68	4.3	0.06	0.79	–0.35	0.86
	C=C	1.339	2.24	–20.1	0.31	0.40	–1.03	1.89
PhNInCH-C(NHCH)$_2$	In–N	1.944	0.85	12.0	0.05	1.29	–0.30	1.39
	N–C	1.377	2.09	–23.1	0.05	0.58	–1.35	1.16
	In–C	2.069	0.73	5.0	0.13	0.85	–0.37	0.98
	C=C	1.382	2.03	–17.2	0.34	0.42	–1.01	1.45

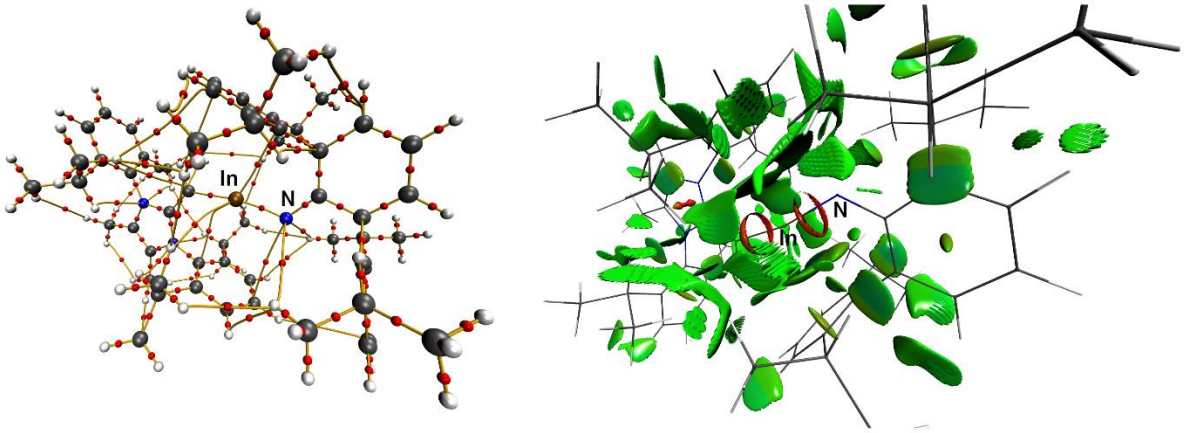

Fig. S57 *left:* AIM molecular graph of **4** with critical points as red spheres; *right: NCI iso*-surfaces of **4** at s(r) = 0.55 color coded with sign(λ_2)ρ in a. u. Blue surfaces refer to attractive forces and red to repulsive forces. Green indicates weak interactions.

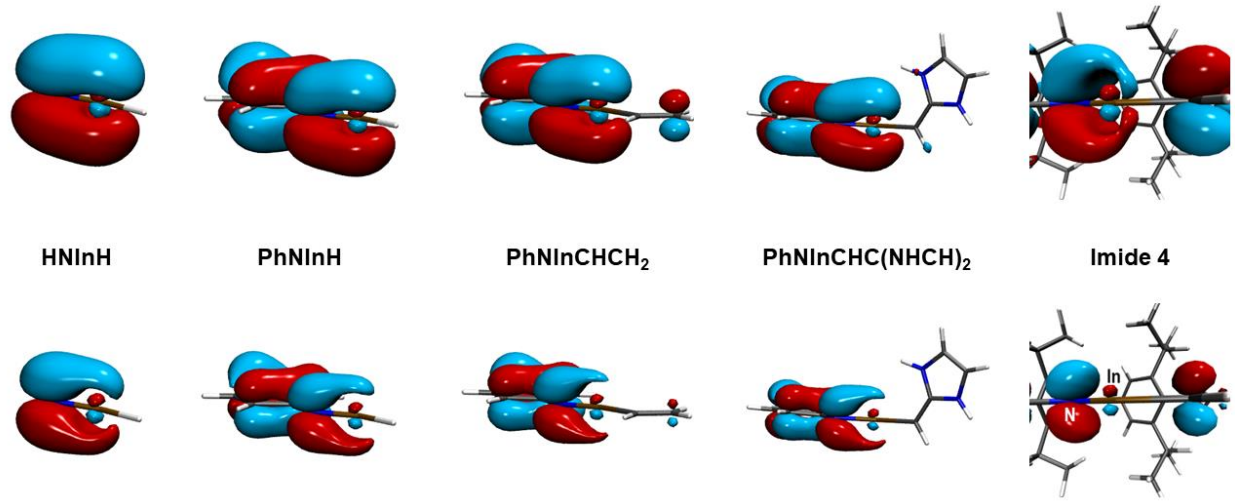

Fig. S58 Highest occupied molecular orbitals of compound **4** and model compounds at *iso*-values of ±0.02 (top) and ±0.04 (bottom).

References

S1. A. B. Pangborn, M. A. Giardello, R. H. Grubbs, R. K. Rosen and F. J. Timmers, *Organometallics*, 1996, **15**, 1518.
S2. I. C. Watson, A. Schumann, H. Yu, E. C. Davy, R. McDonald, M. J. Ferguson, C. Hering-Junghans and E. Rivard, *Chem. Eur. J.*, 2019, **25**, 9678.
S3. M. M. D. Roy, S. R. Baird, E. Dornsiepen, L. A. Paul, L. Miao, M. J. Ferguson, Y. Zhou, I. Siewert and E. Rivard, *Chem. Eur. J.*, 2021, **27**, 8572.
S4. O. T. Beachley, J. C. Pazik, T. E. Glassman, M. R. Churchill, J. C. Fettinger and R. Blom, *Organometallics*, 1988, **7**, 1051.
S5. I. C. Watson, M. J. Ferguson and E. Rivard, *Inorg. Chem.*, 2021, **60**, 18347.
S6. T. B. Ditri, B. J. Fox, C. E. Moore, A. L. Rheingold and J. S. Figueroa, *Inorg. Chem.*, 2009, **48**, 8362.
S7. H. Hope, *Prog. Inorg. Chem.*, 1994, **41**, 1.
S8. G. M. Sheldrick, *Acta Crystallogr. Sect. A*, 2015, **71**, 3.
S9. G. M. Sheldrick, *Acta Crystallogr. Sect. C*, 2015, **71**, 3.
S10. M. D. Pelta, G. A. Morris, M. J. Stchedroff and S. J. Hammond, *Magn. Res. Chem.*, 2002, **40**, S147.
S11. A. Botana, J. A. Aguilar, M. Nilsson and G. A. Morris, *J. Magn. Res.*, 2011, **208**, 270.
S12. M. A. Connell, P. J. Bowyer, P. A. Bone, A. L. Davis, A. G. Swanson, M. Nilsson and G. A. Morris, *J. Magn. Res.*, 2009, **198**, 121.
S13. M. J. Frisch, G. W. Trucks, H. B. Schlegel, G. E. Scuseria, M. A. Robb, J. R. Cheeseman, G. Scalmani, V. Barone, G. A. Petersson, H. Nakatsuji, X. Li, M. Caricato, A. V. Marenich, J. Bloino, B. G. Janesko, R. Gomperts, B. Mennucci, H. P. Hratchian, J. V. Ortiz, A. F. Izmaylov, J. L. Sonnenberg, D. Williams-Young, F. Ding, F. Lipparini, F. Egidi, J. Goings, B. Peng, A. Petrone, T. Henderson, D. Ranasinghe, V. G. Zakrzewski, J. Gao, N. Rega, G. Zheng, W. Liang, M. Hada, M. Ehara, K. Toyota, R. Fukuda, J. Hasegawa, M. Ishida, T. Nakajima, Y. Honda, O. Kitao, H. Nakai, T. Vreven, K. Throssell, J. A. Montgomery, Jr., J. E. Peralta, F. Ogliaro, M. J. Bearpark, J. J. Heyd, E. N. Brothers, K. N. Kudin, V. N. Staroverov, T. A. Keith, R. Kobayashi, J. Normand, K. Raghavachari, A. P. Rendell, J. C. Burant, S. S. Iyengar, J. Tomasi, M. Cossi, J. M. Millam, M. Klene, C. Adamo, R. Cammi, J. W. Ochterski, R. L. Martin, K. Morokuma, O. Farkas, J. B. Foresman and D. J. Fox, Gaussian 16, Revision A. 03, Gaussian Inc., Wallingford CT, 2016.
S14. (*a*) C. Lee, W. Yang and R. G. Parr, *Phys. Rev. B* 1988, **37**, 785; (*b*) A. D. Becke, *Phys. Rev. A*, 1988, **38**, 3098; (*c*) P. J. Stephens, F. J. Devlin, C. F. Chabalowski and M. J. Frisch, *J. Phys. Chem.*, 1994, **98**, 11623.
S15. T. H. Dunning, *J. Chem. Phys.*, 1989, **90**, 1007.
S16. K. A. Peterson, *J. Chem. Phys.*, 2003, **119**, 11099.
S17. (*a*) B. P. Pritchard, D. Altarawy, B. Didier, T. D. Gibson and T. L. Windus, *J. Chem. Inf. Model.*, 2019, **59**, 4814; (*b*) D. J. Feller *J. Comput. Chem.*, 1996, **17**, 1571; (*c*) K. L. Schuchardt, B. T. Didier, T. Elsethagen, L. Sun, V. Gurumoorthi, J. Chase, J. Li, and T. L. Windus, *J. Chem. Inf. Model.*, 2007, **47**, 1045.
S18. W. Humphrey, A. Dalke, and K. Schulten, "VMD - Visual Molecular Dynamics", *J. Molec. Graphics*, 1996, 33.

S19. E. D. Glendening, J. K. Badenhoop, A. E. Reed, J. E. Carpenter, J. A. Bohmann, C. M. Morales, C. R. Landis and F. Weinhold, NBO 6.0, Theoretical Chemistry Institute, University of Wisconsin, Madison WI, **2013**.

S20. R. W. F. Bader Atoms in Molecules. A Quantum Theory; Cambridge University Press: Oxford U.K., 1991

S21. T. A. Keith, AIMAll (Version 15.09.27), TK Gristmill Software, Overland Park KS, USA, 2015 (aim.tkgristmill.com)

S22. J. Contreras-García, E. Johnson, S. Keinan, R. Chaudret, J.-P. Piquemal, D. Beratan and W. Yang, NCIPLOT: a program for plotting noncovalent interaction regions. *J. Chem. Theory Comput.* 2011, **7**, 625-632.